Ambient Ground Vibration Measurements at the Livingston, Louisiana LIGO Site

Alan Rohay, Pacific Northwest National Laboratory

LIGO-C961022-A-D

Table of Contents

List of Appendices

Ambient Ground Vibration Measurements at the Livingston, Louisiana LIGO Site

Alan Rohay, Pacific Northwest National Laboratory

1.0 Introduction

An analysis of ground vibration measurements taken at the Laser Interferometer Gravitational Wave Observatory (LIGO) site at Livingston, Louisiana, was conducted to characterize the ambient seismic noise conditions, anthropogenic noise, and wind and acoustic noise sources. The purpose of this study is to establish site-specific ground vibration statistics for the design of vibration-sensitive systems.

The instrumentation used, and its calibration and noise characteristics are described below in Sections 2 and 3. The method of recording at the LIGO site and the observations that were taken are then described (Section 4). The methods used to prepare spectrograms (a time-frequency analysis), amplitude spectra, and noise amplitude histograms are described in Sections 5, 6, and 7. Plots of the data and spectrograms, amplitude spectra and histograms for 24 one-hour segments of the measurement period are included as Appendices A-D. Section 8 describes the operations of two sets of pipelines that pass beneath the West Arm of the planned LIGO facility during the measurement period, and characterizes the vibrations caused by the pipelines at the ambient measurement sites and at additional measurement sites on and near the pipelines. Descriptions and characterizations of other anthropogenic noise and wind noise are presented in Section 9, including noise associated with trains and aircraft that affect the ambient vibration environment at the LIGO site.

In summary, it was found that the ambient ground vibration at the LIGO site is consistently higher than the LIGO reference design spectrum at frequencies below 5 Hz. This is consistent with previous measurements made at the site in 1988 by the Louisiana State University. Above 10 Hz, the design spectrum nearly always envelops the observed ground vibration spectrum, except when acoustic noise from aircraft is transmitted into the ground.

Below 0.5 Hz, natural "microseism" noise is consistently peaked above 10^{-6} m/sqrt(Hz) near 0.2 Hz. The crude oil pipeline passing beneath the West Arm appears to generate a significant portion of the ambient noise at the West End in the frequency range 0.5 to 10 Hz, and there are significant daily variations in its amplitude. Simultaneous measurements made at varying distances from the pipelines indicate an attenuation of at least 6 dB at a distance of 0.4 km from the crude oil pipeline axis. Trains passing twice daily increased the ambient noise at all three measurement locations. At the South End, the trains generated vibrations exceeding 10^{-6} m/sqrt(Hz) by over a factor of 10 in the frequency range 1 to 5 Hz.

2.0 Instrumentation System Description

The instrumentation used to make the vibration measurements consisted of modern seismological instruments conventionally used to record small earthquake signals. This system consists of three orthogonally-mounted seismometers to sense the ground motion and a recording system that digitally records the data in the field. A low-frequency (infrasonic) microphone was recorded in parallel with the seismic data. Wind speed and direction were also recorded using a separate, low-speed data logger. This section describes the components and systems used to make these measurements, and the parameters used to record the data.

Seismometers. The measurements at the LIGO site were made with three CMG-40T three-component broad band seismometers, manufactured by Guralp Systems, Ltd. and distributed in the U.S. by Digital Technology Associates, Concord, CA. These instruments detect the relative displacement of the seismometer mass due to an input acceleration with a capacitive transducer. This signal is amplified and a feedback force is applied to a coil/magnet assembly to restore the mass position. The instrument has acceleration-, velocity-, and displacement-proportional outputs derived from the feedback signal. The data were collected from the low-gain (nominally 800 V/m/s) velocity output. The velocity output is different for one of the three seismometers, being attenuated by 3 dB (70%) at 0.033 Hz instead of 0.05 Hz as on the other two. Although this does not significantly affect the amplitude response in the frequency band of interest (above 0.1 Hz), it does affect the group delay of the low frequency signals. There are also differences in the high-frequency responses near 50 Hz. The frequency responses and noise floor of the CMG-40T seismometer have been measured and are described in greater detail in the next section on system calibration and noise.

Digital Recorder. The data acquisition systems were two Model 72A-02 and one Model 72A-06 from Refraction Technology, Inc. (Reftek), Dallas, TX. These systems are practically identical. These systems amplify and then digitize up to six input signals with 16-bit precision (24-bit precision on 3 channels of the Model 72A-06) at 1000 samples/s and digitally apply anti-alias filters to the output data streams at selected sub-rates. These data acquisition systems can record each input channel at a different amplification and digitizing rate, and can record continuous data, data from pre-programmed time periods, or can record based on a variety of signal threshold triggers. All data collected at the LIGO site were collected continuously using a sample rate of 250 samples/s and the 16-bit digitizers. The system used stores up to 2.5 Mb of data internally and periodically copies the data to one of two 1 Gb disk drives. Precise time is obtained from a Global Positioning Satellite (GPS) receiver and maintained by an internal crystal oscillator. For these measurements, the GPS system was operated continuously to provide precise synchronization between the three measurement locations. Control of the data acquisition system was provided by a hand-held PC and software provided by Reftek.

Playback and analysis software. The Reftek disk drives were connected to a SUN/UNIX workstation and playback software, obtained from the Incorporated Research Institutions for Seismology (IRIS, Arlington, VA), was used to copy the data from the field disk to the computer system's disk. IRIS software was then used to view the data on the computer

screen, and reformat, merge, and otherwise manipulate the data. All data were copied to 8mm tape in UNIX tar format. The software was operated on computer systems provided by the Physics Department of Louisiana State University during the measurement period. The IRIS software was then used to convert selected portions of the data to SAC format (Seismic Analysis Code, from Lawrence Livermore National Laboratory), and the spectral analyses were conducted using the SAC programs. In addition to the IRIS and SAC software, the Splus statistical package (from StatSci, Seattle, WA) was used to generate histograms and some additional graphics.

Infrasound Microphone. The infrasound instrument used was a Model 2 Microphone from Chaparral Physics Consultants, Albuquerque, NM. It has a 0.4 V/Pa response at the sensitivity selected and its response to pressure is essentially constant between 0.3 and 100 Hz. Its response is attenuated by 3 dB (70%) at 0.1 and 300 Hz. This instrument was not calibrated and has only been used for qualitative comparisons to the seismic noise signals to date. The infrasound signals were recorded as the fourth channel on the Reftek digital recorder at the same rate (250 samples/s) as the seismic data.

Wind measurement system. Wind speed and direction were measured using an F-460 cross-arm assembly from Climatronix, Bohemia, NY, and recorded on a Campbell 21X data logger (Campbell Scientific, Inc., Logan, UT). Wind speed was measured with a cup anemometer and wind direction was measured with a vane. Wind speed and direction were measured every second, and the average wind speed and direction over a one-minute period were calculated and recorded by the data logger. In addition to the one-minute mean, the peak wind speed during the last minute and the time it occurred was also recorded. The data were downloaded to a portable PC and converted to ASCII files using Campbell PC-208 software.

3.0 System Calibration and System Noise

Two of the three seismometers were calibrated previously and the calibration and noise results were reported previously in the report "Ambient Ground Vibration Measurements at the Hanford, Washington, LIGO Site. Some of this information is repeated here for completeness, and a re-calibration of the low-frequency (0.1 to 5 Hz) response of the two original seismometers and the third seismometer is then presented. The new calibration results are in good agreement with the original measurements.The manufacturers measured high-frequency calibration was adopted based on its agreement with the above report's measurements. The high frequency response is not used in this analysis because the response of the seismometers is sufficiently flat to 20 Hz, where the seismometer noise floor and installation or "coupling" resonances begin to degrade the data.

3.1 Seismometer Calibration

Calibration method. Electrical signals were input to the calibration coil of the seismometers to check the calibration constants of the seismometers. Two types of input signals were used, step offsets (for low-frequency response measurement), and sinusoidal inputs. These two methods were previously used to measure the frequency response of the two

original seismometers. Only the low-frequency step calibration was conducted at the end of the Livingston measurements on all three seismometers. This consisted of inputting a step voltage into the calibration coil, repeated over twenty times at 45-s intervals with alternating polarity. The seismometer velocity outputs were digitized at 250 samples/s at a gain of 1, and the calibration input signal was recorded as a fourth channel. The input and output signals recorded on the Reftek disk were then copied to the workstations for spectral analysis.

Low Frequency Response. Spectral analysis was performed on both the calibration signal and the output signals of the nine components tested using the step signals. The spectra of the inputs and outputs (or their derivatives) were calculated over 20 different step intervals and the average taken to reduce the variance. The ratio of the output to input voltage spectra (obtained by converting the input acceleration spectra to velocity spectra and possibly removing the pre-whitening effect from differentiation) was calculated, and normalized to the calibration circuit resistance and the feedback coil constant appropriate to each component. The result is shown in Figure 3-1 for the three 3-component seismometers, normalized to the velocity transduction constants provided by the manufacturer. The original values agree with those measured to within 5% above 0.1 Hz. This calibration begins to fail at frequencies higher than approximately 2 Hz because background noise at this location is high and the high-frequency power in the step inputs is relatively low.

Although all three seismometers are practically flat to velocity from 0.1 to over 20 Hz, there is a phase response difference at frequencies below 0.5 Hz that can slightly affect the calculation of signal differences or signal correlations between the seismometers. Although the phase response and group delay have been measured from these step calibrations, this report will use the smoother results that can be generated analytically for equivalent seismometers corresponding to these measured amplitude responses. The two original instruments have a response that is simulates a seismometer with a 20-s period; the third instrument has a 30-s period. These values are in good agreement with those provided by the manufacturer.

High Frequency Response. The high frequency response provided by the manufacturer is shown in Figure 3.1 as the smooth roll-off at frequencies above 20 Hz. All nine components are shown. The two points indicated as squares in Figure 3-1 show the range of measured high-frequency responses of the two original three-component seismometers at 50 and 100 Hz. The high-frequency response is within about 10% of the predicted values.

The importance of making a correction for this high-frequency response is diminished because of the problems with coupling of the seismometers to the soil, resulting in an amplifying resonance in the frequency range above 40 Hz. The noise spectra at the LIGO site, including the resonant amplification caused by the coupling problem, are practically always a factor of 10 or more below the LIGO design spectrum.

3.2 Seismometer Noise

Estimates of the seismometer noise floor and electronic system noise were made previously using the two original seismometers, as described in the Hanford Ambient Vibration

report. At a quiet site near the Hanford LIGO, signal differences between two identical seismometers were spectrally analyzed using the same methods as used to calculate the spectra of the Livingston LIGO measurement sites. Figure 3-2 shows the spectrum of the signal obtained by subtracting each corresponding component of the time series from the other. The latter represents the portion of the signal that is not common to both sensors and which is interpreted as sensor noise. However, there are additional signal differences that are due to the method of emplacement, including misalignment of the horizontal components and possible differences in coupling on the concrete floor. Assuming each of the two sensors contribute equally to this noise signal, the noise caused by each sensor would be estimated to be reduced by a factor of sqrt(2) relative to the values plotted in the figure. At frequencies above 20 Hz, signal difference spectra were previously observed to be as large as the independent signal's spectra, so it is clear that only sensor noise is recorded and not actual ground motion from 20-100 Hz, or levels below 10^{-12} m/sqrt(Hz). The sensor noise is more than a factor of 10 below the LIGO design spectrum from 0.1 to 100 Hz, except for a band near 1 Hz where the seismometer noise is only 6 to 8 times lower than the LIGO design spectrum.

3.3 Amplifier and Digitizer Noise

Figure 3-2 provides a comparison of the CMG-40T signal difference spectra for all three channels and an estimate of the noise generated by the Reftek amplifier and digitizer (lowest curve). The two horizontal signal difference spectra are offset by factors of 10 for clarity. The vertical noise spectrum is approximately a factor of two higher than those of the horizontals to nearly 10 Hz. The lowest curve is a spectrum estimated from a simulated white noise signal with a r.m.s. amplitude corresponding to 1 count on the digitizer. (The evenly-spaced spikes in this spectrum are an artifact of the random number generator, as using different seeds changed their position). At the gain actually used in making the LIGO site measurements, this corresponds to 0.89 microvolts r.m.s. Actual tests by Reftek indicate that at this gain, the noise is approximately 1.2 uV, so that the noise plotted here should be increased nominally 30%. Actual quantization noise due to rounding (a signal with a uniform distribution between -0.5 and +0.5 counts) was also checked and is found to be a factor of 1/sqrt(12) below the plotted estimate, in agreement with theory. This figure shows that the seismometer noise signal is well resolved by the Reftek system at the gain used, but the margin was quite small at frequencies near 10 Hz.

3.4 Coupling

Returning to the high frequency noise difference spectra in Figure 3-2, there a large increase in the noise signals for the two horizontal sensors at frequencies between 70 and 80 Hz. A second peak at approximately 90 Hz is also observed. The first is attributed to an amplification of the actual noise by a rocking oscillation of the seismometers, termed a "coupling" problem. The effect is much smaller for the vertical channel (not offset in this plot). The second peak at 90 Hz may also be due to a coupling problem, but may be affected by the vibration of the disk drive that is used to record the data. The coupling problem (and sometime the disk drive signal) will also appear in the actual LIGO data,

although the coupling problem is ultimately found to be worse in the soil compared to the hard concrete surface at the Nike missile bunker.

4.0 Description of Noise Measurements

Measurement Period. Continuous seismic data were recorded at the LIGO site from October 26 to November 3, 1995. The seismic systems at the South End and West End were installed on October 26. On October 27 the third seismic system was installed at the Corner, along with the infrasound microphone and wind measurement system. All these systems (seismic, acoustic, and wind) operated over the weekend until Tuesday, October 31, when the sites were revisited. Moderate rain had flooded the microphone installation at the Corner shortly before recovering the disks from this site. The failure of the microphone system was coincident with a temporary problem noted on the seismic signals, but the seismic signals had returned to normal by the time of the site visit. Seismic data from the South End and West End sites was normal throughout the 5-day period (mid-day Thursday to mid-day Tuesday).

Sunday	Monday	Tuesday	Wednesday	Thursday	Friday	Saturday
				299 (10/26) S End Start W End Start	300 (10/27) Corner Start	301 (10/28)
302 (10/29) Central Standard Time begins	303 (10/30)	304 (10/31) Microphone Removed, New Disks	305 (11/01)	306 (11/02) Heavy Rain & Flooding	307 (11/03) Recorders Removed	308 (11//04) Seismic Sensors Removed
309 (11//05)	310 (11//6)	311 (11//07)	312 (11//08) Pipeline			

All three sites continued to operate until Thursday, November 2, when heavy rain flooded the instrument vaults, immersing most of the equipment. Although the recorders continued to function, the seismometer signals became erratic Thursday morning. The recording systems were removed on Friday, and the seismometers and remaining equipment were removed Saturday. Although neither the seismometers nor the recording systems and disks appeared to be damaged, various internal fuses were blown and the interconnecting cables and plugs were damaged and/or shorted. Data collected between Tuesday, October 31 and Thursday morning, November 2, appeared to be normal on the seismic channels at all three locations.

In summary, the data collection program produced valid seismic data measured simultaneously at all three sites for a 6-day period from mid-day Friday, October 27 to Thursday

morning, November 2. Wind measurements were made at the Corner throughout this period. The acoustic microphone operated for the first four days of this period.

On Wednesday, November 8, the systems were re-deployed at various distances from two pipelines that cross the West Arm of the LIGO site. These measurements are described in Section 8. Some of these data were not usable because of damage to the cables, when condensation apparently generated cross-connections between some channels or interrupted power to the seismometer system.

Timing of Seismic Data. Time on all recording systems was synchronized to Greenwich Meridian Time (GMT) and day of year (termed "Day" in this report). In this report, a one-hour period will be referred to as "Hour", so that referring to Day 300, Hour 22 refers to the time period 22:00-23:00 GMT on Day 300. It is important to correlate the observed noise phenomena with anthropogenic noise sources that may occur at times better correlated with local time and calendar day. The measurement period unfortunately included the change from Central Daylight Time (CDT) to Central Standard Time (CST). GMT is 5 hours advanced from CDT from the beginning of the measurements to Sunday, 2:00 a.m. CDT, or Day 302 07:00 GMT. Hour 06 (the one-hour period beginning at 06:00 GMT and ending at 07:00 GMT) corresponds to 1:00 - 2:00 a.m. CDT. This one-hour period is immediately followed by the one-hour period 1:00-2:00 a.m. CST, which is Hour 07 (07:00 to 08:00 GMT). From this time on is GMT is 6 hours advanced from local time (CST).

Timing on all three seismic recording systems was synchronized to external GPS clocks that operated continuously at each site. The recording system is programmed to gradually adjust its internal time to maintain a time difference of less than 0.1 milliseconds, and revises the rate of time adjustment whenever the time difference exceeds 0.1 milliseconds. If a comparison of the internal and external clocks indicates a difference of 16 milliseconds, the internal time is abruptly changed ("jerked") into conformance with the external clock.

During the deployment at the Livingston LIGO sites, prior to the flooding, the timing systems maintained accuracies of better than 0.05 milliseconds at the two End sites, but the timing system at the Corner sometimes drifted by up to 0.25 milliseconds when the satellite clock lost sufficient satellite signals for time locking. Although the performance of the Corner site timing system was inferior to the other two, the larger inaccuracies only represent a maximum time difference of 1/4000 of a second, which is small in comparison to the 1/250 of a second sampling interval.

Measurement Locations. Measurement locations were selected to be as near to the surveyed locations of the Corner and Ends as was convenient. At the Corner, the site was moved approximately 100 m North from the survey markers to avoid a roadway. The two End measurement sites were situated about 30 m external to the surveyed locations. The entire area had been cleared of trees and bushes, leaving a relatively flat grassy surface along both arms. Trees left from the logging and bushes left from the grubbing were no closer than 50 m from any of the measurement sites.

One of the auxiliary outputs of the GPS clock used to synchronize time to GMT is the latitude and longitude of the site. However, this output was not available because the software for the clocks does not allow location determination in parallel with continuous time synchronization. The locations of the measurement sites were instead determined with a separate, hand-held GPS location system. Below is a comparison of the locations obtained from Woodward-Clyde Engineers for the LIGO site (map dated 12/22/94). The distance and azimuth between the corner and the end stations were calculated to be within 23 m of the 4 km length specified, and the azimuths of the two arms were within 0.01 degrees of being perpendicular.

Location Name	Latitude	Longitude	Distance	Azimuth
LIGO Corner	30.5630	90.7744	-	-
LIGO West End	30.5519	90.8143	4.022	252.28
LIGO South End	30.5284	90.7616	4.023	162.28

The table below gives the locations where the seismic measurements were actually taken, and the distances and azimuths to the surveyed locations above.

Seismometer Station Location Name	Latitude	Longitude	Distance From LIGO	Azimuth From LIGO
LIGO Corner Seismic	30.5637	90.7749	0.097	326.95
LIGO West Seismic	30.5515	90.8145	0.051	203.02
LIGO South Seismic	30.5283	90.7615	0.013	139.12

The azimuths from the surveyed sites to the measurement sites are calculated precisely, but are not accurate because the distances from the survey points and measurement locations are small, comparable to the accuracy of the GPS locations. Figure 4-1 shows an areal view of the LIGO site.

Equipment Installation. A 55-gallon drum (approximate dimensions 4' high and 2.5' in diameter) with an open bottom and a removable lid was emplaced at one end of a trench dug in the clay soil so that the top of the drum was just exposed to the surface. This housed batteries and the Reftek data acquisition system and disk.

A second drum, cut to 3' length, was emplaced approximately 1' below grade in at the other end of the trench, approximately 8' from the first. The trench was then filled to grade except for the area near the barrel for the seismometer. A cement paving stone approximately 1.5' in diameter was leveled in the clay exposed at the bottom of this drum, and the

seismometer was set on the paving stone and oriented using a compass to an estimated precision of 2 degrees.

The cable from the seismometer was fed to the data acquisition system through holes cut in the sides of the drums. A lid was placed on the seismometer barrel and was covered to grade to dampen acoustic noise. The seismometer cable was buried to prevent damage from rodents and to reduce electrical noise.

A set of color photographs is available which illustrate the stages of the installation and document the locations of the measurement sites.

Seismometer orientation. The orientation of the LIGO facility was measured from a map that indicated the orientation of the LIGO arms were 18 degrees counter-clockwise from the principal directions. The geodetic calculations using the latitude and longitude from this map agree with this orientation. The seismometers were oriented using a magnetic compass to an estimated precision of 2 degrees. This compass measured the orientation of the LIGO arms to be only 19 degrees counter-clockwise from magnetic North, instead of the 22.5 degrees that would be expected from the 1980 magnetic declination (+4.5 degrees) on a U.S. Geological Survey map. The seismometers' orientations and the LIGO arms' orientations were all measured consistently, and no orientation error has been introduced. The compass was later found to give the correct azimuths at the Hanford LIGO site.

Data recording setup. All measurements were made at a gain of 128 at a sample rate of 250 samples/s. This gain level represented a compromise between recording higher noise levels and the resolution of lower noise levels at high frequency.

The disk was connected to the switched power connection of the data acquisition system, so that the disk drive only consumed power when data was dumped from memory to disk. The vibration caused by the disk drive operating was reduced by wrapping the disk drive in foam rubber, it is not observable in the ambient noise measurements described here. However, this noise was observable during the later surface noise measurements made at the oil pipelines.

Approximately 150 Mb of data were collected at each site each day, which fills the 1 Gb disk drives roughly every 5 days.

Infrasound measurements. Infrasound data was recorded in parallel with the seismometer signals at the Corner.The microphone was emplaced in a shallow pit covered by two furnace filters taped between two3'x3' pegboard panel (the pegboard has 1/4" holes at 2" spacing in it). This was found to give sufficient isolation from the wind, and is not thought to affect the amplitude of the low-frequency pressure fluctuations. The acoustic system was damaged by rain and disconnected November 30.

Wind measurements. Wind speed and direction data were collected from Friday, October 27, (when the Corner seismic system was installed) to the last day of seismic data collection, Friday, November 3. The assembly has a cup anemometer and a wind vane at each end of a 1-m arm. This assembly was mounted at the top of a rigid tripod assembly

approximately 2.5 m high. The orientation of the wind vane was set by compass to 4.5 degrees West of magnetic North, which was indicated to be true North based on the USGS map. (This orientation was not set with the same convention as the seismometers, which were oriented parallel to the LIGO arms.) The data logger's time was synchronized to within approximately 5 s of the time base of the Reftek seismic recorder.

Observations of anthropogenic noise sources. The LIGO site is bordered by forested land to the north, but is near roads and rural homes on the west, south, and east sides. During various site visits, various audible and visual cues to potential noise sources were noted. There were observations of both low-flying propeller-driven airplanes (strongly audible) and high-flying jet aircraft (generally barely audible). It was usual to observe other vehicles on the dirt roads in the area, mostly groups of hunters with dogs (after dark), and hunters hunting for lost dogs (during the day). On several occasions, chain saws were audible from the forest to the north of the Corner and West End sites, and also from the direction of homes to the south of the West and South Ends. There were groups of cows about at all measurement locations. A railway was noted, located about 2.5 km south of the South End.

Data selected for analysis. The data were plotted for each day and each seismic component. These plots were used primarily to identify sections of data that were affected by a variety of noise phenomena, or that indicated malfunctions of the systems due to flooding of the installations. These plots are included as Appendix A.

For the purpose of characterizing the spectra over a 24-hour period, the time period from Day 303, Hour 06 Through Day 304, Hour 05 was selected. This period corresponds to Monday, October 30, 00:00 to 24:00 CST. This period was chosen instead of the preceding Sunday because there appeared to be more seismic and acoustic noise on the Monday period, without many direct (vehicle drive-by) signals that strongly affect the results.

Data from several other days will also be used for special studies of wind effects, anthropogenic noise, and other low-frequency noise that was observed to vary from day to day. Spectrograms of the vertical seismic signals and microphone were generated for these other days to identify time periods for these special studies. These spectrograms (described in the next section) principally illustrate the high-frequency (above 5 Hz) noise variations that generally characterize most anthropogenic noise sources. A subset of these spectrograms, corresponding to the 24-hour period selected, is included in Appendix B.

5.0 Spectrograms

Acceleration and Infrasound Spectrograms. Spectrograms are included in Appendix B for the vertical channel of the seismic signals for the same period that are used to calculate the 24-hour spectra and histograms (Sections 6 and 7, below), as a means of identifying the particular phenomena that affect the spectra and histograms. The spectrograms were constructed by calculating the amplitude spectrum of 720 sequential 5-second segments of a one-hour time series (900,000 points). The time series data had previously been differentiated to acceleration to flatten the spectrum between 5 to 100 Hz (this also makes the scal-

ing parallel to the LIGO design spectrum in the range 10 to 100 Hz).The display of a spectrogram consists of arranging each spectrum (one from each 5 s of data) into a sequential table, so that the table entries correspond to the spectral amplitude at each frequency as a function of time. This table or matrix of amplitudes can then be color-coded, gray-scaled, or contoured to produce a quantitative representation of the time-frequency patterns of spectral amplitude variations. For the Livingston data, color spectrograms were produced for the appendices, and a variation on the gray-scale spectrograms was used to create the spectrograms in the figures of this report.

Black-and-white (or binary gray-scale) spectrograms, are generated by subtracting the mean spectral amplitude from each spectrum and then plotting in black the positive values of the resulting difference. This works well in identifying narrow-band features, but has a side effect of obscuring or whitening the appearance of the spectrogram in adjacent bands. A time series plot of the acceleration signal is included above the spectrogram at fixed scale on all the spectrograms for reference to absolute noise levels.

An example of an acceleration spectrogram is shown in Figure 5-1. Spectrograms were also calculated in the same way for the infrasound signals the same day (October 30), and an example is shown in Figure 5-2. These two spectrograms are for a quiet period at the Corner measurement site. For comparison, Figure 5-3 shows an acceleration spectrogram at the Corner during daytime hours, when a vehicle passed the site, and Figure 5-4 shows the corresponding infrasound spectrogram. Figure 5-5 shows an example from the West End when several aircraft flew overhead, and Figure 5-6 shows an example from the South End when a train passed to the south.

6.0 Hourly Spectra

Amplitude spectra are presented in Appendix C that were prepared from one-hour segments of data for a 24-hour period at all three sites. The hourly spectra for Monday, October 30 from 00:00 CST to 24:00 CST correspond to Day 303 Hour 06 through Day 304 Hour 05. Examples of the spectra for a quiet period are shown in Figures 6-1 to 6-.5 for all three components at the Corner site and the vertical components of the South End and West End. The spectra are in units of log-amplitude spectral density; they equal one-half the log-power spectral density.

The amplitude spectra were calculated by averaging 39 180-s windows that overlapped the adjacent windows by 90 s. A 50% cosine taper was applied to each of the windows so that the effect of the overlap is practically compensated, and the windows have an effective length of approximately 90 s. Each window was first de-meaned prior to tapering, and scaled by the appropriate velocity transducer constant. The FFT was then taken of each window, and the result divided by 2*pi*f to obtain a displacement spectrum, and squared to produce a power spectrum. Corrections for the window length and taper were made, and the results saved to temporary files. Averaging is done in two ways: the simple mean of the power spectra is calculated frequency-by-frequency, and the mean of the logarithm of the power spectrum is similarly calculated. Claiming that the distribution of the power spectra is nearly log-normal, the latter provides a robust central estimate that should be close to

the median of the distribution. The mean power spectrum is equivalent to the mean-squared amplitude spectrum. The spectra are presented on a log displacement amplitude scale. Therefore, the "median" estimate represents the median amplitude spectrum of a log-normal distribution of amplitude spectra, and the "mean" estimate represents the r.m.s. amplitude spectra.

The r.m.s. amplitude spectra are more strongly affected by temporally-limited noise events during the one-hour periods. Figure 6.6 shows an example when a small earthquake signal was present, Figure 6-7 shows an example when a train passed to the south of the site, and Figure 6.8 shows an example when a vehicle was driven past one of the sites. These and other noise phenomena will be described in greater detail in a later section. Identification of the source of the noise variability is needed to chose whether it is most appropriate to use the r.m.s. or median spectra for any particular application.

A comparison of the individual amplitude spectra to the r.m.s. amplitude spectrum indicates that the r.m.s. spectra are exceeded by 1 to 3 of the individual spectra, suggesting an approximate interpretation as the 97th to 90th percentile (respectively) of the distribution of the 39 total spectra. The 90th-percentile approximation generally applies to those instances when the difference between mean and median is small (temporal noise variations are small), and the 97th-percentile approximation generally applies to those instances when the difference between mean and median is large (when there are significant bursts of noise). If the cause of the noise burst is known, a determination can be made as to the representativeness of the r.m.s. spectrum versus using the "best estimate" median value.

It is apparent in practically all of the spectral plots that the poor coupling of the seismometer to the clay soil is making the measurements inaccurate near 40-70 Hz, particularly for the two horizontal components. The apparent amplification of noise now covers a wider range than was observed when the instruments were calibrated/compared on a solid concrete floor. For the horizontal components, there sometimes appears to be an artificial "hole" in the spectrum at about 35 Hz.

When the noise levels above 40 Hz approach the 10^{-12} level (the lowest level shown in these spectra), the noise is actually at the noise floor of the seismometer as indicated by the seismometer difference spectra. Because of the coupling problem and the limited noise resolution at high frequency, the spectra have not been corrected for the amplitude roll-off of the seismometers' response, which would merely amplify these effects. The raw (uncorrected) spectra are accurate to within 10% for all frequencies between 0.1 and 30 Hz. At 50 Hz, the seismometer response is attenuated by 30%.

7.0 Hourly Histograms

Histograms of the signal amplitudes were prepared from one-hour segments of data of the same 24-hour period used for calculating the spectra at each of the three sites. The histograms for the 24-hour period and the three sites are included in Appendix D.

The histograms are derived from a set of band-pass filters that isolate the motions in the frequency bands 0.5-1 Hz, 1-2 Hz, 2-4 Hz, 4-8 Hz, and 8-16 Hz. The data were first filtered and decimated to 50 samples/s with the same anti-alias filter as is applied by the Reftek recorder. This filtering maintains the full signal amplitude to a frequency of 40 Hz. The data were then demeaned, a taper applied to the 0.36 seconds of the beginning and ending of the data (2/10,000 of the data was affected), and a high-pass, 8-pole Butterworth filter was applied at 0.5 Hz. The stronger filtering below 0.5 Hz was needed to reduce the rising amplitude of the low-frequency microseism noise. These time series were corrected by the appropriate velocity-transducer constants and integrated to produce displacement time series. A set of 4-pole Butterworth band-pass filters was then applied at the above frequency limits to produce separate displacement time series for each band (only a low-pass was needed for the lowest frequency band, having already applied the 8-pole high-pass at 0.5 Hz). The spectral amplitudes are reduced 3 dB (to 70%) at the upper and lower band limits by the Butterworth filters. The spectral effects of the different filters on an example signal are shown in Figure 7-1. The band-passed time series were then segmented into short time samples that corresponded to a single cycle of the lowest frequency represented in each band. This results in the time sampling shown below for each one-hour period.

Frequency Band (Hz)	Sample Length (s)	Number of Samples
0.5 - 1	2	1800
1 - 2	1	3600
2 - 4	0.5	7200
4 - 8	0.24	15000
8 - 16	0.12	30000

The r.m.s. amplitude was calculated in each sample, and a cumulative histogram of the number of times r.m.s. ground displacements exceeded levels spaced at logarithmic intervals of 0.05 units were calculated.

Figures 7-2 to 7-6 show examples of the histogram from one of the quietest periods for all three components at the Corner and for the vertical components at the South End and West End. Note that the scale of these histograms has been increased to an upper limit of 10^{-6} m; histograms previously calculated for the Hanford LIGO site had a maximum of 10^{-7} m. There was a slight, brief exceedance of 10^{-6} m in the set of histograms for the two horizontal channels at the West End and the north component at the Corner during Hour 14 Day 303 for the frequency band 0.5-1.0 Hz. Figure 7-7 shows the effect on the North Component at the West End. A smaller effect is also seen in this set of histograms for the frequency band 1.0-2.0 Hz. This noise burst at relatively low frequency is caused by a magnitude 5 earthquake that occurred at 1448 GMT near the west coast of southern Mexico.

The effects of short-duration noise events that may occur during each one-hour period generate a characteristic effect on the histograms that is a complementary presentation of the differences described in the previous section between the r.m.s. and median spectra. For example, the r.m.s. noise spectra in Figure 6-6 are increased by the earthquake in the low-frequency range. The histogram of Figure 7-7 corresponding to this Hour has the low-

frequency bands shifted to the right (higher amplitudes) at lower probability of exceedance values (approximately 10%). Figure 7-8 and 7-9 show the histograms corresponding to the train and car effects shown on the spectra in Figures 6-7 and 6-8.

8.0 Pipeline Noise

There are several identifiable sources of noise at the Livingston LIGO facility, primarily resulting from anthropogenic sources including pipelines, train traffic, and aircraft. One of the most significant noise source appears to be a crude oil pipeline that crosses the West Arm of the LIGO site and most strongly affects the West End measurements.

The potential noise effects of the pipelines are expected to be largest at the West End compared to the Corner or South End measurement sites, and to be larger still at the point where the pipelines cross the West Arm. These pipelines and their levels of operation during the measurement period are described below, followed by a description of data analyses that sought to detect and characterize the seismic vibrations from the pipelines at the West End measurement location. Limited measurements made directly over the pipelines (and at short distances away) were also collected and analyzed, and these results are described at the end of this section.

8.1 Description of Pipelines

Two sets of pipelines cross the West Arm of the LIGO site along two north-south-oriented right-of-ways (see Figure 4-1). The flow of material within the pipelines and/or pressure fluctuations from nearby pumps may generate seismic vibrations that are transmitted into the ground along the pipelines. The western right-of-way crosses the LIGO West Arm 0.5 miles from the West End (approximately one-fifth of the distance from the West End to the Corner), and contains the three Transcontinental pipelines. The eastern right-of-way crosses the LIGO West Arm 0.8 miles from the West End (approximately one-third of the distance from the West End to the Corner), and contains the two Shell pipelines, called the "Capline" and the "Choctaw pipeline", and the smaller Enterprise pipeline.

Transcontinental Gas Pipelines. This set of three pipelines crosses the LIGO West Arm along the western right-of-way 0.5 miles from the West End. One 24-inch-diameter and two 30-inch-diameter pipelines carry natural gas (gaseous phase). The pressure is estimated to be approximately 750 psi (52 times atmospheric pressure) near the LIGO site. The combined flow of natural gas through all three pipelines averages 1.0 to 1.2 billion ft^3/day (equivalent volume at 1 atmosphere or14.7 psi). Flow rates during the period of measurements ranged from 0.93 to 1.07 billion ft^3/day. Flow in the pipelines is to the north, generally driven by Compressor Station 62, located 70 miles to the south, but during periods of high need Station 63, located 35 miles to the south, will also be used. During the measurement period, pressure measurements at Station 62 and 63 were within a ten percent of 900 and 825 psi, respectively. Station 62 has nine integral compressors ranging in horsepower from 1440 to 5500, and all operate at 325 r.p.m.

These three pipelines have been in continuous operation over the past 10 years. During the measurement period there were no significant fluctuations or interruptions in the operation of this pipeline. Station 63 was not operating during the measurement period, but 3% of the gas flow was being diverted to a gas storage field (Station 64) at a branch in the pipeline from Station 63, thereby reducing the operating pressure and flow somewhat near the LIGO site.The pressure at the LIGO site is estimated to drop an additional 75 psi in the 35 miles between the measurement point to the south. In the period of time following the pipeline vibration measurements, Station 63 has been brought on line and is scheduled to remain operational until further notice, potentially increasing pressure levels and noise near the LIGO site.

Shell "Capline". The Capline is the easternmost of the three pipelines within the eastern right-of-way and carries a wide variety of crude oil grades northbound in a 40-inch diameter pipe. The Capline is pressurized at the St. James pump station (Mile Pole 0) to pressures ranging from 500 to 700 psi and is later measured in the range 250 to 400 psi at the block valve at Mile Pole 28 (located twelve miles south of the LIGO site). The Capline is repressurized at the Pine Grove Station (Mile Pole 46), six miles north of the LIGO site. Throughputs on the Capline ranged from 0.95 to 1.2 million barrels/day during the measurement period. During this time, the Capline experienced two periods of downtime, from 3:30 a.m. to 6:55 a.m. CDT on October 27, and from 9:28 p.m. CST November 2 to 7:46 a.m. CST November 3. This first of these two periods was observed at the West End seismic site. The second period when this pipeline was not operating occurred after the flooding and has not been examined. During the first shutdown, all 5 of the pump units at the St. James pump station were off and the pressure measured at Mile Pole 28 dropped to 60 psi for two hours.

The Capline flow rate throughout the year reaches a maximum of 1.2 million barrels/day, so the pipeline was flowing practically at the maximum during the measurement period. Capline flows are maintained above 0.7 million barrels/day to minimize the mixing of different crude oil grades in the pipeline. Once or sometimes twice per week, the flow in the Capline will be shut off for several hours, when oil is input to the pipeline network at a different point, north (downstream) of the Livingston area. Two of these characteristic periods of downtime were during the measurement period. The grade of oil is changed 3-5 times per day, with each "batch" containing 200,000-300,000 barrels. Oil batches are changed on an irregular schedule throughout each day. A "pig" is sent through the Capline only 2-3 times each year to clean the inside of the pipeline (it is not used to separate different grades of crude oil). The pig is a 40" diameter rubber sphere weighing about 1500 lbs. An instrumented device for measuring the condition of the pipe is only used once every 5-6 years. No "pigs" were run through the pipeline during the measurement period.

Shell Choctaw Pipeline. The Choctaw pipeline is 20 inches in diameter, and is the western-most of the three pipelines within the eastern right-of-way. The Choctaw carries liquid CO2 at pressures between 1200 and 1350 psi. This pipeline is operated solely by the natural pressure at the source well (there are no pumps), and to a lesser extent by gravity. The density of the liquid is approximately 22 lbs/ft^3 at 105^{o}F at the top of the well, but is cooled to ground temperature (50^{o}F) in the pipeline and there has a density of approxi-

mately 53 lbs/ft^3. Flow of material is to the south, even though the pressure increases southward due to gravity. During the measurement period, the operating pressure measured at Mile Pole 142 (2 miles south of the West Arm) was constant within 3% of 1300 psi. Throughputs on the Choctaw averaged 6.7 million ft^3/day during this time period. The flow in this pipeline does not vary significantly throughout the year and the flow rate during the measurement period is near the maximum of the range.

Enterprise Pipeline. Enterprise operates a 6 inch diameter pipeline down the center of the eastern right-of-way, between Shell's Choctaw pipeline and Capline. The Enterprise pipeline carries liquid propane at pressures ranging from 600 to 1400 psi. The LIGO facility is about half-way between two pumping stations 20 km north and south of the site. This pipeline routinely transports 500 to 700 barrels/hour, up to 1000 barrels/hour during the months of November-February. During the measurement period, the system was operating in the 500 to 700 barrels/hour range, but was shut down over the weekend, from approximately 6 a.m. CDT Saturday, October 28, to 7 a.m. CST Monday, October 30. On November 8, when measurements were being taken at the pipelines, this pipeline was shut down at 8:40 p.m. CST, but the data taken after 7:40 p.m. were suspect and were not examined.

Summary of Pipeline Information. The table below summarizes the overall characteristics of the pipelines. Clearly, the Capline oil pipeline has the largest mass flux of any of the pipelines, and this pipeline therefore is expected to have the largest potential for generating vibrations. This pipeline carries a wide variety of crude oil grades and these will have different densities and viscosities, and has weekly shutdowns.

	Western Right-of-Way	**Eastern Right-of-Way**		
	Transcontinental	**Choctaw**	**Enterprise**	**Capline**
Diameter (in.)	24 30 30	20	6	40
Material Description	Natural Gas	Liquid CO2	Liquid Propane	Crude Oil (various)
Pressure (psi)	750 (est.)	1300	600-1400	250-400
Flow Volume 10^6 ft^3/day	1000 @s.t.p. 20 @51atm.	0.13	0.1	6.2
Est. Flow Rate(ft/s)	18	0.7	5.8	8.2
Density, lb/ft^3	0.036	53	32	44
Mass Flow 10^6 lbs/day	0.7	6.7	3	260

Volumes in the above table were calculated based on a 42 gallon or 5.6 ft3 barrel. Densities of propane and crude oil are estimated from average specific gravities of 0.5 and 0.7 relative to the density of water. Density of natural gas was estimated from the average specific gravity of 0.55 relative to air compressed to 52 atm. (750 psi). Flow rates are estimated from the flow volume divided by the pipeline cross-section area.

8.2 Pipeline Noise at West End

Measurements taken on Friday morning, October 27 at the West End measurement location provide isolation of the noise component due to the Capline. The Capline was shut down from 03:30 to 06:51 CDT, corresponding to the middle of Hour 08 and the end of Hour 11 on Day 300. Spectrograms were generated for the frequency range 0-25 Hz for all three components of motion at the West End for Hours 06 - 14 that span the period when the Capline was shut down and re-started. Figures 8.2-1 to 8.2-3 show the acceleration time series and black-and-white spectrograms from the selected eight hour period. The effect of the pipeline is strongest on channel 2 or the "North" component, (actually N18°W, parallel to the South Arm but also most nearly parallel to the pipeline). On shutdown, there is an increase in the noise amplitude and then a repetitive, decaying series of impulsive signals that are interpreted to be due to a "water-hammer" or "surging" effect of the pressure drop that ultimately propagates back and forth in the pipeline. This can be seen more clearly in the one-hour spectrogram shown in Figure 8.2-4. The restarting of the pipeline flow is less definitive. The time that the pumps were noted to be restarted corresponds to a large spike in the time series of Figures 8.2-2 and 8.2-3 (the two horizontal components) at just after 21,000 s on the time series, but there are additional, or unrelated, noise sources that gradually increase the noise in this frequency band (also note the sudden onset of two lines in the spectrograms at 2 and 4 Hz) prior to the onset of flow. It therefore appears that there are other unrelated noise sources active during this period. After the reported time of restart, there is a gradual increase in the amplitude and bandwidth of the noise, suggesting a relationship to increasing flow rates.

Figures 8.2-5 to 8.2-13 show the spectra for the three components at the West End for a one-hour period each before, during, and after the shutdown. Noise on the vertical channel is not much different between the periods before and during shutdown, but is significantly greater after the shutdown. The spectral signature of the pipeline noise prior to the shutdown on the horizontal channels is an increased, modulated (or scalloped) spectrum between 2 and 8 Hz. In contrast, the noise spectra after restart are increased to higher levels on all three components over a broader frequency range that extends below 1 Hz. During this later period, the modulated spectrum, observed prior to the shutdown, is generally superseded by this relatively smooth noise increase. Either this pipeline generates varying levels and spectral characters of noise when operating conditions or states change, or another noise source is superimposed over the pipeline noise during the later period.

Low Frequency Spectrograms. The variability of low-frequency noise, potentially due to the Capline, or due to other noise sources that might be superimposed upon this source, was investigated by generating low-frequency spectrograms (0.5 to 5 Hz) for several entire days of measurements. These spectrograms and time series are for the vertical and infrasound channels only, and are included in Appendix E.

Figures 8.2-14 to 8.2-16 show examples of the spectrograms in Appendix E, regenerated as black-and-white spectrograms, for the vertical components at the three measurement sites for Day 303 (6 p.m. Sunday, October 29 to 6 p.m. Monday, October 30). Figure 8.2-17 shows the spectrogram for the Corner site's infrasound microphone signal for this same time period. The left half of the spectrograms, 0-43,200 seconds, corresponds to night-

time, 6 p.m. to 6 a.m., and the right half of the spectrograms, 43,200 to 86,400 seconds, corresponds to daytime, 6 a.m. to 6 p.m.

There is generally an increase in seismic (and acoustic) noise during working hours. Similar increases are observed at all three measurement sites during daylight hours, but each site has distinctly different characteristics during daylight hours. The Corner and South End sites have numerous high-amplitude short duration noise bursts, compared to the West End, where a steady noise is observed for the morning hours 6 a.m. to 1 p.m. CST (Figure 8.2-16). A similar noise was present for a shorter time period the previous Saturday. Monday, October 30, was the day chosen for complete analysis (the spectrograms, spectra, and histograms in Appendices B, C, and D), and appears to have as much or more low-frequency noise during daylight hours compared to the other days when measurements were taken (see Appendix E).

It was noted above that the Enterprise pipeline was shut down over the weekend from approximately 6:00 a.m. CST Saturday, October 28, until 7:00 a.m. CST Monday, October 30. No significant reduction of noise was observed at the time of shutdown at the West End measurement location. The noise increase observed Monday morning at 6 a.m. CST continued unchanged only until 1 p.m. that day but the pipeline continued to be operated at nominal flow volume throughout the remainder of the measurement period. Therefore, this 7-hour noise burst cannot be attributed to the Enterprise pipeline.

Although there is a definite relationship between the noise at the West End and the operation of the crude oil "Capline", there are other anthropogenic noise sources that contribute to the daily variation of noise at all three sites, and these can have amplitudes as large as those attributed to the pipeline. Many of these other sources can be associated with working hours, but the sources for these noise signals have not been identified. Changes in the viscosity of the crude oil in the Capline might account for changes in the noise levels at the West End measurement site. However, these changes do not occur on a regular daily schedule and occur more frequently (several times each day) than the observed "daily" noise fluctuation.

8.3 Noise Measurements near the Pipelines

After the measurements were made at the Corner, South End, and West End locations, the systems and cables were repaired from water damage and redeployed at various distances (see Figure 4-1 for measurement locations) from the two pipeline right-of-ways for periods ranging from one to 4 hours. In many cases problems were noted in the field that indicated un-characteristic noise signals were being recorded. On later analysis, it was determined that cabling was sometimes developing cross-channel connections from condensation and these data had to be discarded. Other data were also noted to be uncharacteristic of previous measurements and were also discarded. There were measurements made at several sites for several components that appeared to be correct and these are presented here.

The installations made at the pipelines were made by setting the concrete paving stone on the grassy surface, and packing soil beneath it until a stable platform was obtained for the

seismometer. The seismometers were oriented so "North" was directed N20°W parallel with the South Arm of the LIGO facility. The seismometer and pad were then covered with a 55-gallon barrel cut to 2/3 height, and lined with 3" thick foam rubber for thermal and acoustic isolation. The recorders and batteries were simply set on the soil adjacent to the barrel. A set of color photographs is available that illustrate these measurements and that document the measurement locations. When some electrical connections were determined to be failing, some shorter cables had to be used that had not been damaged, resulting in placing the disk drive in close (3 feet) proximity to the seismometer. This generated some periodic noise when the disk drive operated.

Measurements made November 8 directly over the Transcontinental and Shell pipelines were limited to the vertical channel due to failure of connecting cables. Spectra for the two sites for the same half-hour period are shown in Figures 8.3-1 and 8.3-2. The spectra virtually overly one another at frequencies below 3 Hz, but the measurements made over the Shell pipelines exceed those measured over the Transcontinental pipelines from 3 to 10 Hz. The spectra for the Shell pipeline look similar and have comparable amplitudes to those measured at the West End (0.8 miles from the Shell pipelines) during the measurement period. Considering that the distance from the Shell pipelines to the Transcontinental pipelines is approximately 0.25 miles, this can be interpreted as a measure of the attenuation with distance of the vertical-component noise from the Shell pipeline.

The noise measured near 3 Hz at the Transcontinental pipeline (western right-of-way) is reduced by a factor of 2 (6 dB) compared to that measured at the Shell pipeline (eastern right-of-way). At 7 Hz is the reduction is approximately a factor of 3 (10 dB). These measurements, made simultaneously, are indicative that the noise from the Shell pipeline is greater than that from the Transcontinental pipelines during the measurement period, and that the noise from the Shell pipelines is attenuated by at least the above factors in the 0.25 miles (0.4 km) distance from the Shell pipeline to the Transcontinental pipeline. Because the Transcontinental measurement site was at a point further south than the Shell measurement site, this interpretation also assumes that the pipeline noise is generated uniformly along the north-south pipelines.

Above 20 Hz, there appear to be resonance or coupling effects on the vertical-component spectra measured on the Transcontinental pipeline (Figure 8.3-2). This type of spectral feature is usually not this large on the vertical channels, and may be due to the installation of the seismometer pads on the natural grass-covered surface at the pipelines. These spectral features may be related to the gas pipelines, but are probably indicative of a resonance of the seismometer pad on the underlying grassy surface.

Three-component measurements were successfully made later at two additional locations 0.1 and 0.3 miles east of the Shell pipeline. The spectra for these two different time periods are shown in Figures 8.3-3 to 8.3-8.

This later set of measurements also indicate that the high-frequency (above 10 Hz) spectral differences between sites are artifacts of the installations. There is some evidence for attenuation of the noise with distance in these later measurements, but the evidence for temporal variability of multiple sources of noise in the previous section makes this inter-

pretation ambiguous. For some pairs of components and locations, a 40-50% reduction of noise may be observed over the distance difference of 0.2 miles (0.3 km) within a limited and variable frequency band in the range 2-10 Hz. The differences in the shape characteristics of these spectra suggest that characteristics of the noise source (or sources) did change with time and that concluding distance attenuation of the pipeline noise with distance has been measured from these later data is not justified. Simultaneous measurements are essential to the measurement of the attenuation of pipeline noise, and different instruments and buried installations are needed to accurately measure the high-frequency (above 10-20 Hz) noise amplitudes.

9.0 Other Noise Sources

9.1 Train Traffic

An Illinois Central Railroad passes approximately 1-1/2 miles south of the South End station of the LIGO site. Long-duration (10 minute) noise increases were observed on the time-series traces each day, generally during Hour 02 and Hour 05, corresponding to 7-8 p.m. and 10-11 p.m. CST. The spectrogram for the Hour 05 train was shown in a previous section for the South End site (see Figure 5-6). Spectrograms for the Corner vertical component and infrasound channel are shown in Figures 9.1-1 and 9.1-2. These spectrograms are dominated by a high-frequency signal, but a low-frequency signal can also be observed (see Figure 5-6 where the seismic signal is stronger at the South End, and the color spectrograms in Appendix B). The high-frequency component consists of a multiple-banded signal that sometimes shifts in frequency in a complex way (considered to be related to the speed of the engine), but which has an overall frequency sweep consistent with a doppler shift. The low-frequency component does not appear to have similar structure. The high frequency component is observed most clearly on the infrasound microphone spectrogram (located at the Corner) and the pressure and seismic displacement are highly correlated, indicating that the high-frequency noise is transmitted to the site acoustically.

The seismic signal is strongest at the South End but is observed at all three measurement sites, and can be observed on the low-frequency spectrograms in Appendix E at approximately 10,000 and 20,000 seconds into the time series and spectrograms, and in the black-and-white spectrograms shown previously (see Figures 8.2-14 to 8.2-16).

Illinois Central Railroad's Baton Rouge office confirmed that trains pass Livingston at about these times each day, but in addition, trains also pass at 2-3 a.m. and 8-9 a.m. local time. A search for similar effects during these periods indicates that these two morning trains did not generate signals as large as the evening trains (02 and 05 GMT), although other noise sources sometimes obscured the 8-9 a.m. train signal.

Figures 9.1-3 to 9.1-5 show the spectra of the Hour 05 train signal at the three sites for the vertical component (spectra for all components are included in Appendix C). The r.m.s. spectrum is increased by a factor of three in the frequency range from 1 to 5 Hz. Figure 9.1-6 shows the train's effect on a set of histograms for the vertical channel at the South End (histograms for all components are included in Appendix D). At probability levels

below 10%, the two bands 1-2 and 2-4 Hz exceed the amplitude of the 0.5-1 Hz band (normally the largest). The 4-8 Hz band is also affected by the train signal.

9.2 Acoustic Phenomena

There is an overall similarity between the spectrograms of the acoustic microphone and the vertical seismic signal at the Corner measurement site. In many cases, some of the larger episodes of higher noise on the seismic channel can be attributed to anthropogenic acoustic noise that is transmitted into the ground at the measurement site, particularly at high frequencies. Such noise phenomena affect different components of the LIGO facility in ways that are different from noise transmitted through the earth. In fact, it appears that much of the high-frequency noise can be attributed to atmospheric sound sources. Appendix F contains a set of infrasound spectra for the 24 hours of October 30.

Low Frequency Acoustic Noise. The acoustic spectra measured at Livingston have a significantly different character than observed at Hanford. Some of this difference may be due to improved shielding from wind-induced noise and significantly lower winds during the measurement period. At low frequency, the Livingston infrasound noise is sometimes peaked at 0.6-0.8 Hz during quiet periods (Figure 9.2-1). At Hanford, the spectrum of infrasound was peaked at frequency below 0.2 Hz and was interpreted as the equivalent "micro-barom" signal with the same source as the 0.15 Hz "microseismic" noise. This infrasound noise is sometimes correlated with the low-frequency seismic signals in its temporal variation in this frequency range (0.6-0.8 Hz).

Line spectra. These features appear as spikes in the spectra and as horizontal lines in the spectrograms. The spectrograms shown previously for the vertical and infrasound channels (see Figures 5-1 and 5-2) tend to emphasize a set of high frequency lines above 30 Hz. These are not as notable as previously observed at Hanford. The most conspicuous line in the spectra occurs at 10 Hz for the infrasound microphone and for the vertical seismic channels (Figures 9.2-1 and 9.2-2). Additional lines at approximately 2.1 and 6.5 Hz are evident at lower frequencies in the acoustic spectra, and these are common to nearly all the acoustic spectra in Appendix F. In contrast, the seismic spectra do not appear to admit the 2 Hz acoustic noise, but another spike appears at 5 Hz on some of the horizontal channels (see Figure 9.2-3 for example). The 5 Hz line was not present in the acoustic spectrum, and the 10 Hz spectrum is diminished, suggesting the 5 Hz noise is ground transmitted and the 10 Hz is acoustically transmitted into the ground. At higher frequencies, the spectral lines are more variable, but commonly include spikes at 20 and 30 Hz as shown in Figure 9.2-1 and 9.2-2. Line spectra at the other two stations are consistent with the above comments relating to the 5, 6.5, and 10 Hz spectral lines, and also commonly exhibit the 20 and 30 Hz or other additional line spectra. These higher-frequency line spectra are possibly electromagnetic pickup by the electronics, but experience at other sites (especially at the Hanford LIGO site) indicates that acoustic noise with very narrow bands can explain these features.

Aircraft "Glide Tones". These are common features in the infrasound spectrograms and occur as sigmoidal or "s-shaped" patterns in the spectrograms. Figure 9.2-4 shows a one-hour black-and-white spectrogram with several high-amplitude examples of these fea-

tures. The aircraft glide tones can be a dominant source of acoustic noise, as shown by the relatively high-amplitude signal at 1000 s in Figure 9.2-5. These signals are transmitted into the ground and are recorded on the seismic channel. The corresponding seismic spectrograms are shown in Figures 9.2-6 and 9.2-7, and the corresponding seismic spectra are shown in Figures 9.2-8 and 9.2-9.

During the quietest periods at the LIGO site, the same frequency range occupied by the aircraft glide tones is discerned to have very faint tones that decrease linearly with time instead of with the characteristic s-shaped pattern described above. The source of these signals is not known, but could be due to very distant or very high aircraft. Although these are also observed on the seismic channel, they do not form a distinct temporal increase in the time series, but may represent a minimum background of acoustic noise that will always be present.

Also distinct from the glide tones are "amorphous acoustic bursts" that can be seen frequently in the spectrograms of the acoustic and seismic signals in Appendix B (see Figures 9.2-4 through 9.2-7 for additional examples). These are not related to bursts in wind speed, and wind speeds for the day chosen for analysis have maximum peak wind speeds of approximate 4 m/s (see nest section); such winds do not usually create significant noise at high frequencies. These are not associated with a corresponding low-frequency noise that is observed when the source is a passing vehicles as shown previously in Figures 5-3 and 5-4. The source of the amorphous acoustic bursts has not yet been identified with a particular anthropogenic or natural source, but they do have an effect on the spectra comparable to the aircraft glide tones.

9.3 Wind Speed

Wind speed measurements for the entire measurement period are shown in Figure 9.3-1, and for October 30 for a 24-hour period that was chosen for analysis. Peak wind speeds during the day chosen for analysis never exceeded 5 m/s. Two one-hour segments of data from the end of Day 305 were chosen to observe any potential wind speed effects. The wind speeds measured during these two hours at the Corner are shown in Figures 9.3-3 and 9.3-4. The spectrograms of the three components of the seismic signals at the Corner are shown in Figures 9.3-5 through 9.3-10. The spectrograms for the moderate wind period show a change in the low-frequency portion (below 20 Hz) during the period of maximum winds shown in Figure 9.3-3.

Amplitude spectra for the 10-minute period of highest winds are compared to those of a 10-minute period of minimal winds several hours later in Figures 9.3-11 to 9.3-16. The wind effect is observed in the frequency range from below 1 Hz to approximately 20 Hz on all three components of the seismic signal. The noise increases by about a factor of 3 over most of this frequency range, and produces a relatively smooth, featureless spectrum in this band that tends to obliterate other spikes or scallops that were present when wind speeds were minimal.

10.0 Conclusion

In summary, it was found that the ambient ground vibration at the LIGO site is consistently higher than the LIGO reference design spectrum at frequencies below 5 Hz. This is consistent with previous measurements made at the site in 1988 by the Louisiana State University. Above 10 Hz, the design spectrum nearly always envelops the observed ground vibration spectrum, except when acoustic noise from aircraft is transmitted into the ground.

Below 0.5 Hz, natural "microseism" noise is consistently peaked above 10^{-6} m/sqrt(Hz) near 0.2 Hz. The crude oil pipeline passing beneath the West Arm appears to generate a significant portion of the ambient noise at the West End in the frequency range 0.5 to 10 Hz, and there are significant daily variations in its amplitude. Simultaneous measurements made at varying distances from the pipelines indicate an attenuation of at least 6 dB at a distance of 0.4 km from the crude oil pipeline axis. Trains passing twice daily increased the ambient noise at all three measurement locations. At the South End, the trains generated vibrations exceeding 10^{-6} m/sqrt(Hz) by over a factor of 10 in the frequency range 1 to 5 Hz.

Acknowledgment. Shannon Goodwin provided substantial support in the collection of the field data and gathering the information on the pipeline operations. Warren Johnson, Bill Hamilton, and especially Monica Lee, of the Physics Department at Louisiana State University, graciously provided me the use of their offices, lab space, and computers during the collection of these data.This work was directly supported by the LIGO Project, Caltech, and I would like to especially acknowledge the encouragement from Lisa Sievers, Rick Savage, and Fred Asiri.

I also acknowledge the assistance of the pipeline operators who provided information regarding the pipeline operations. Information about the Transcontinental pipeline was provided by Lou Thibodeaux and David Bonvillain of Williams Field Services in Gibson, LA. Information on the Shell Pipeline was provided by Gerald Yandell, Assistant Supervisor of Oil Movements at the Shell Pipeline Corporation Office in Houston, TX. Information about the Enterprise pipeline was provided by Bob Raburn in Gonzales, LA.

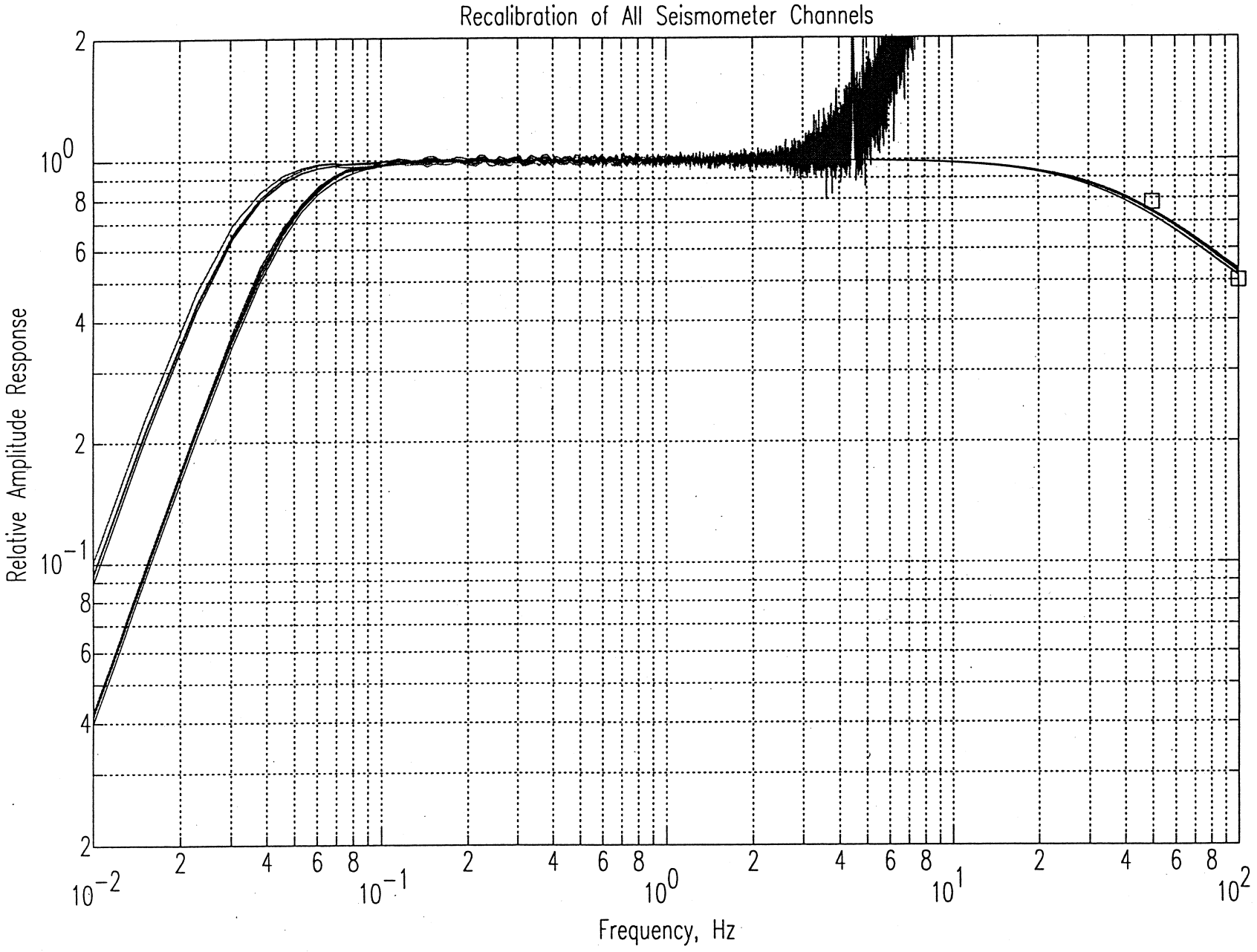

Figure 3-1. Results of final calibration check on all seismometer channels after completion of Livingston measurements. The 30-s period and 20-s period low-frequency responses of the seismometers are shown. The manufacturers calibration curves at high frequency are shown relative to those measured (squares at 50 and 100 Hz).

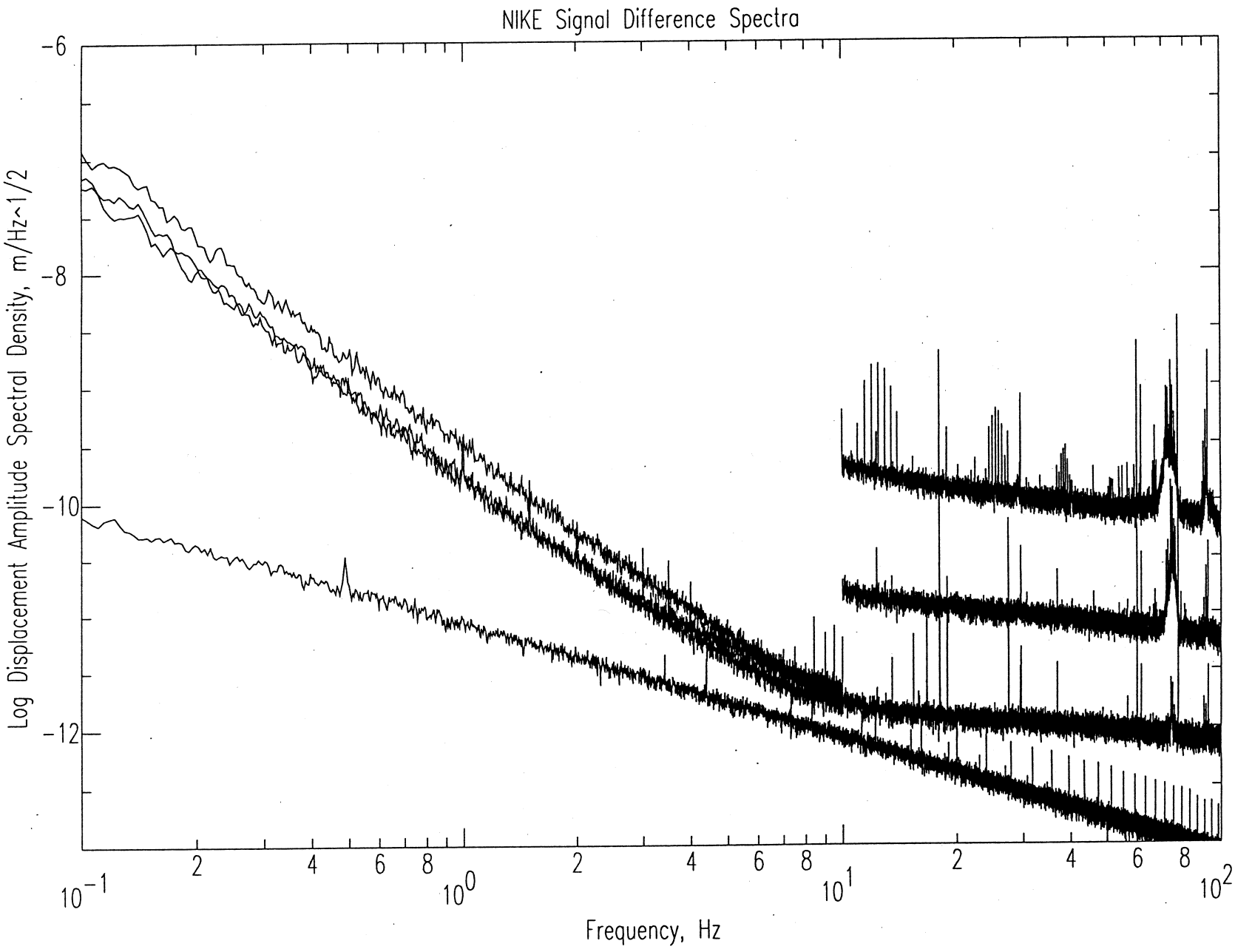

Figure 3-2. Original noise spectra estimated from signal-difference spectra measured at a quiet site. The two horizontal noise spectra are shown offset above 10 Hz to illustrate the coupling resonance at 70-80 Hz. The lower curve is an estimate of the amplifier noise of the recording system.

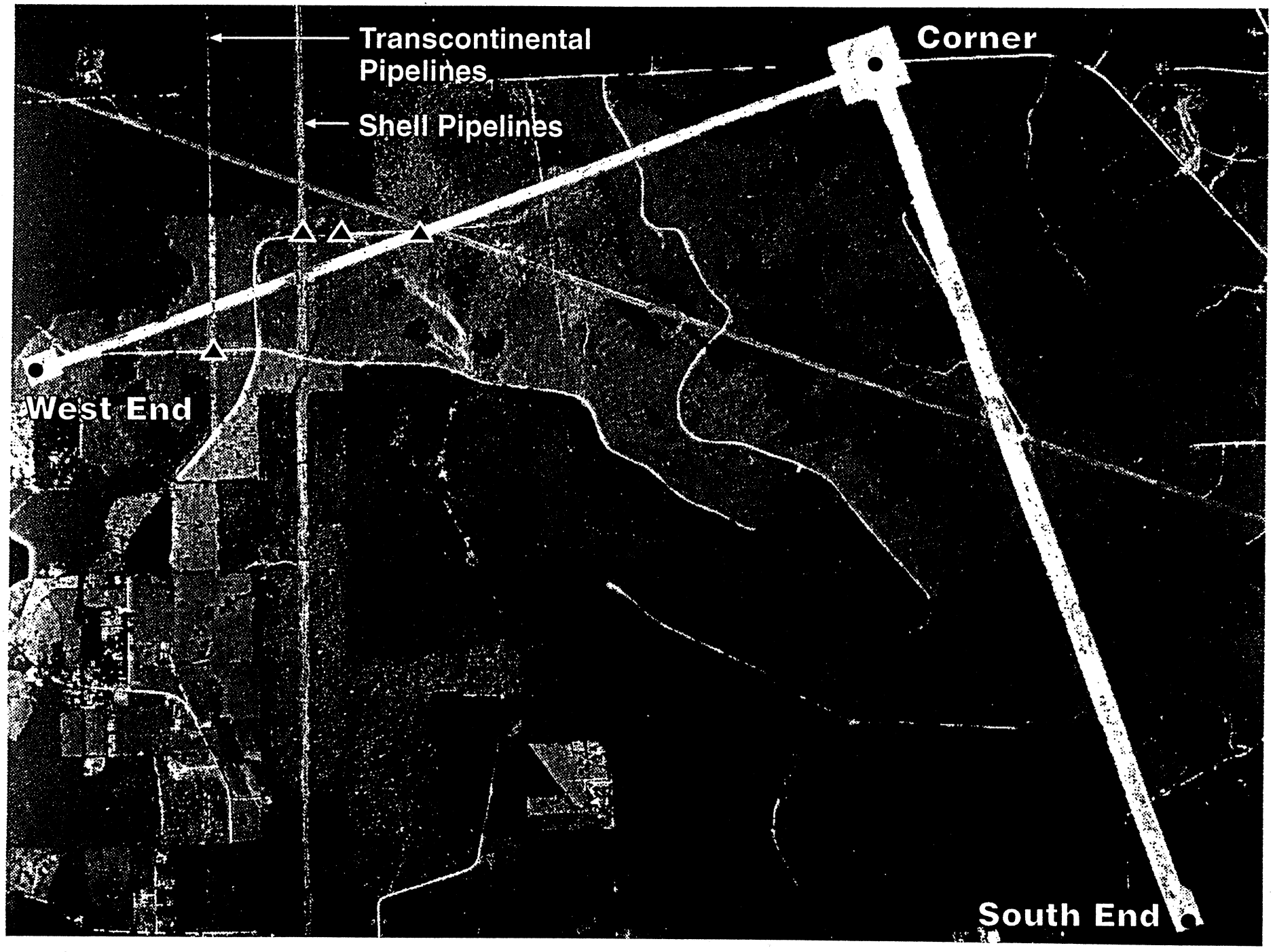

Figure 4-1. Areal view of the Livingston, Louisiana, LIGO site. The measurement locations for the ambient vibration measurements are shown at the Corner and Ends (dots). Triangle represent measurement locations for the pipeline measurements. The position of the pipeline right-of-ways is also shown.

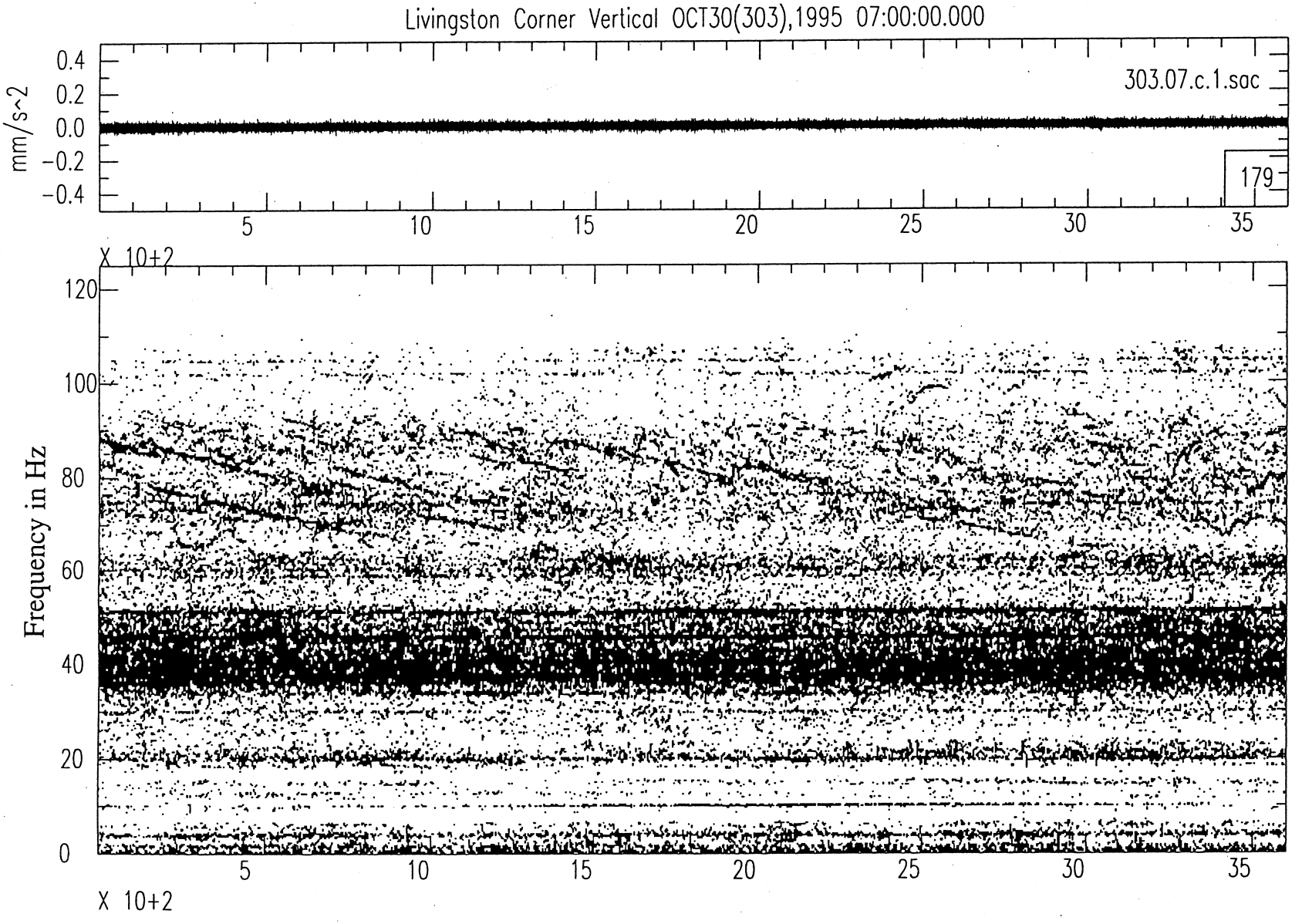

Figure 5-1. Black-and-white vertical-component spectrogram for one of the quietest periods (1 to 2 a.m.) observed at Livingston. Long-duration sweep-tones are observed in the background between 60 and 90 Hz.

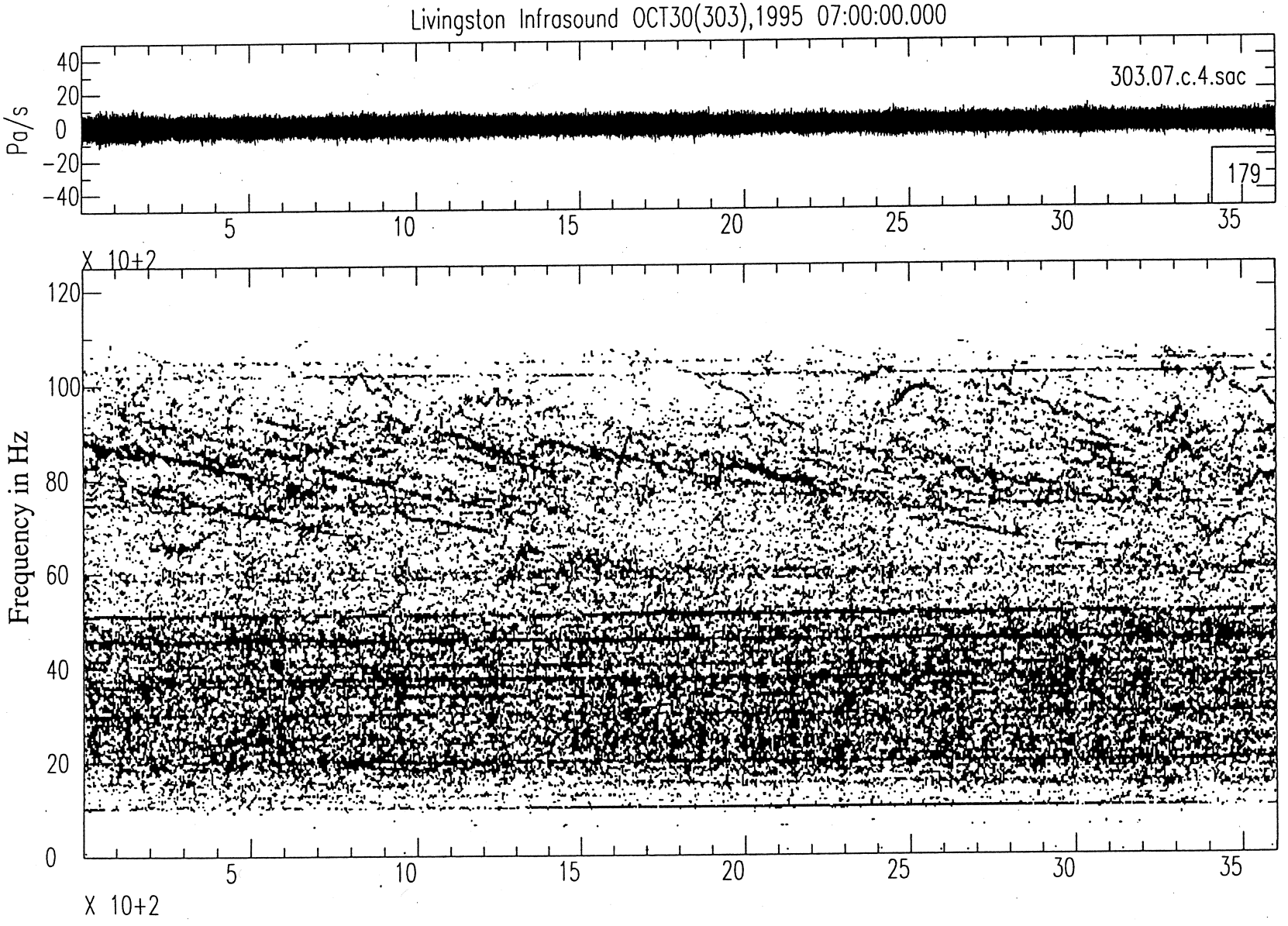

Figure 5-2. Black-and-white infrasound spectrogram for the period shown in Figure 5-1. Many of the same features can be observed, including line-spectra, that are transmitted into the ground and appear on the seismic spectrogram.

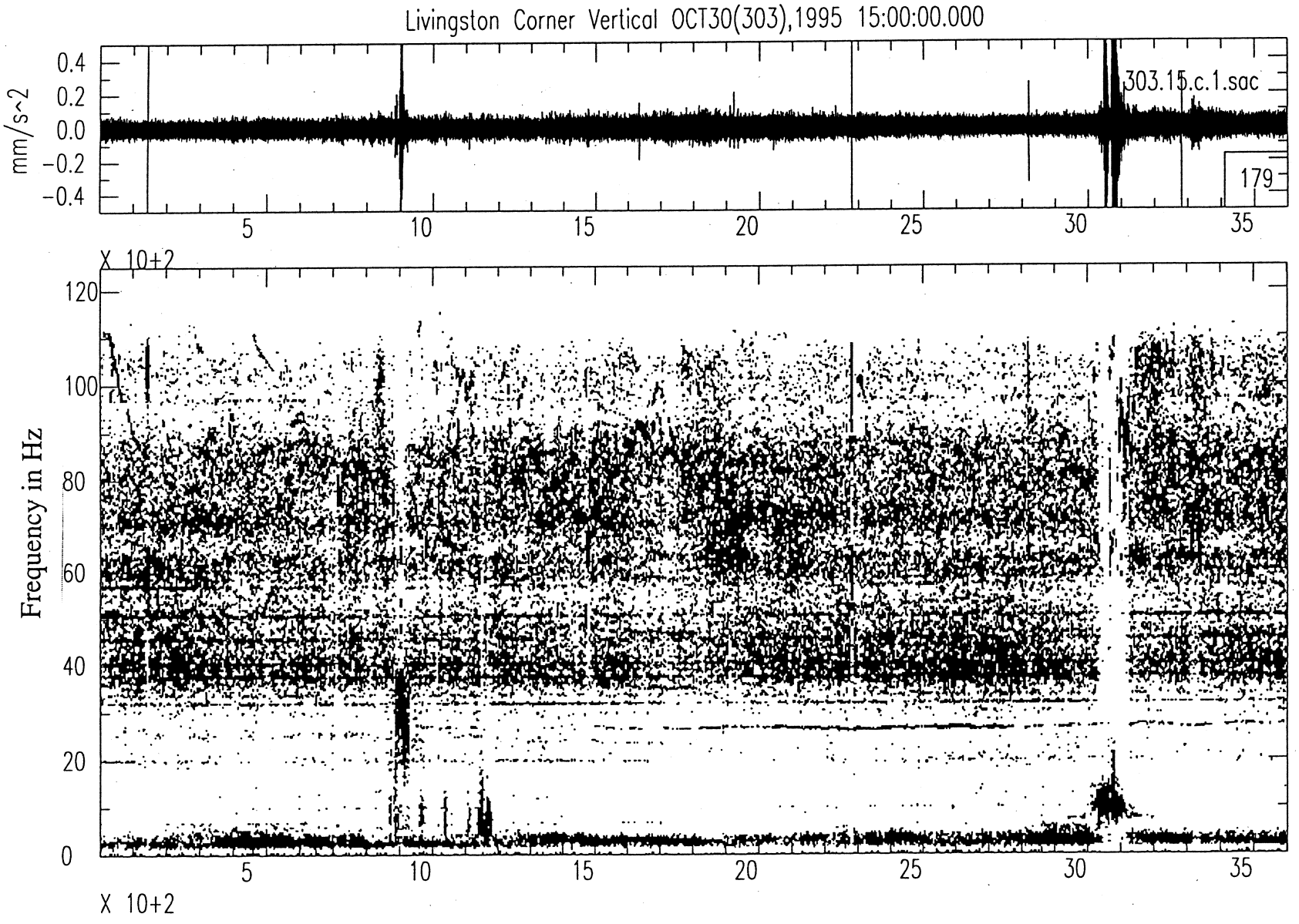

Figure 5-3. Black-and-white spectrogram showing the seismic effect of a passenger vehicle passing near the Corner. The seismic signal is seen at low frequencies near 10 Hz at time 3100 seconds.

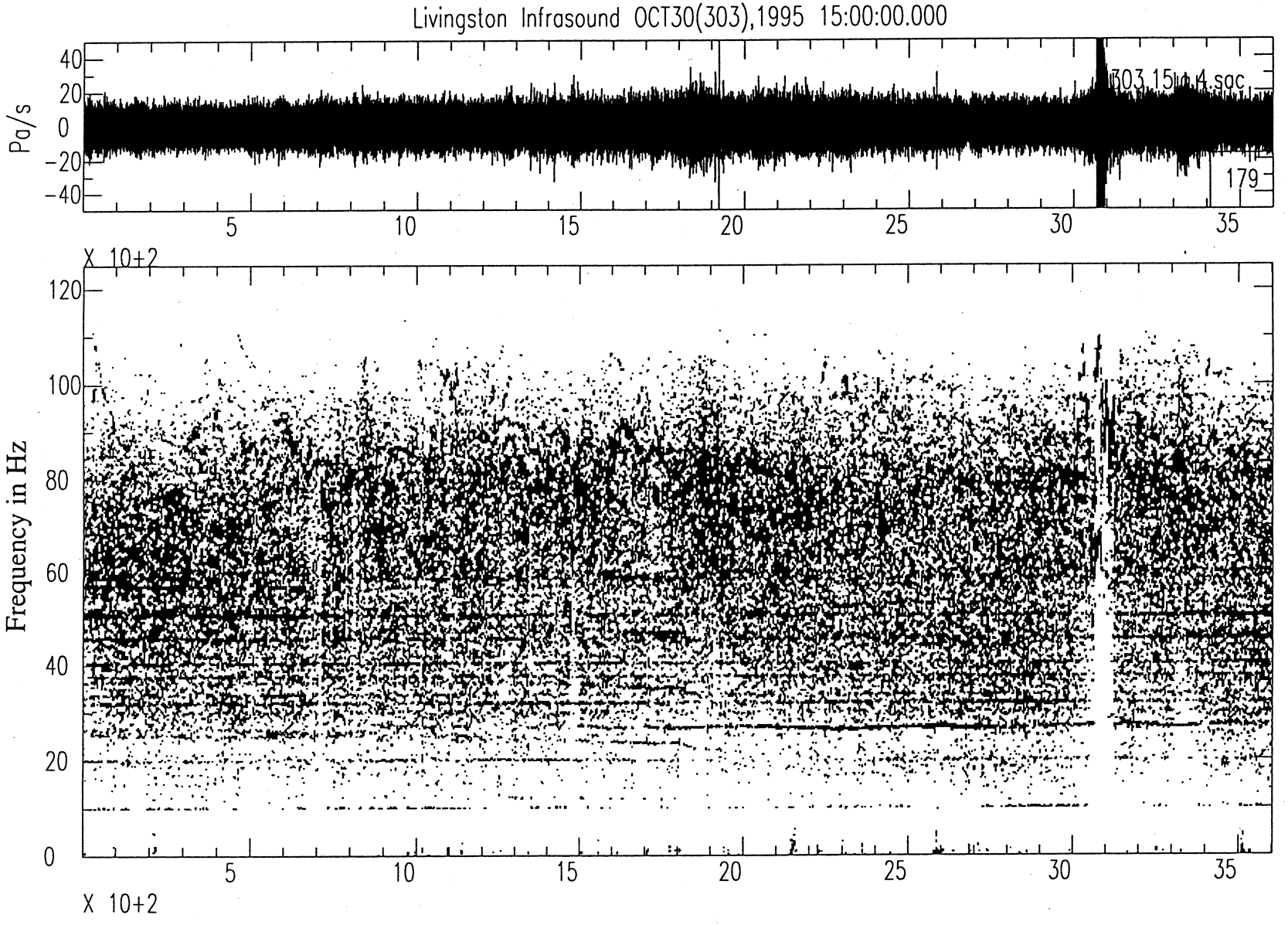

Figure 5-4. Black-and-white spectrogram showing the infrasound effect of a passenger vehicle passing near the Corner. The acoustic signal is dominated by high frequencies instead of the low frequencies in the seismic spectrogram in Figure 5-3.

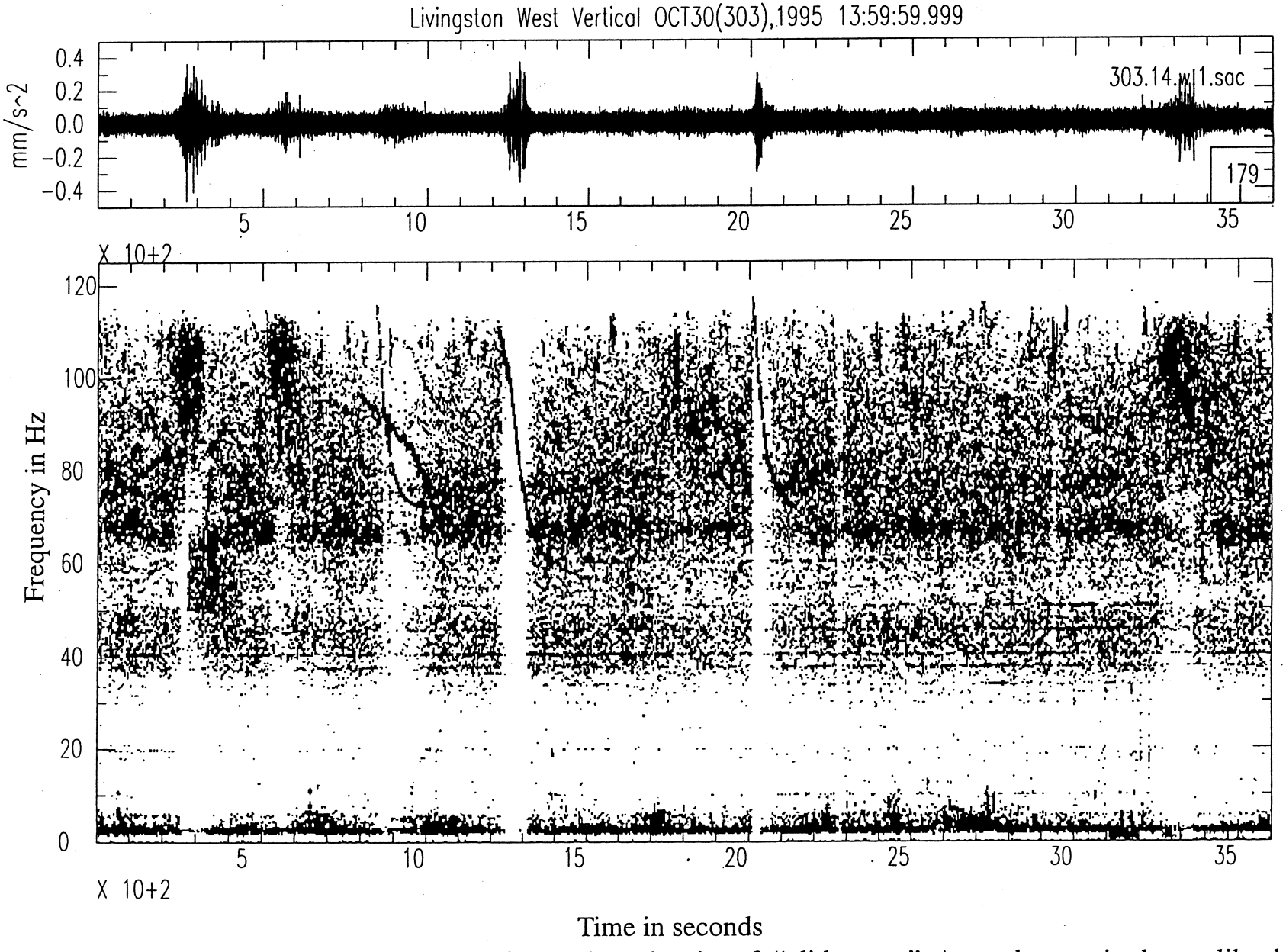

Figure 5-5. Black-and-white spectrogram of several nearby aircraft "glide tones". Amorphous noise bursts like those at 300 and 3400 seconds are frequently observed.

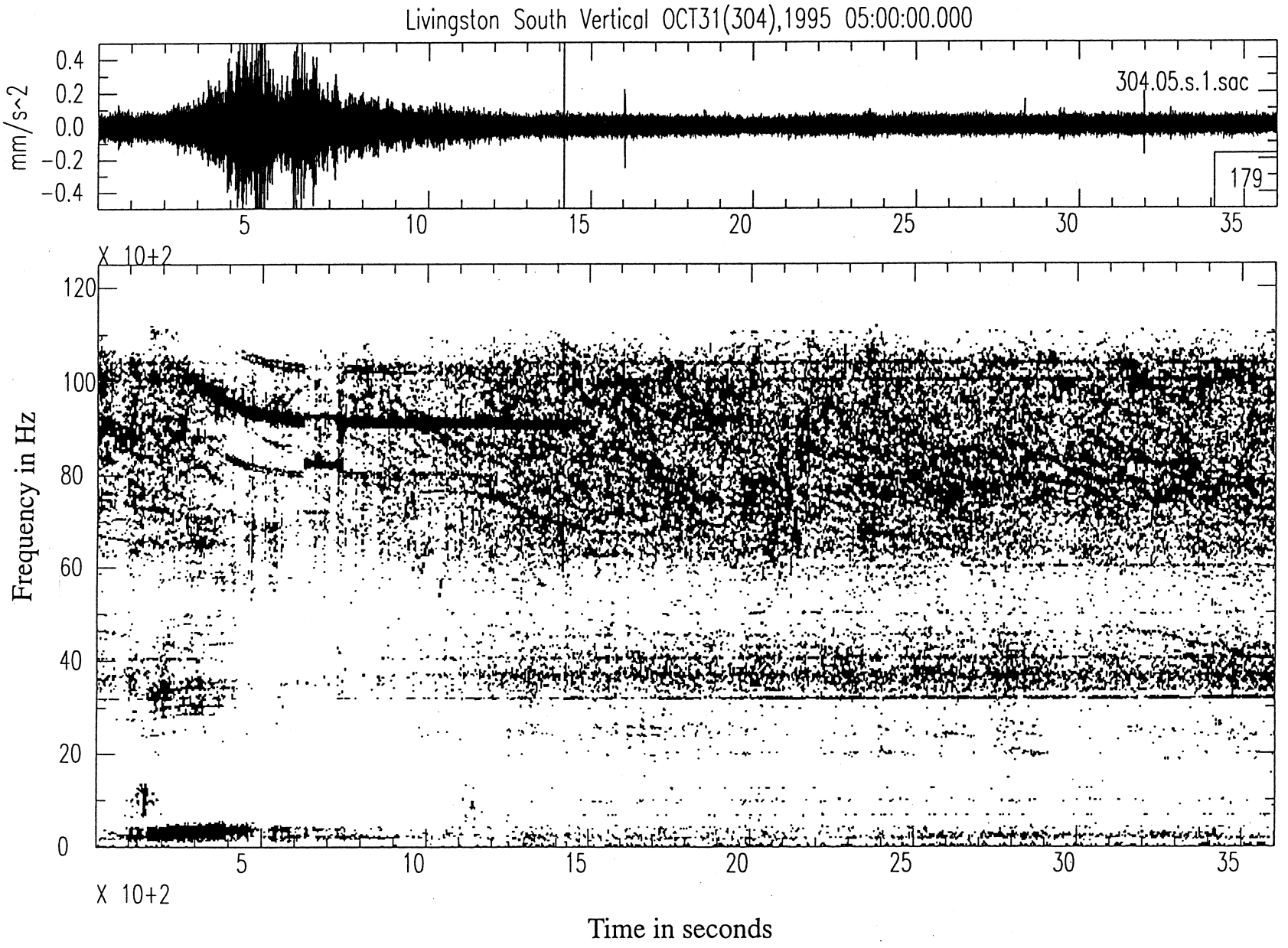

Figure 5-6. Black-and-white spectrogram of a train passing the South End of the Livingston LIGO site. A set of high-frequency acoustic signals and a low-frequency (less than 5 Hz) signal are observed.

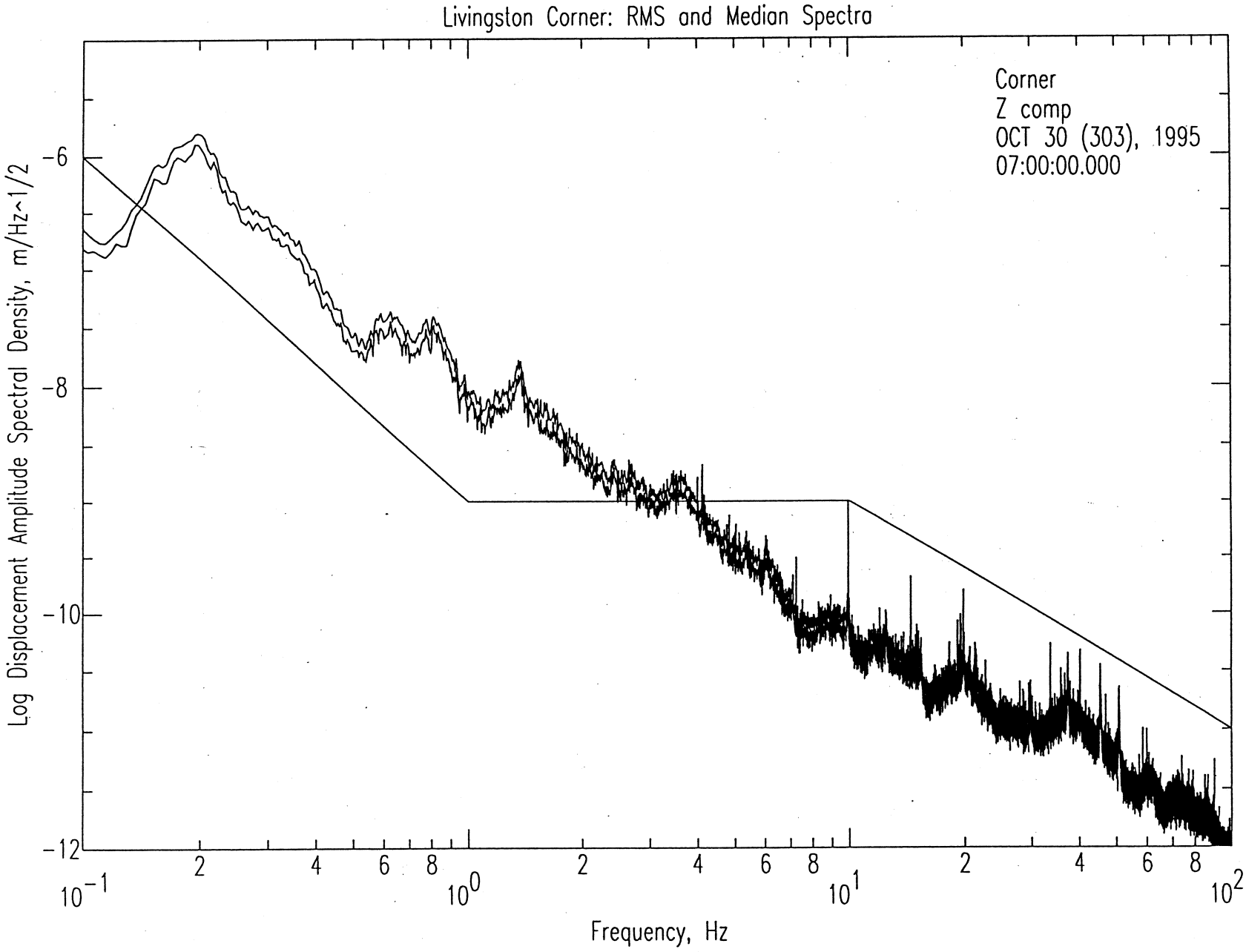

Figure 6-1. Amplitude spectra (median and r.m.s.) for a quiet one-hour period at the Corner. This period corresponds to the spectrogram shown in Figure 5-1. Vertical component is shown.

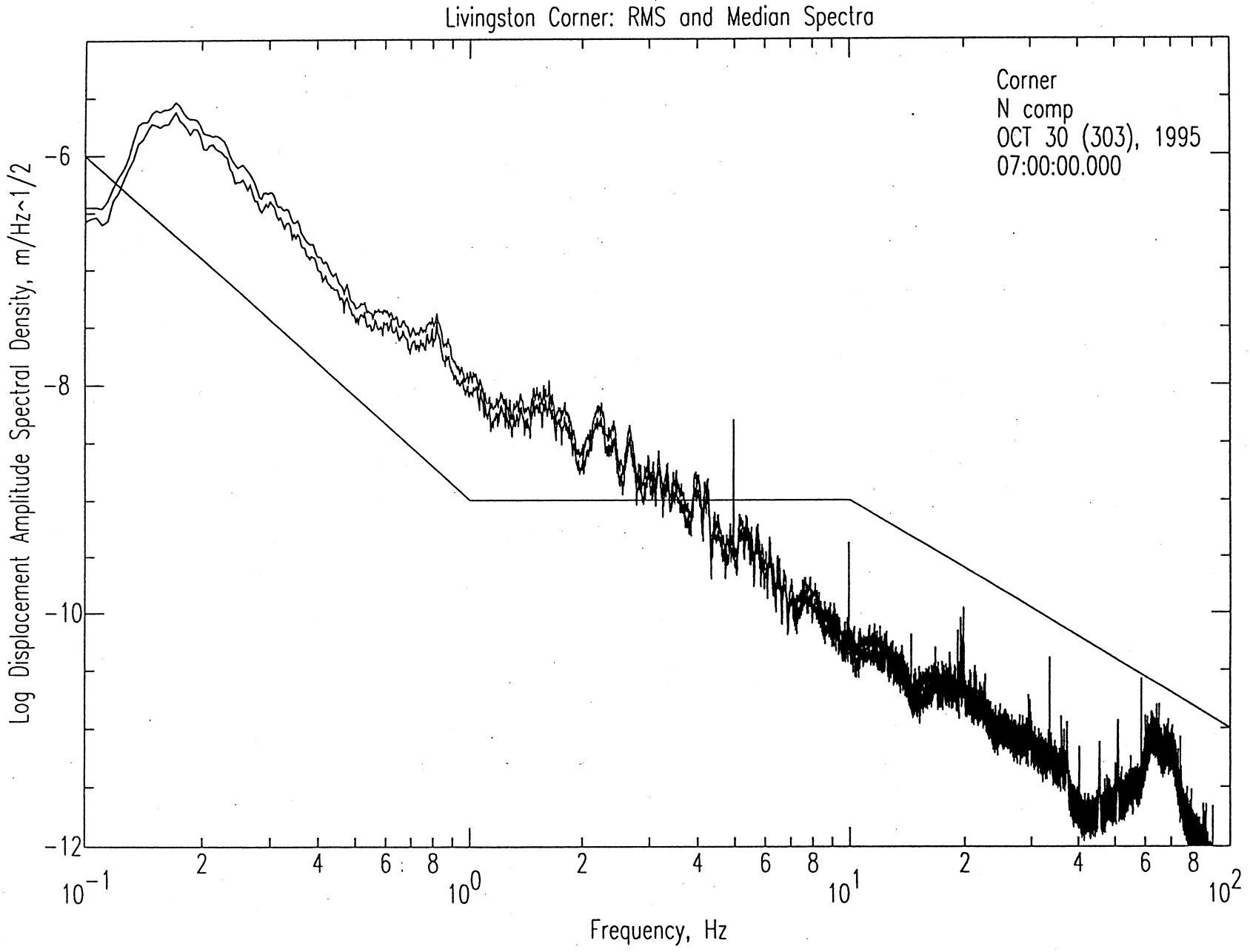

Figure 6-2. Amplitude spectra (median and r.m.s.) for a quiet one-hour period at the Corner. This period corresponds to the spectrogram shown in Figure 5-1. North component is shown.

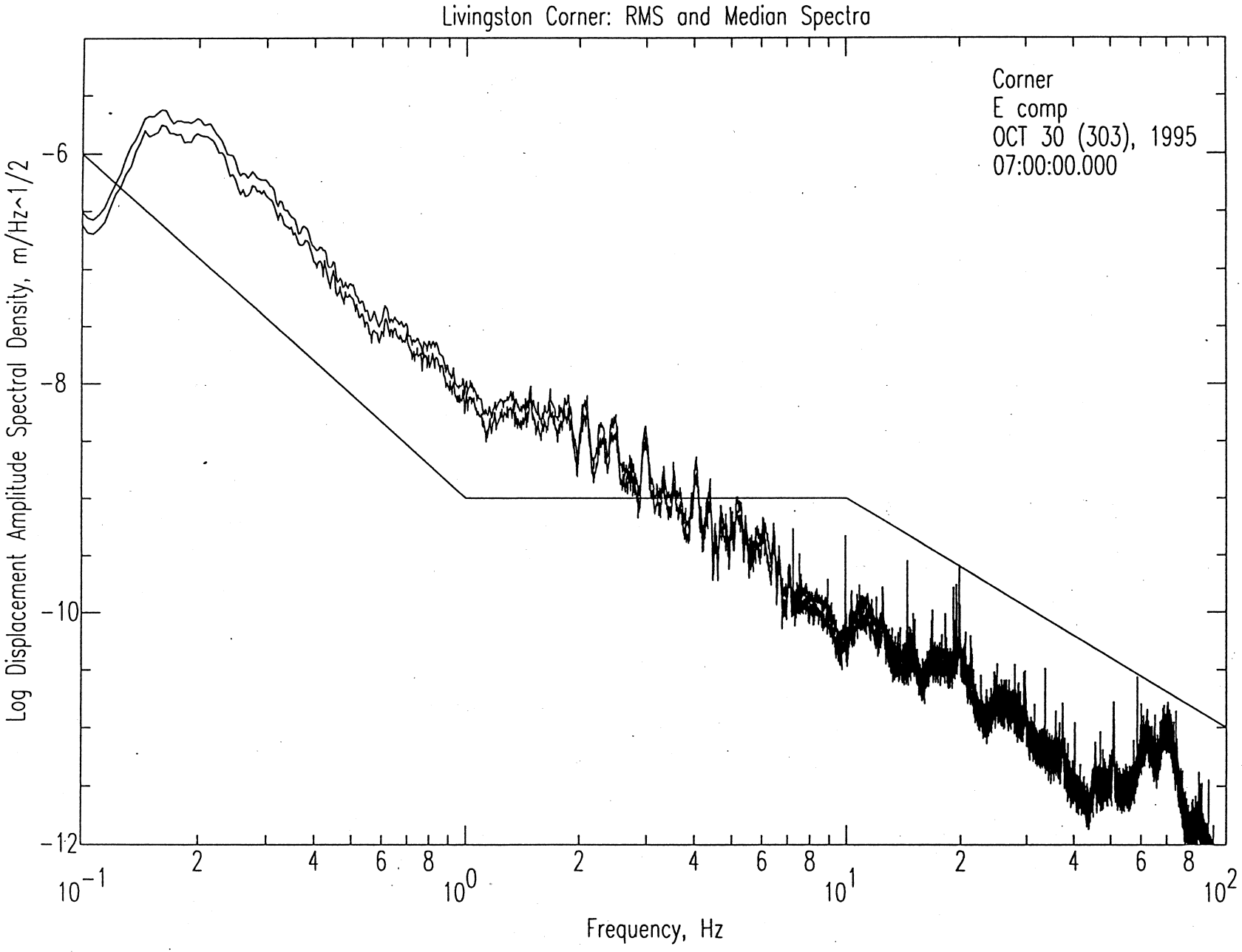

Figure 6-3. Amplitude spectra (median and r.m.s.) for a quiet one-hour period at the Corner. This period corresponds to the spectrogram shown in Figure 5-1. East component is shown.

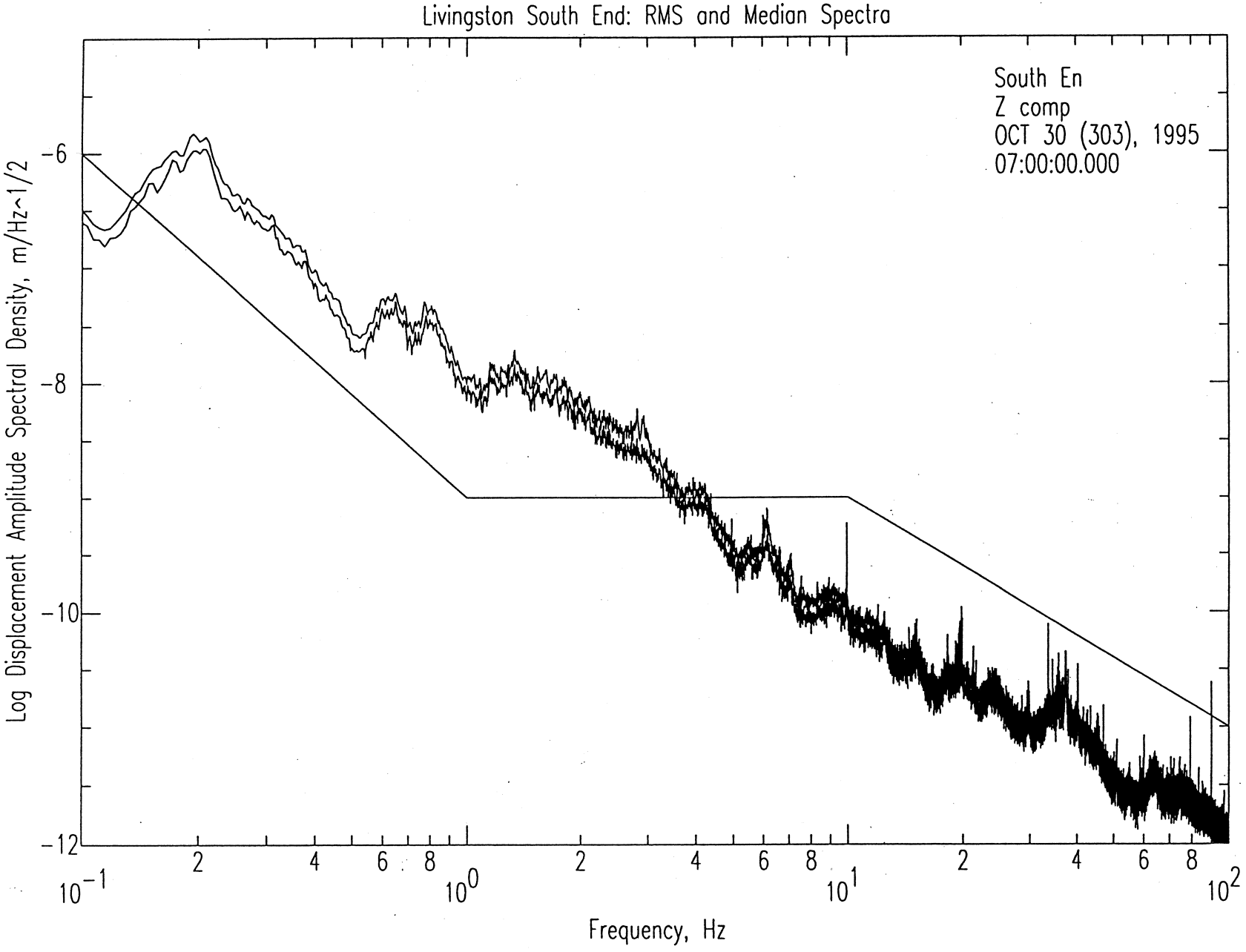

Figure 6-4. Amplitude spectra (median and r.m.s.) for a quiet one-hour period at the South End. This period corresponds to the same time period as the spectra shown in Figure 6-1. Vertical component is shown.

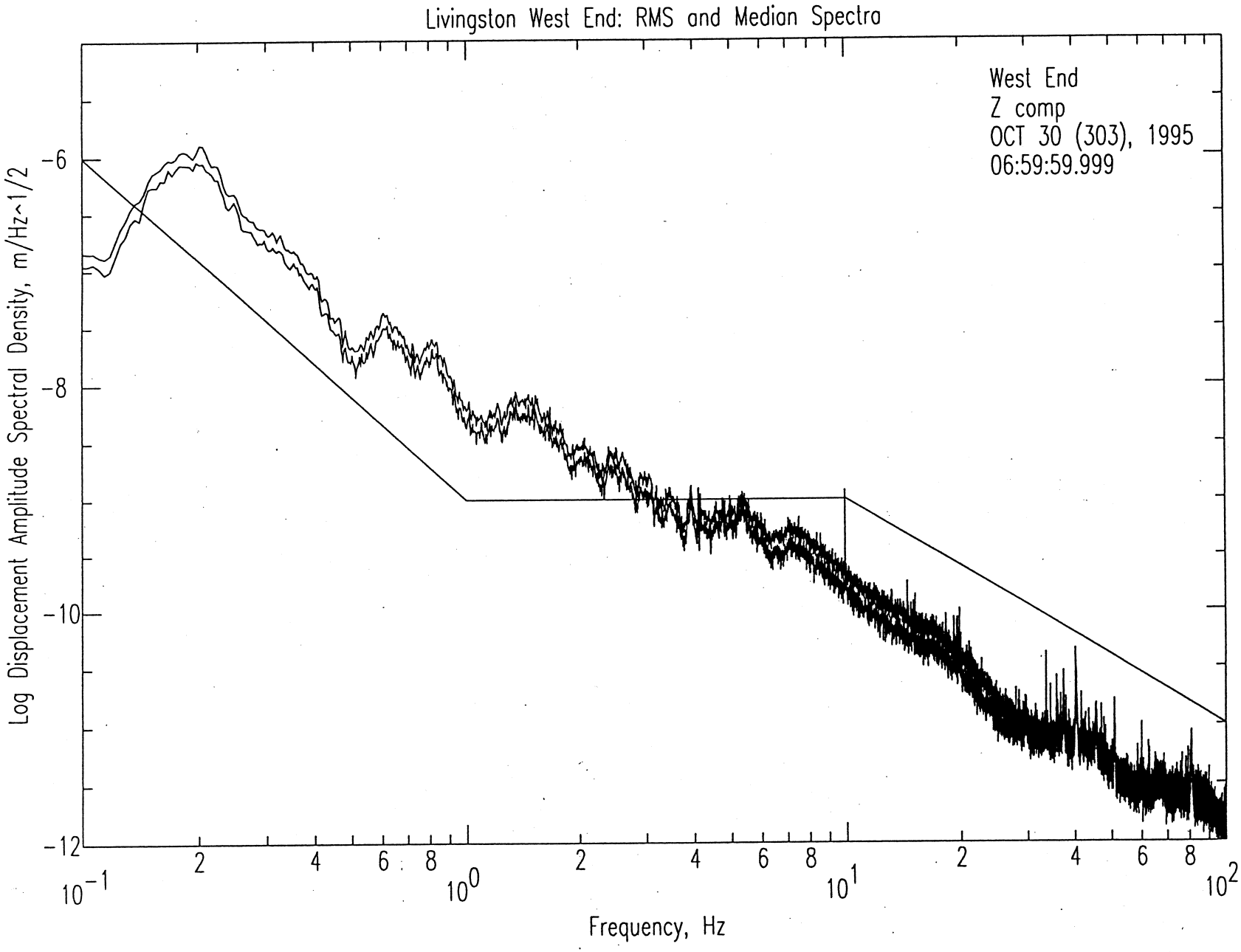

Figure 6-5. Amplitude spectra (median and r.m.s.) for a quiet one-hour period at the West End. This period corresponds to the same time period as the spectra shown in Figure 6-1. Vertical component is shown.

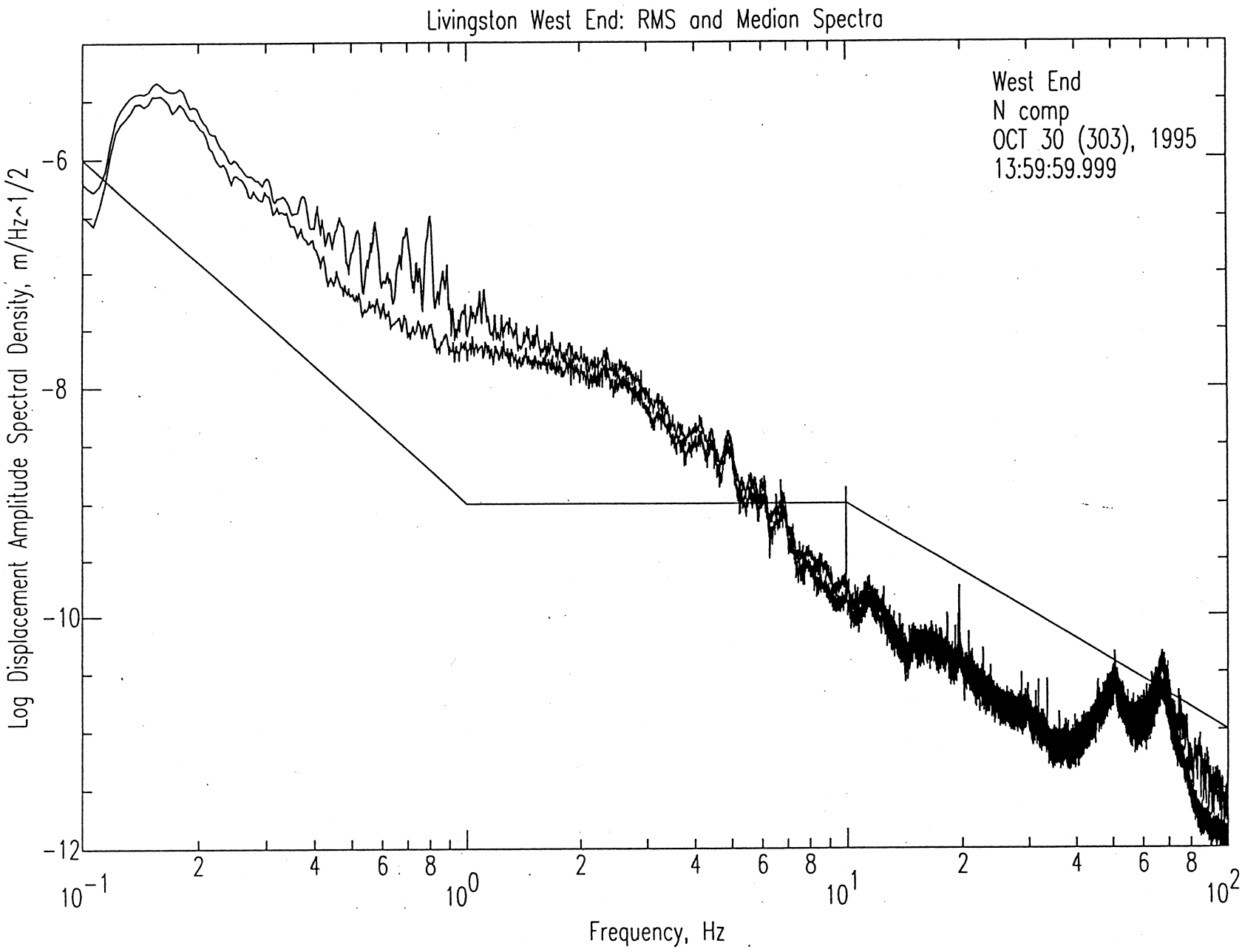

Figure 6-6. Amplitude spectra (median and r.m.s.) for a one-hour period when an earthquake signal was present. The short-duration earthquake signal elevates the r.m.s. spectrum near from 0.3 to over 1 Hz without affecting the median spectrum. The effect of the aircraft "glide tones" raises both spectra at high frequency (40-70 Hz). These spectra correspond to the signals shown in the spectrogram in Figure 5-5.

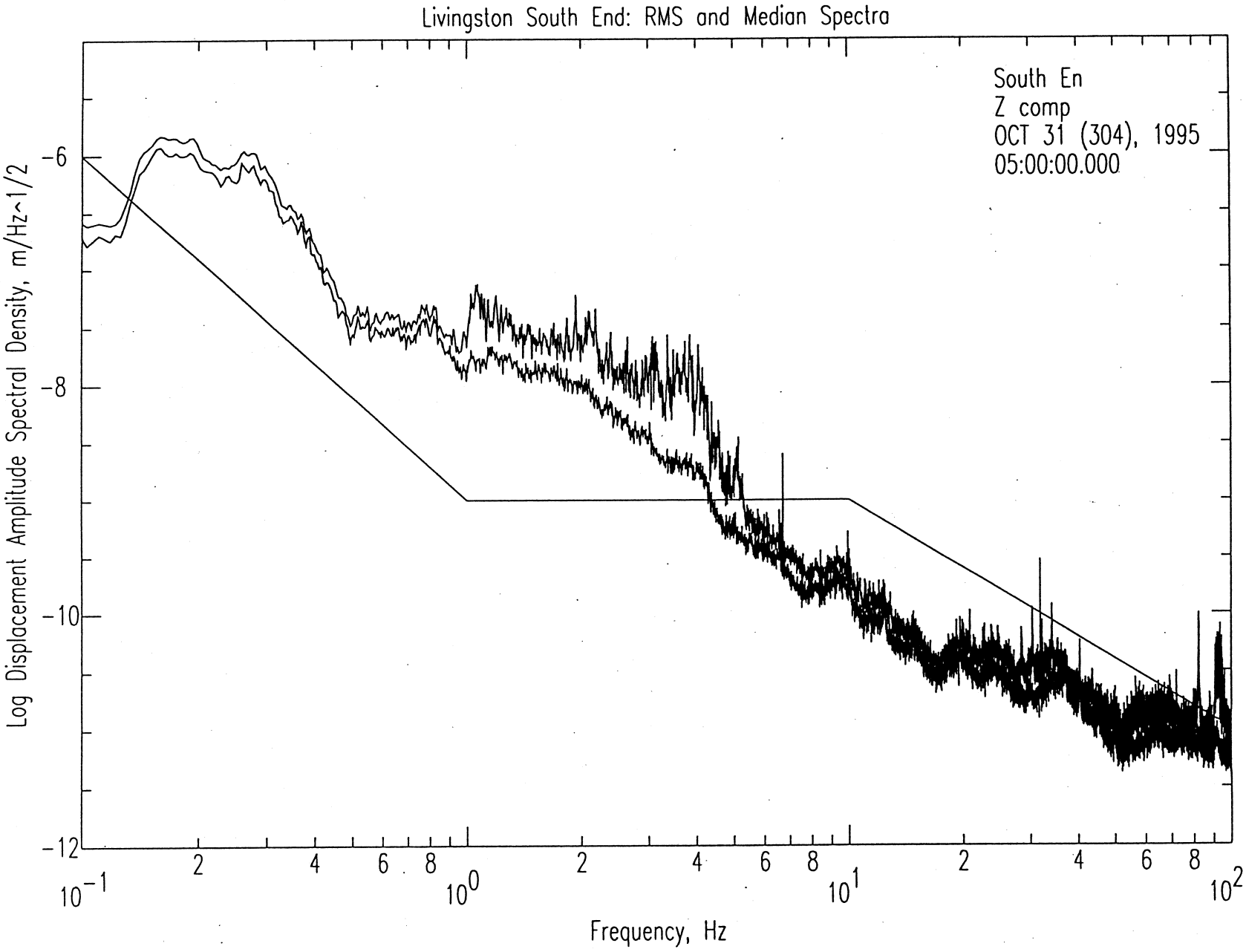

Fgure 6-7. Amplitude spectra (median and r.m.s.) for a one-hour period when a train passed the South End. The seismic signal affects the r.m.s. spectrum from 1 to 5 Hz. Acoustic signal at 95 Hz is transmitted into the ground. These spectra correspond to the signals shown in the spectrogram in Figure 5-6.

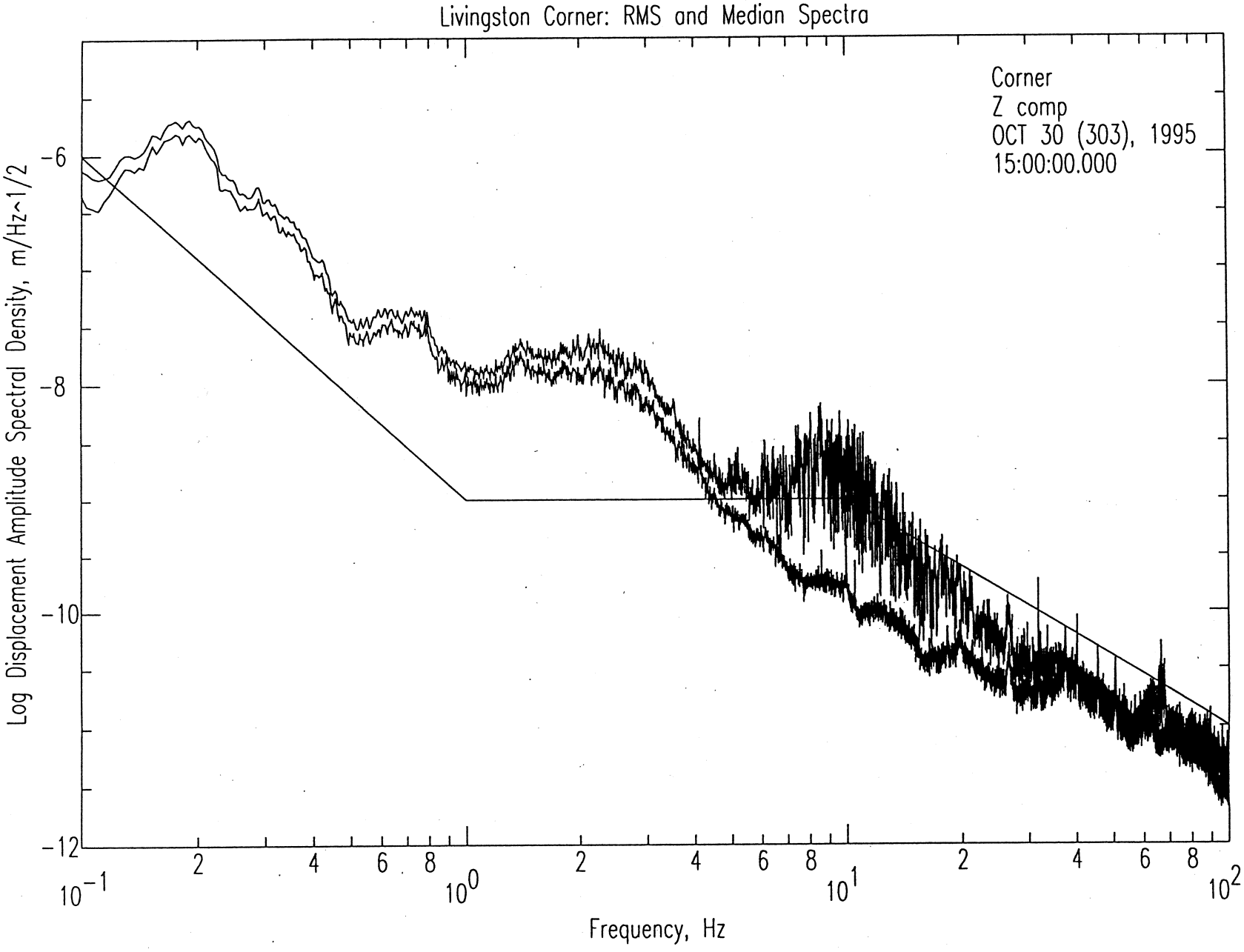

Figure 6-8. Amplitude spectra (median and r.m.s.) for a one-hour period when a passenger vehicle passed near the Corner. The r.m.s. spectrum is increased from 5 to over 20 Hz. These spectra correspond to the signals shown in the spectrogram in Figure 5-3.

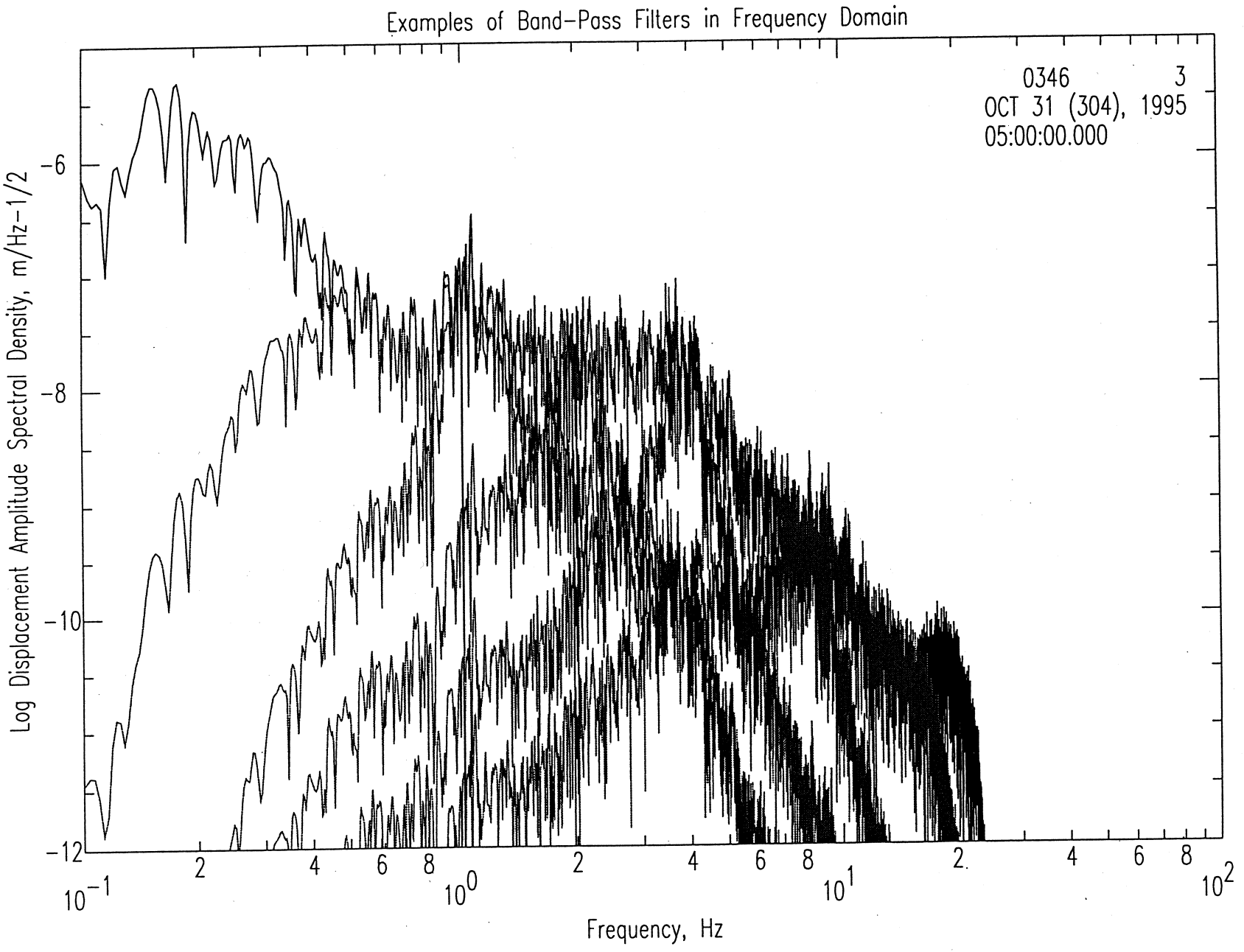

Figure 7-1. Effect of band-pass filtering. A 4-pole Butterworth filter is used to separate noise into the frequency bands 0.5-1.0 Hz, 1.0-2.0 Hz, 2.0-4.0 Hz, 4.0-8.0 Hz, and 8.0-16.0 Hz. An 8-pole filter is used at 0.5 Hz.

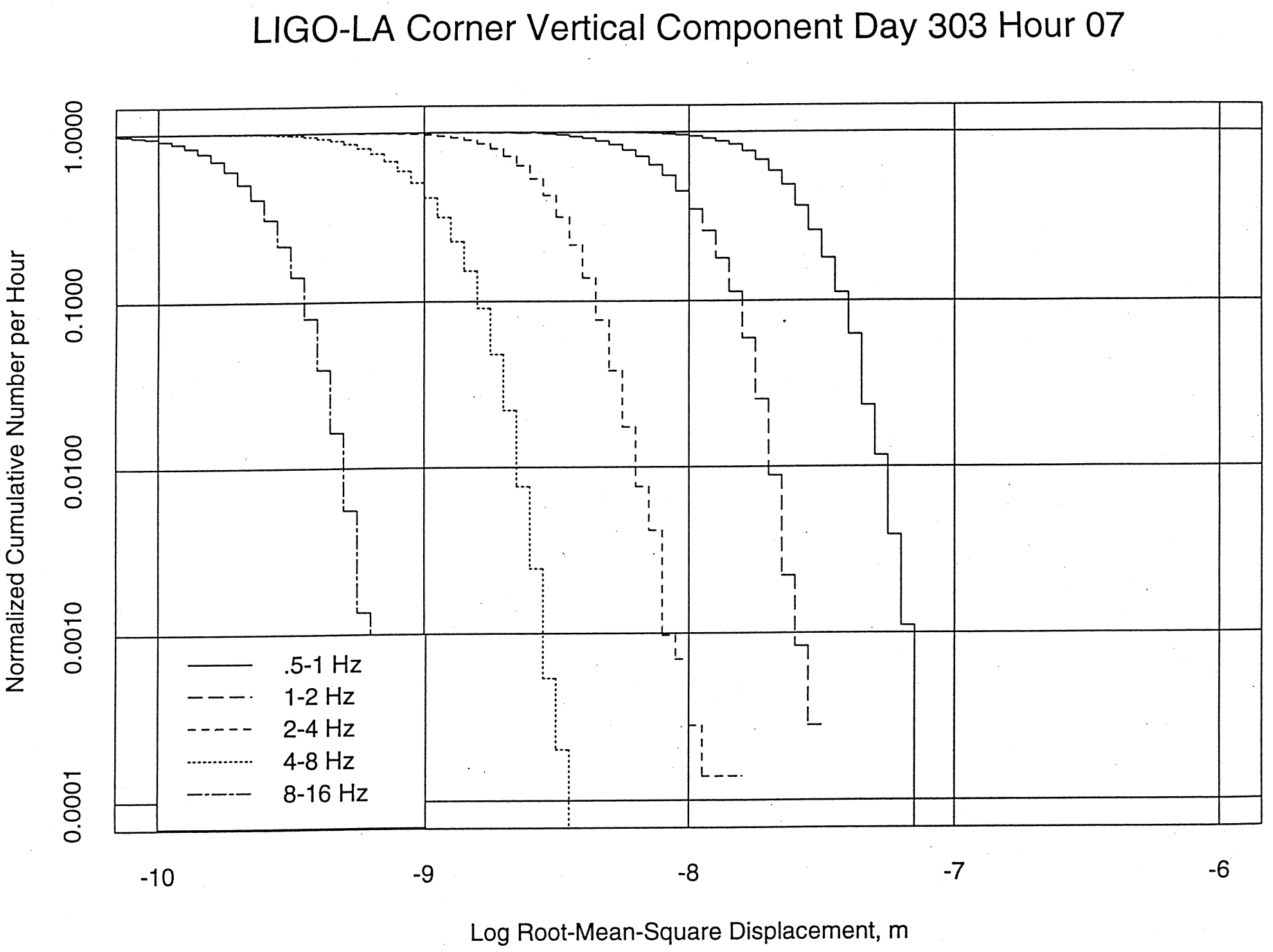

Figure 7-2. Vertical displacement amplitude distribution at the Corner for the five frequency bands. This time period corresponds to the quiet period shown as a spectrogram in Figure 5-1 and the amplitude spectra shown in Figure 6-1.

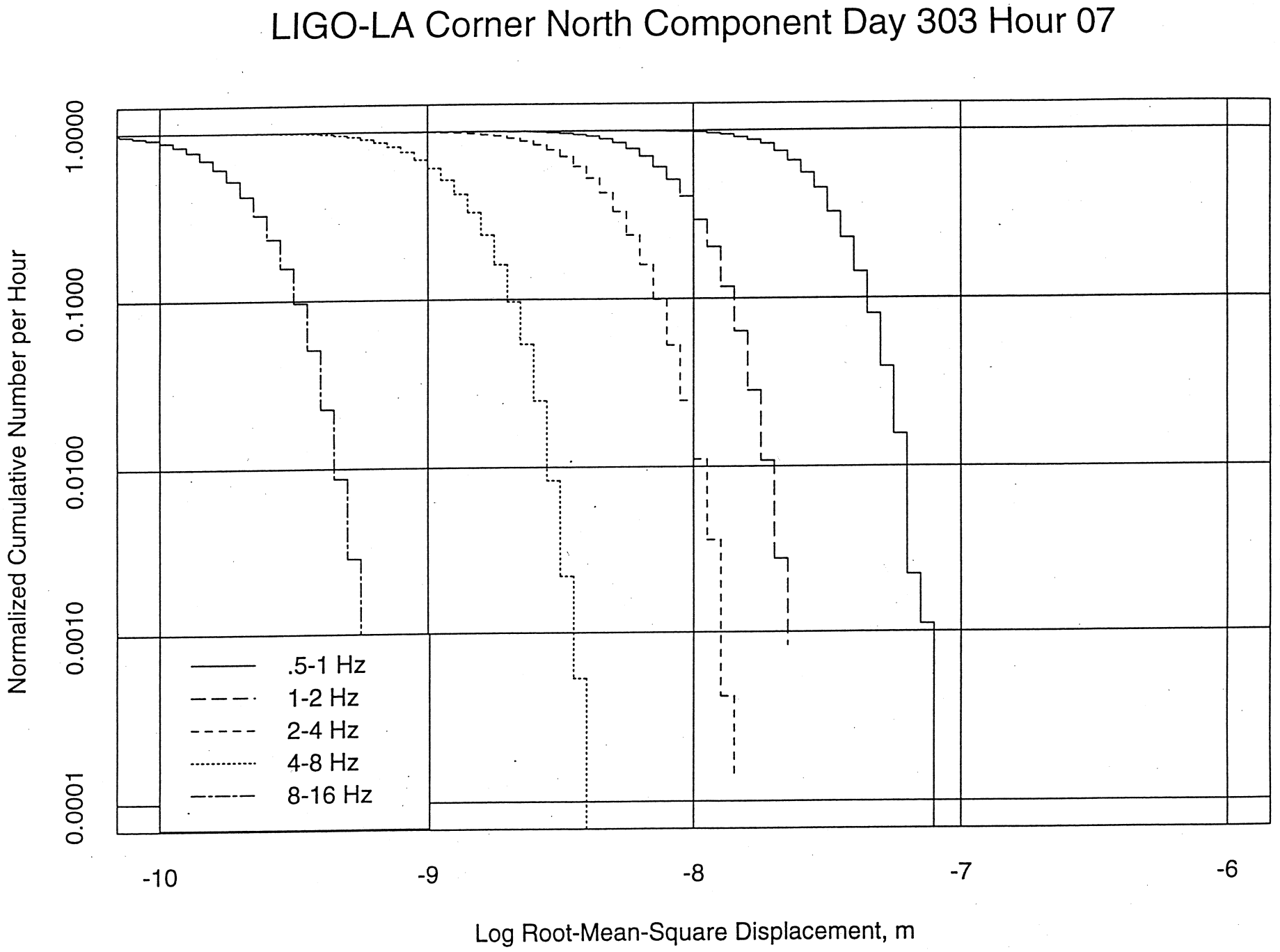

Figure 7-3. North-component displacement amplitude distribution at the Corner for the five frequency bands. This time period corresponds to the quiet period shown as a spectrogram in Figure 5-1 and the amplitude spectra shown in Figure 6-2.

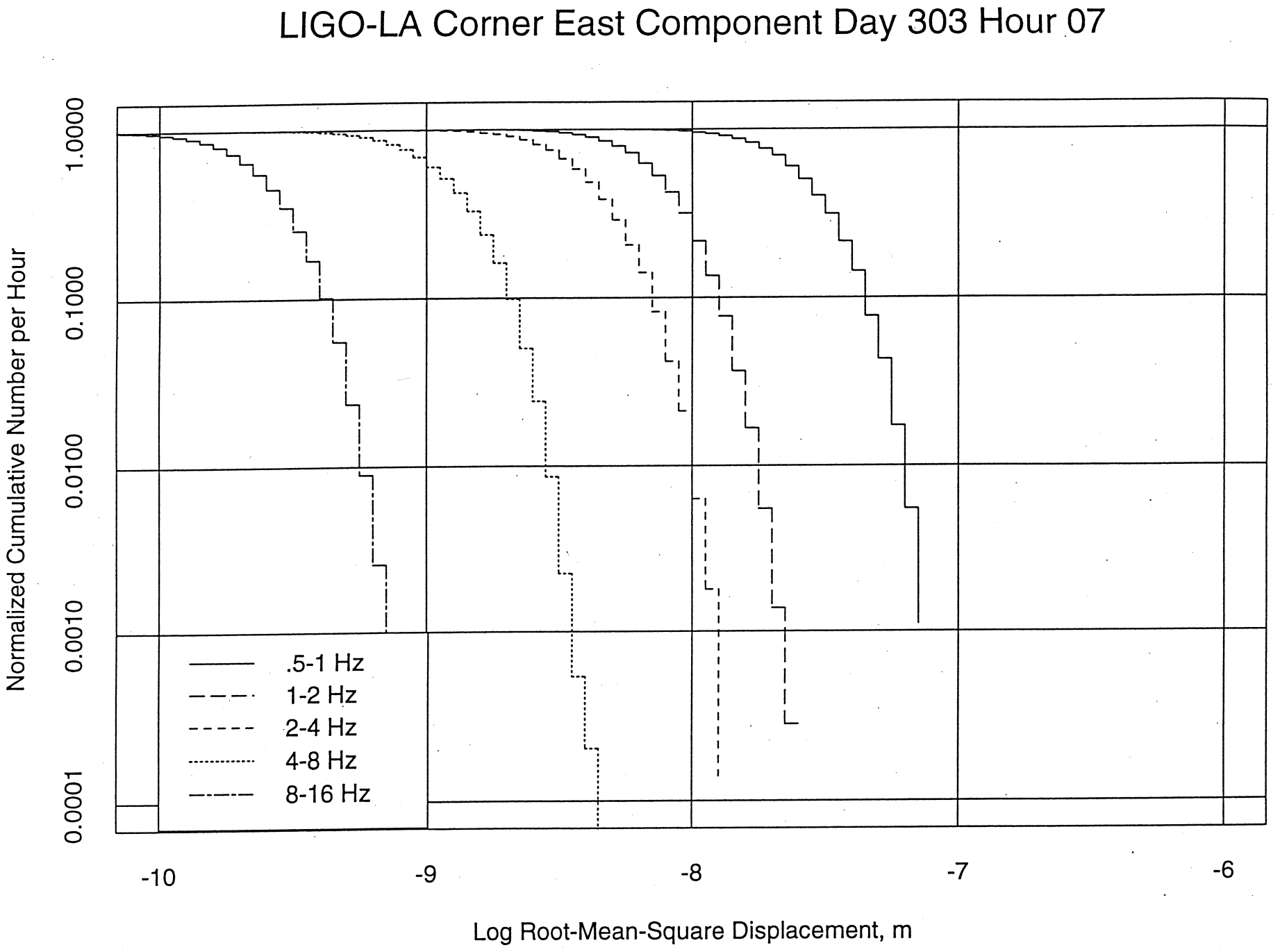

Figure 7-4. East-component displacement amplitude distribution at the Corner for the five frequency bands. This time period corresponds to the quiet period shown as a spectrogram in Figure 5-1 and the amplitude spectra shown in Figure 6-3.

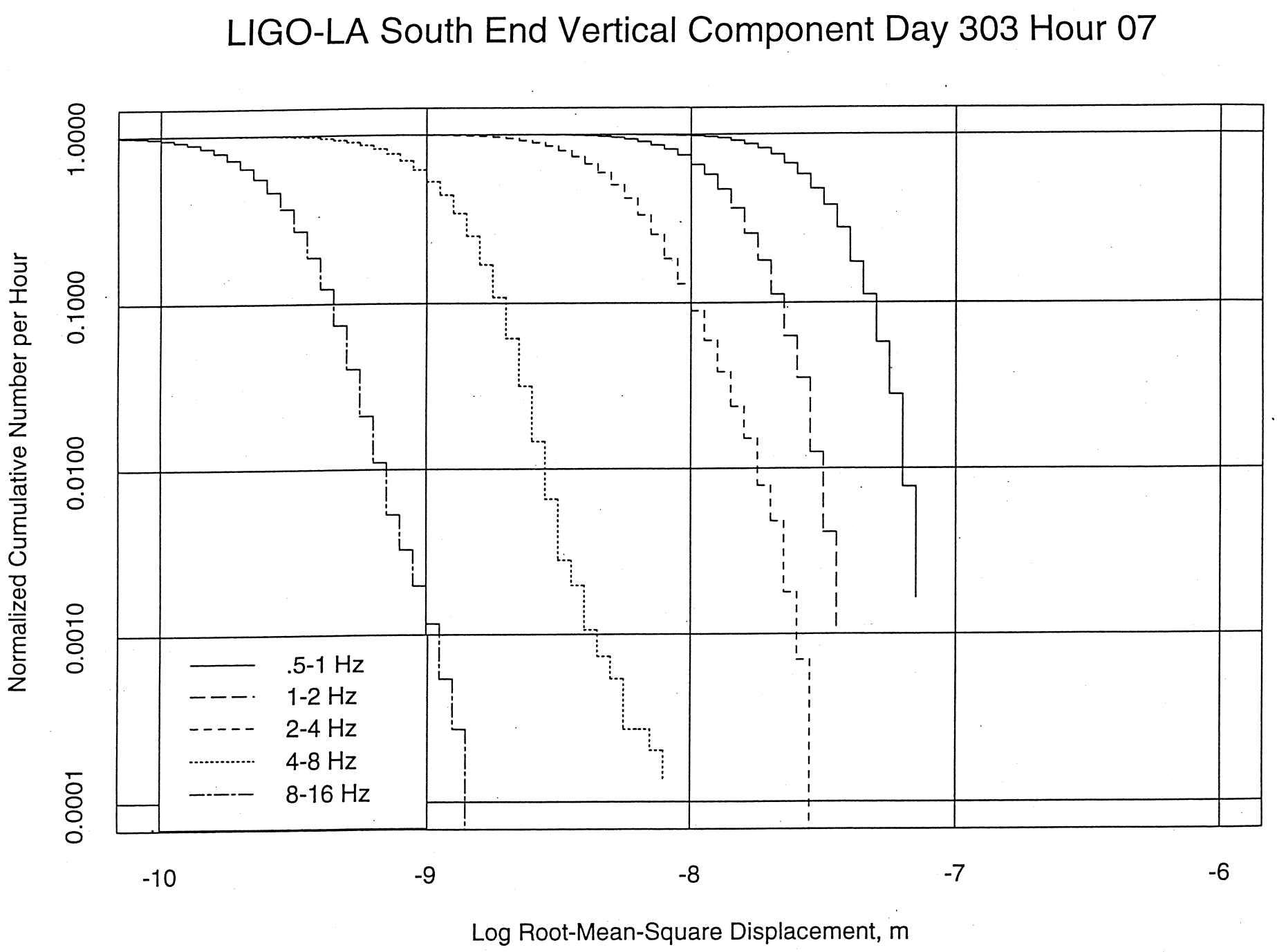

Figure 7-5. Vertical displacement amplitude distribution at the South End for the five frequency bands. This time period corresponds to the quiet period shown in the amplitude spectra shown in Figure 6-4.

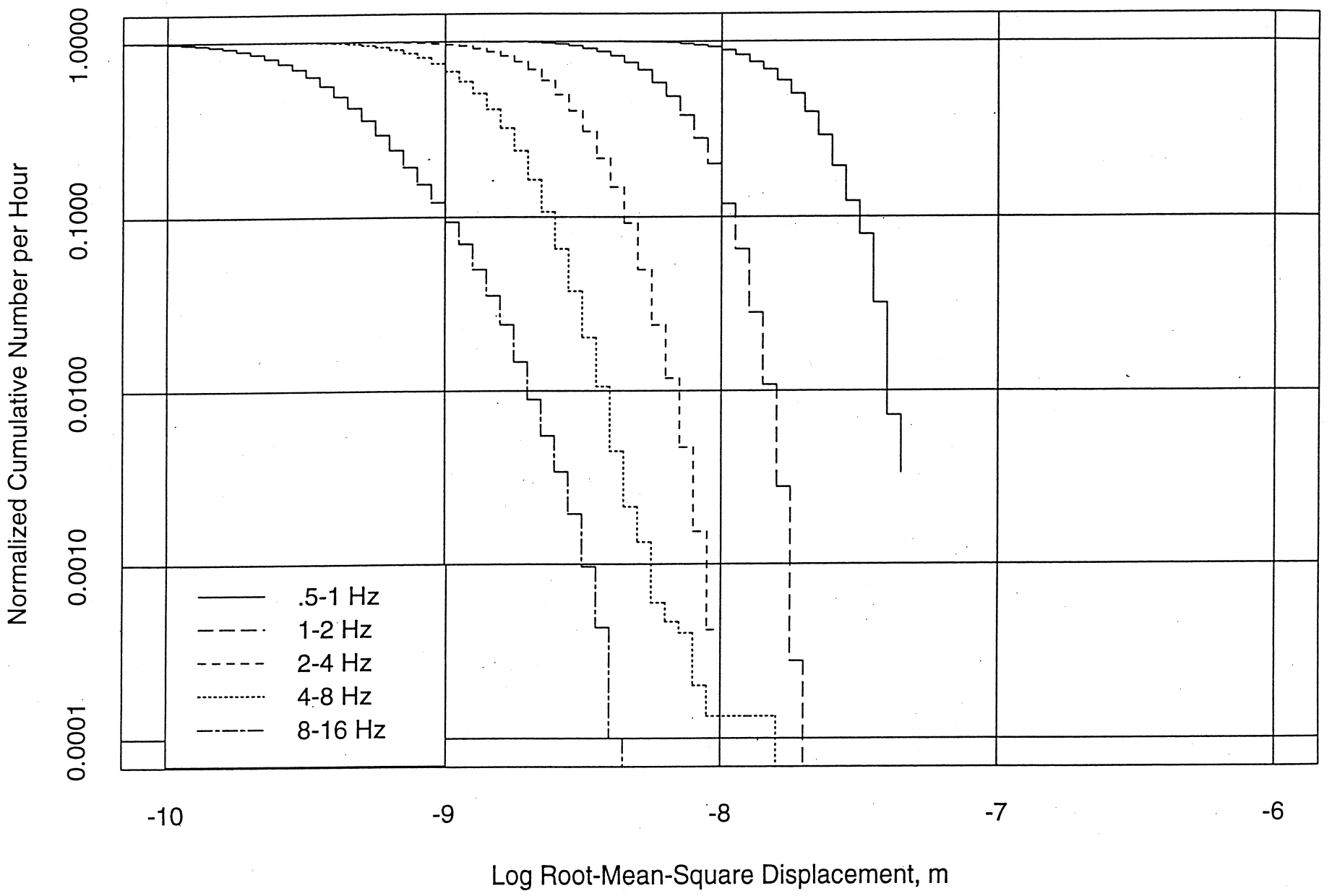

Figure 7-6. Vertical displacement amplitude distribution at the West End for the five frequency bands. This time period corresponds to the quiet period shown in the amplitude spectra shown in Figure 6-5.

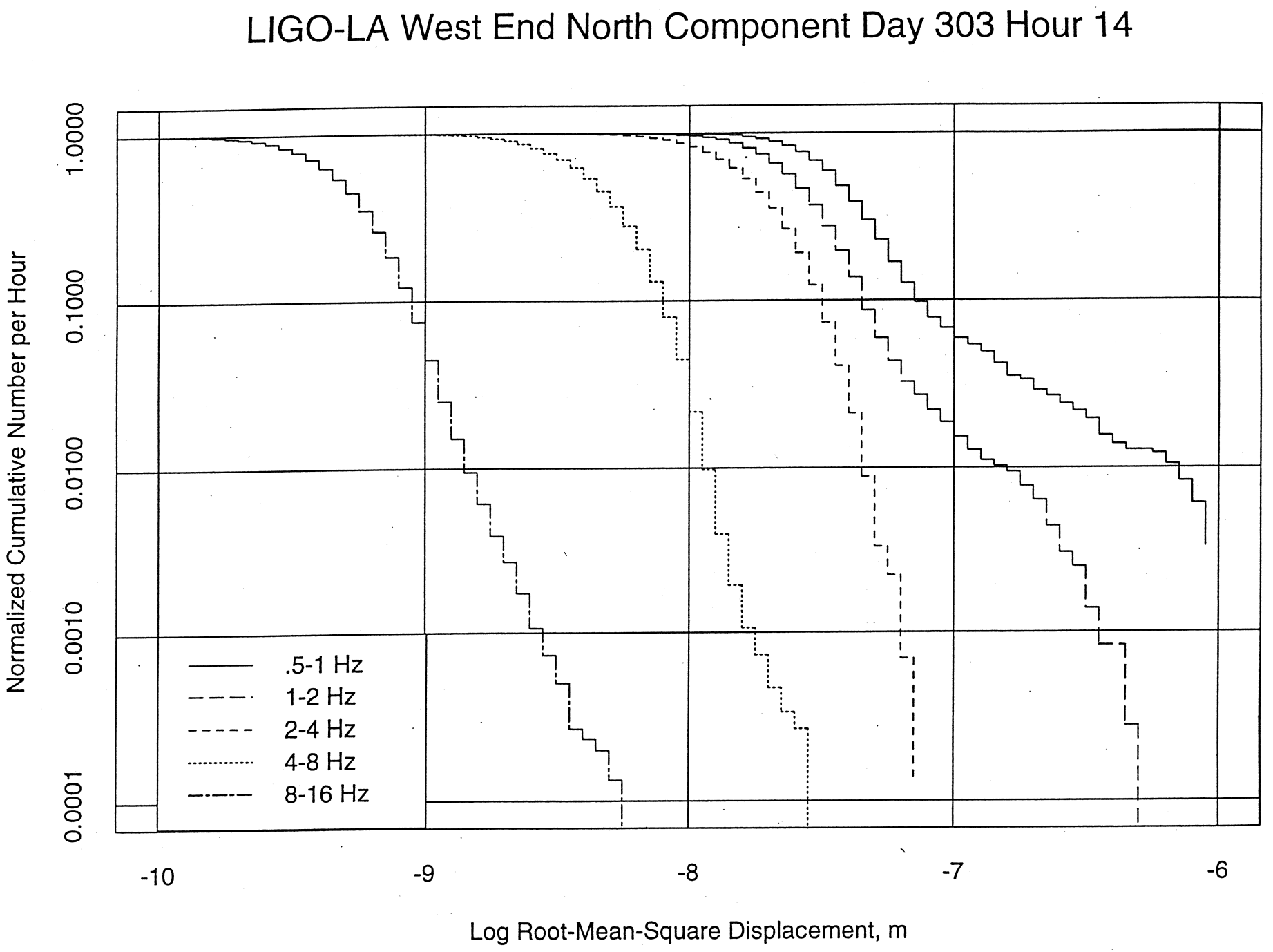

Figure 7-7. North-component displacement amplitude distribution at the West End for the five frequency bands in a time period when an earthquake occurred. The spectrum corresponding to this time period was shown in Figure 6-6. The amplitude distribution for the two low-frequency bands are affected about 10% of the time period.

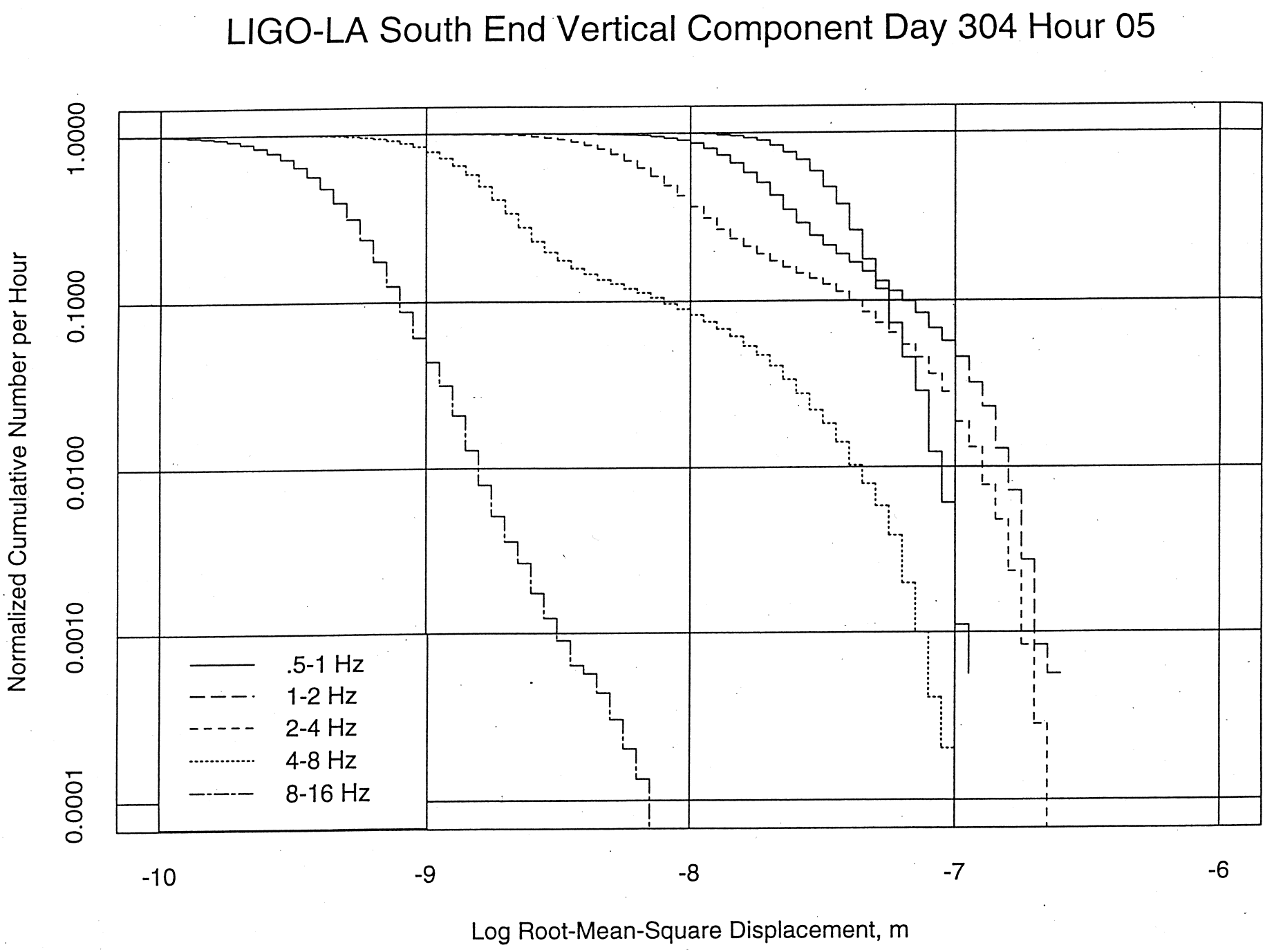

Figure 7-8. Vertical-component displacement amplitude distribution at the South End for the five frequency bands in a time period when a train passed the site. The spectrum corresponding to this time period was shown in Figure 6-7.The train principally affects the middle frequency ranges 1-8 Hz.

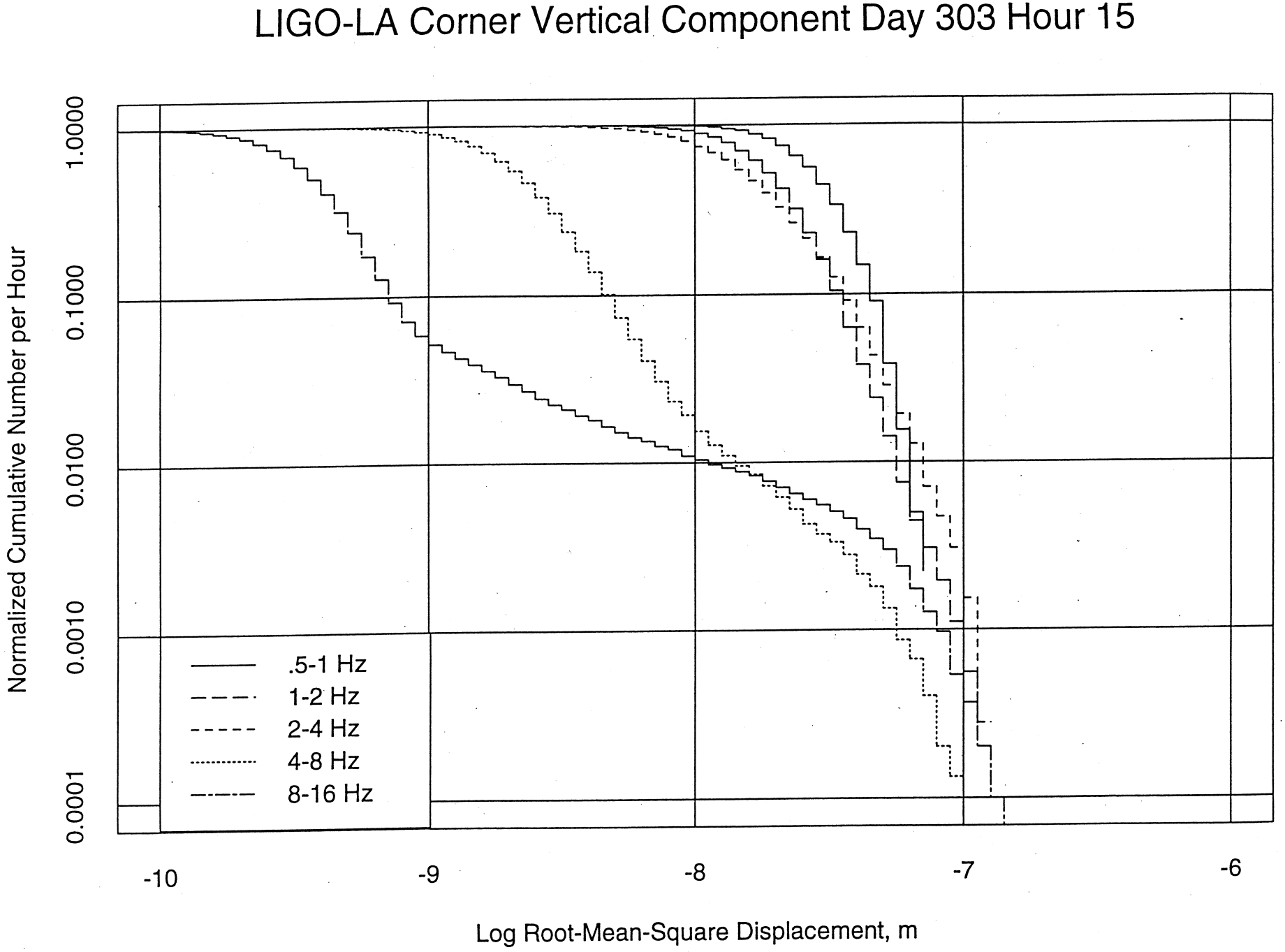

Figure 7-9. Vertical-component displacement amplitude distribution at the Corner for the five frequency bands in a time period when a passenger vehicle passed the site. The spectrum corresponding to this time period was shown in Figure 6-8. The vehicle principally affects the highest frequency ranges 4-16 Hz.

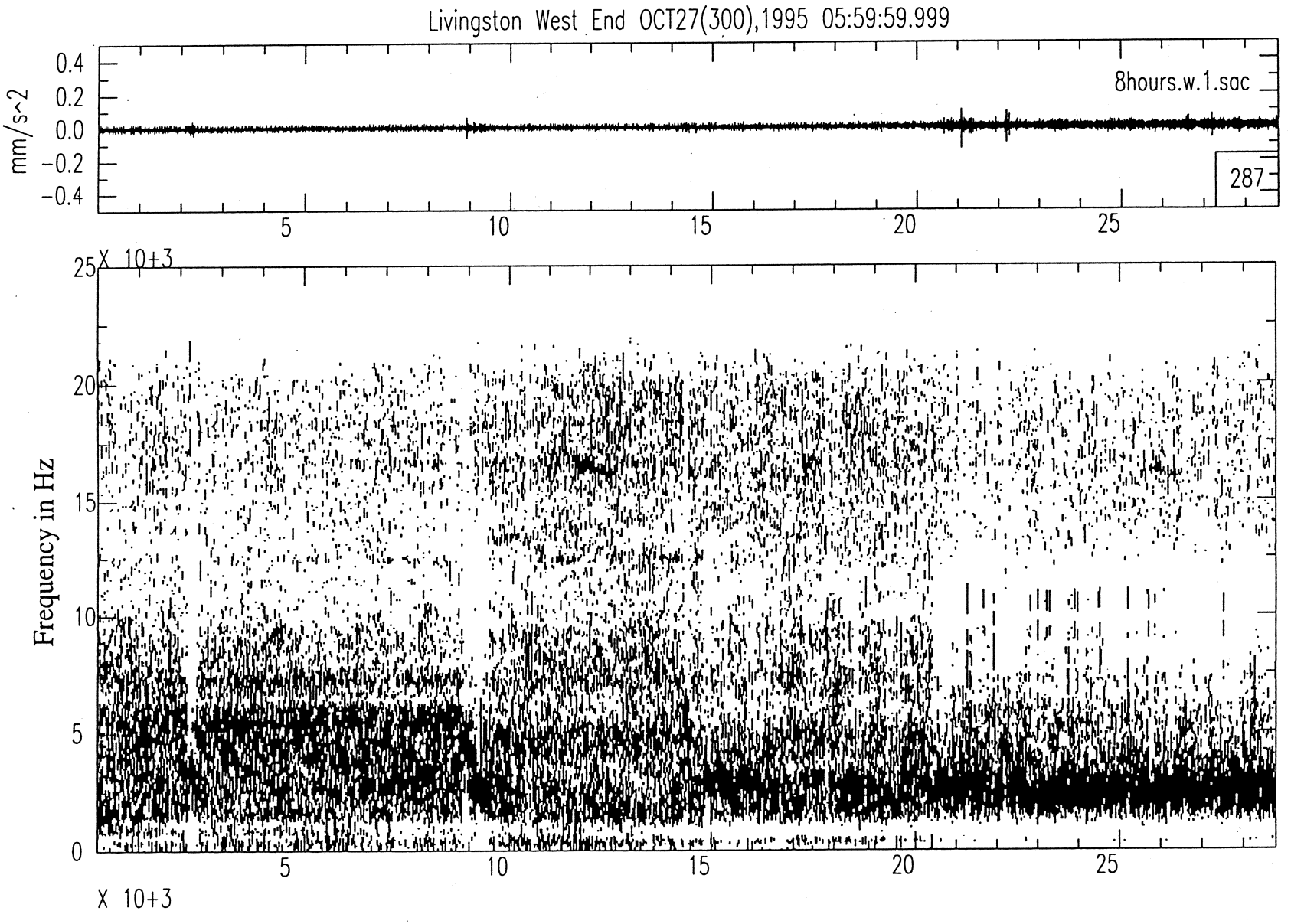

Figure 8.2-1. Black-and-white 0-25 Hz spectrogram of the vertical component at the West End when the crude-oil "Capline" was shut down. The period of shutdown was from approximately 9000 to 21000 seconds on the 8-hour time period shown. Noise at West End is reduced in the band 1-7 Hz.

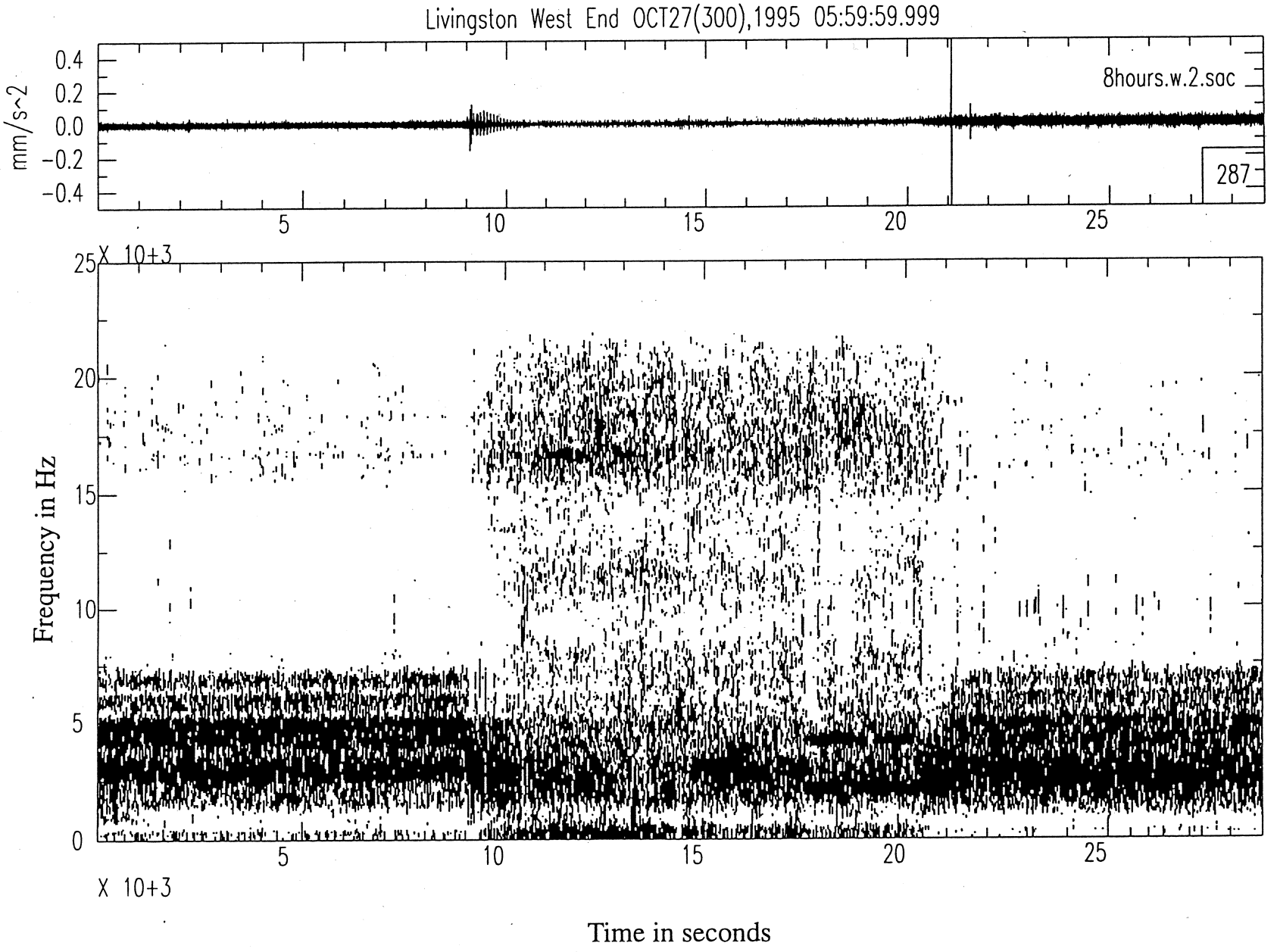

Figure 8.2-2. Black-and-white 0-25 Hz spectrogram of the north component at the West End when the crude-oil "Capline" was shut down. The period of shutdown was from approximately 9000 to 21000 seconds on the 8-hour time period shown. Noise at West End is reduced in the band 1-7 Hz.

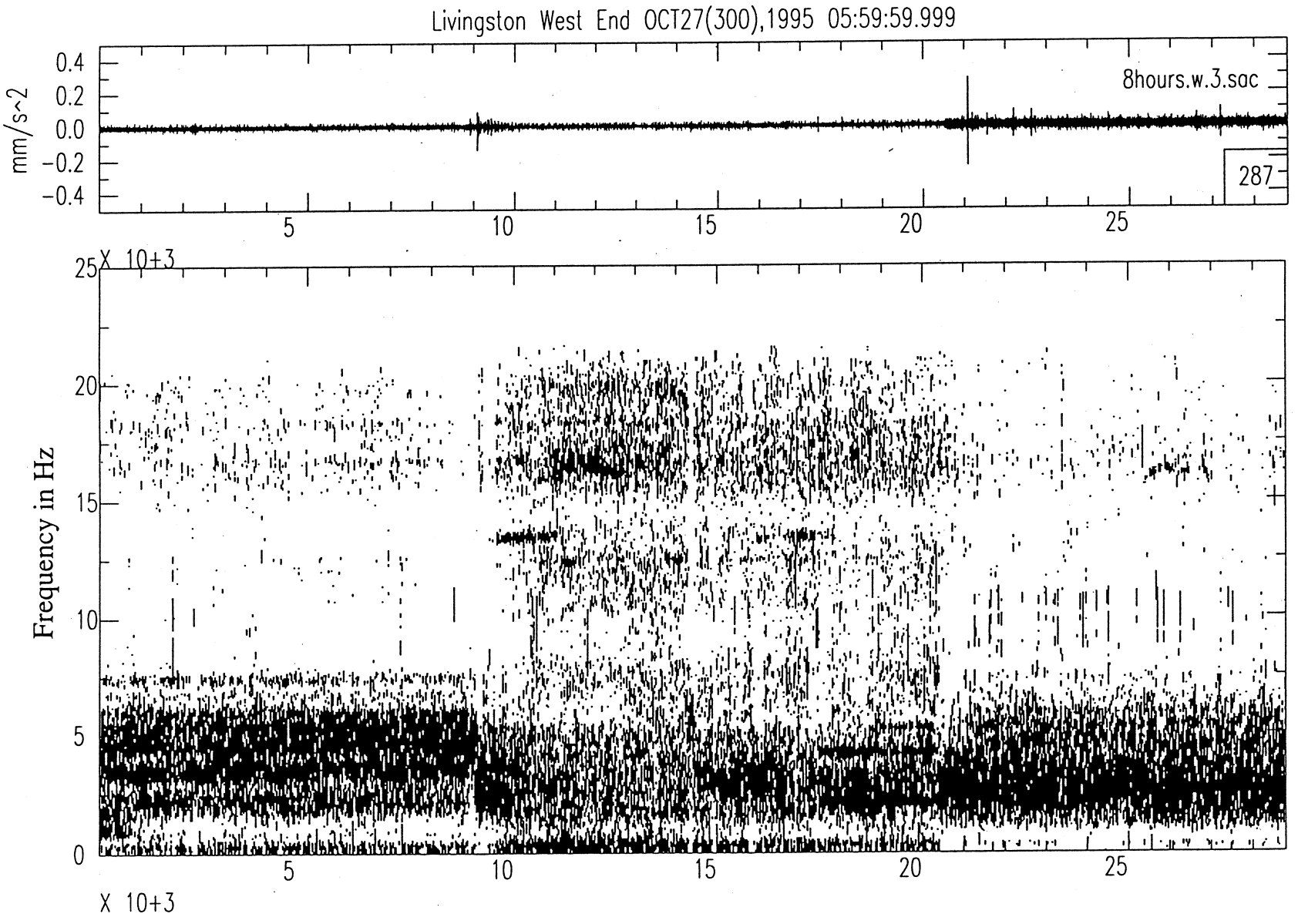

Figure 8.2-3. Black-and-white 0-25 Hz spectrogram Hz of the east component at the West End when the crude-oil "Capline" was shut down. The period of shutdown was from approximately 9000 to 21000 seconds on the 8-hour time period shown. Noise at West End is reduced in the band 1-7 Hz.

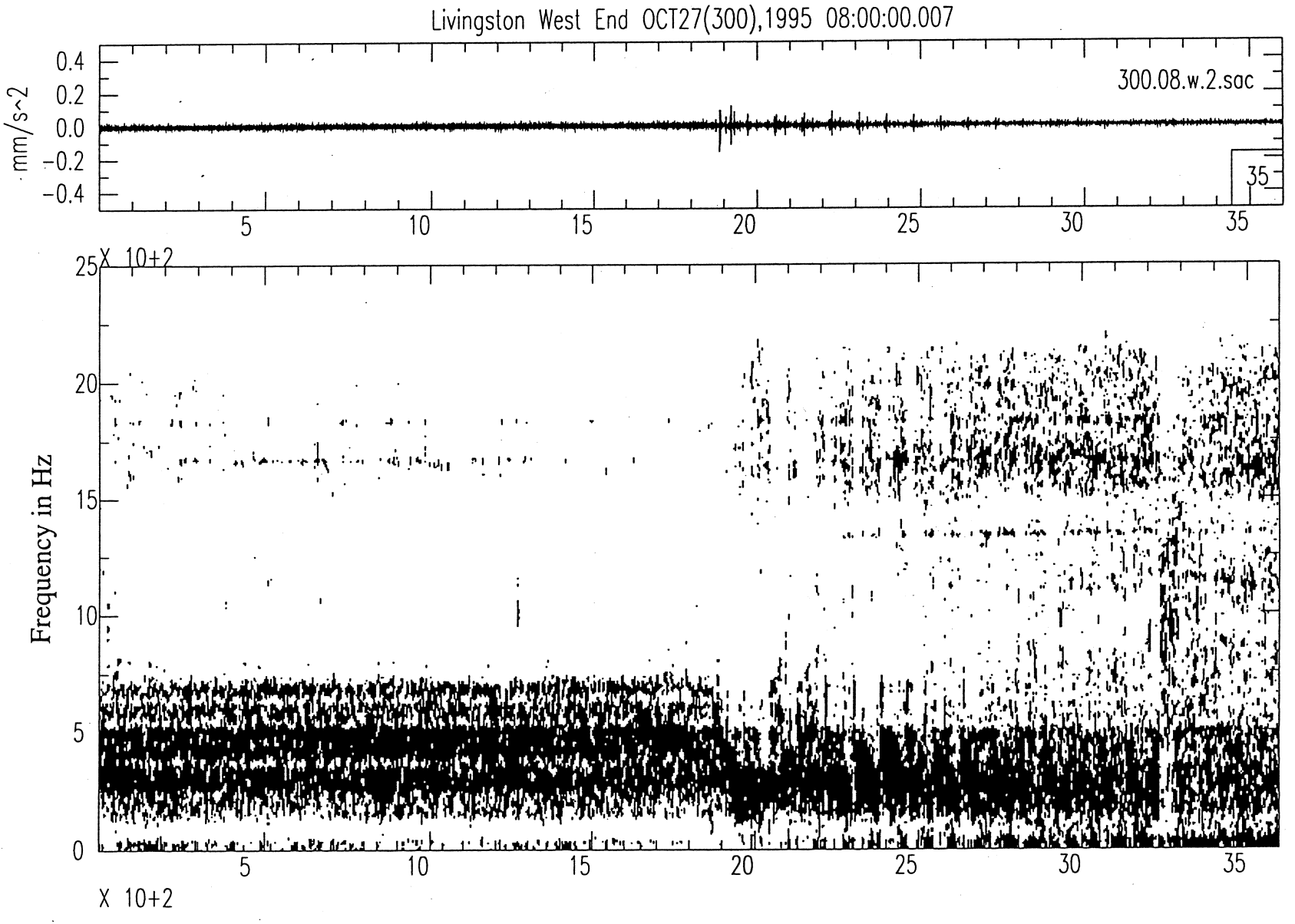

Figure 8.2-4. Black-and-white 0-25 Hz spectrogram of the north component at the West End when the crude-oil "Capline" was shut down. This shows a one-hour period when the shutdown occurred at about 0830 GMT. The "water-hammer" or "surging effect can be seen on the decaying, evenly-spaced noise bursts following the shutdown.

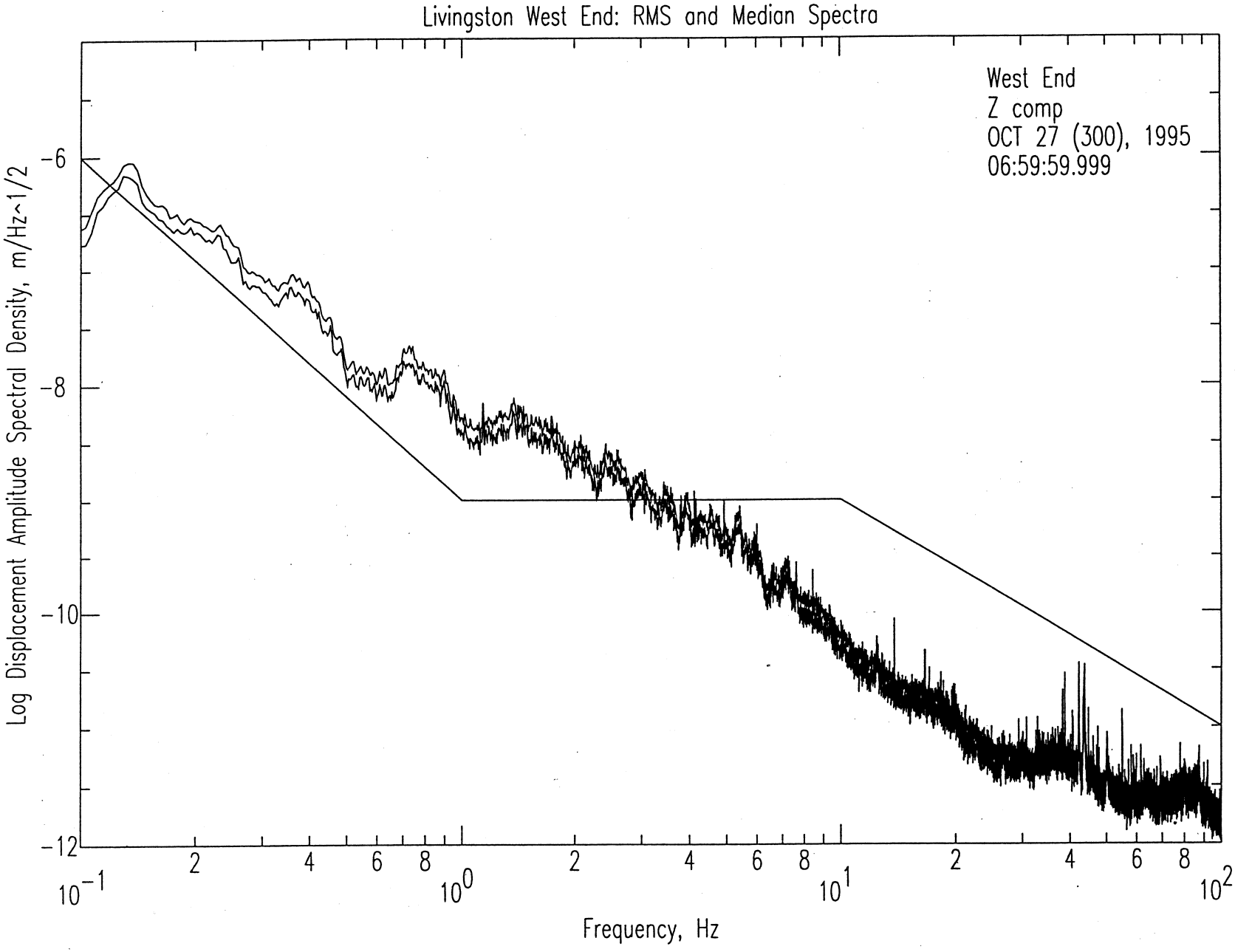

Figure 8.2-5. Amplitude spectra (median and r.m.s.) for a one-hour period at the West End prior to the "Capline" shutdown at 0830 GMT. Vertical component is shown.

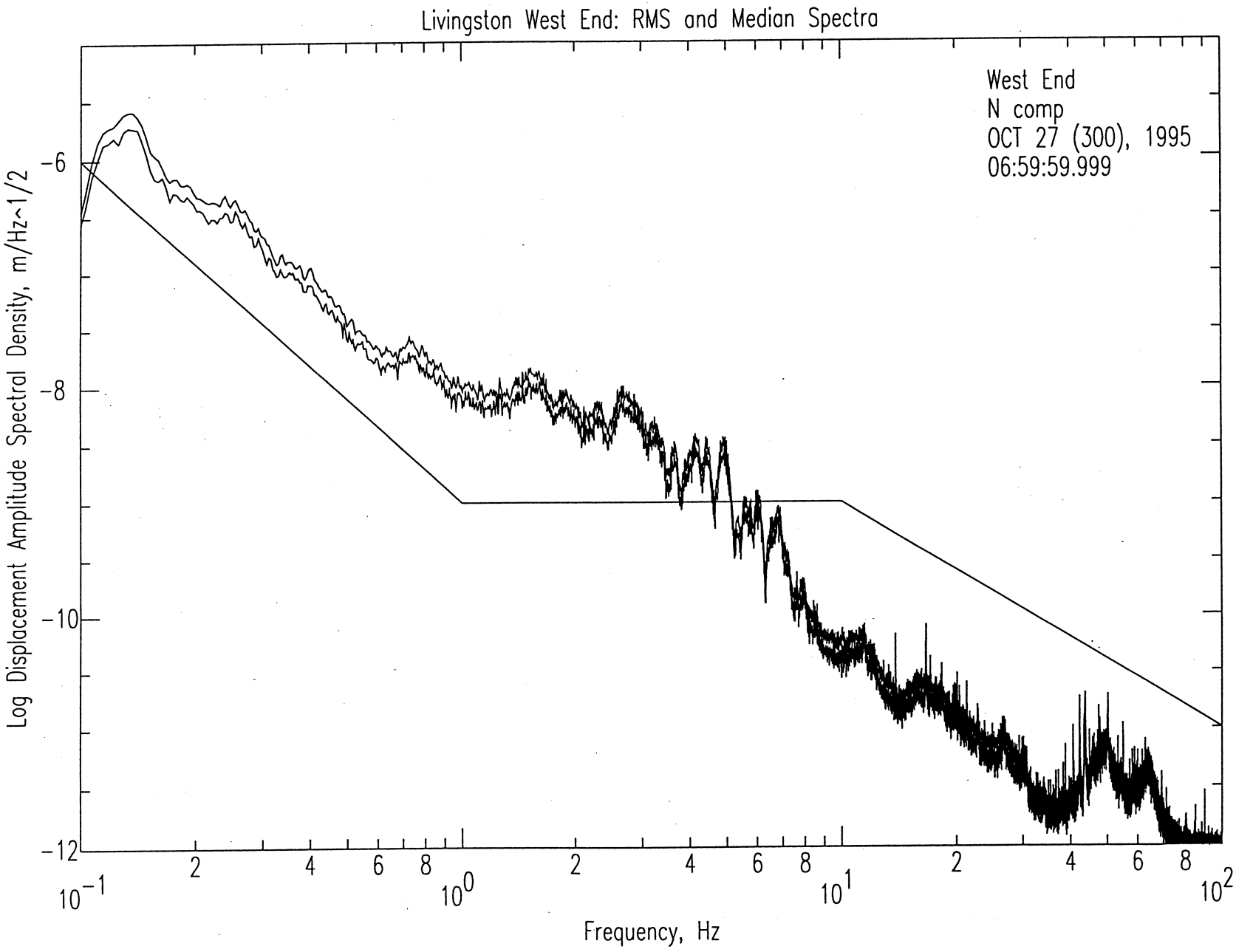

Figure 8.2-6. Amplitude spectra (median and r.m.s.) for a one-hour period at the West End prior to the "Capline" shutdown at 0830 GMT. North component is shown.

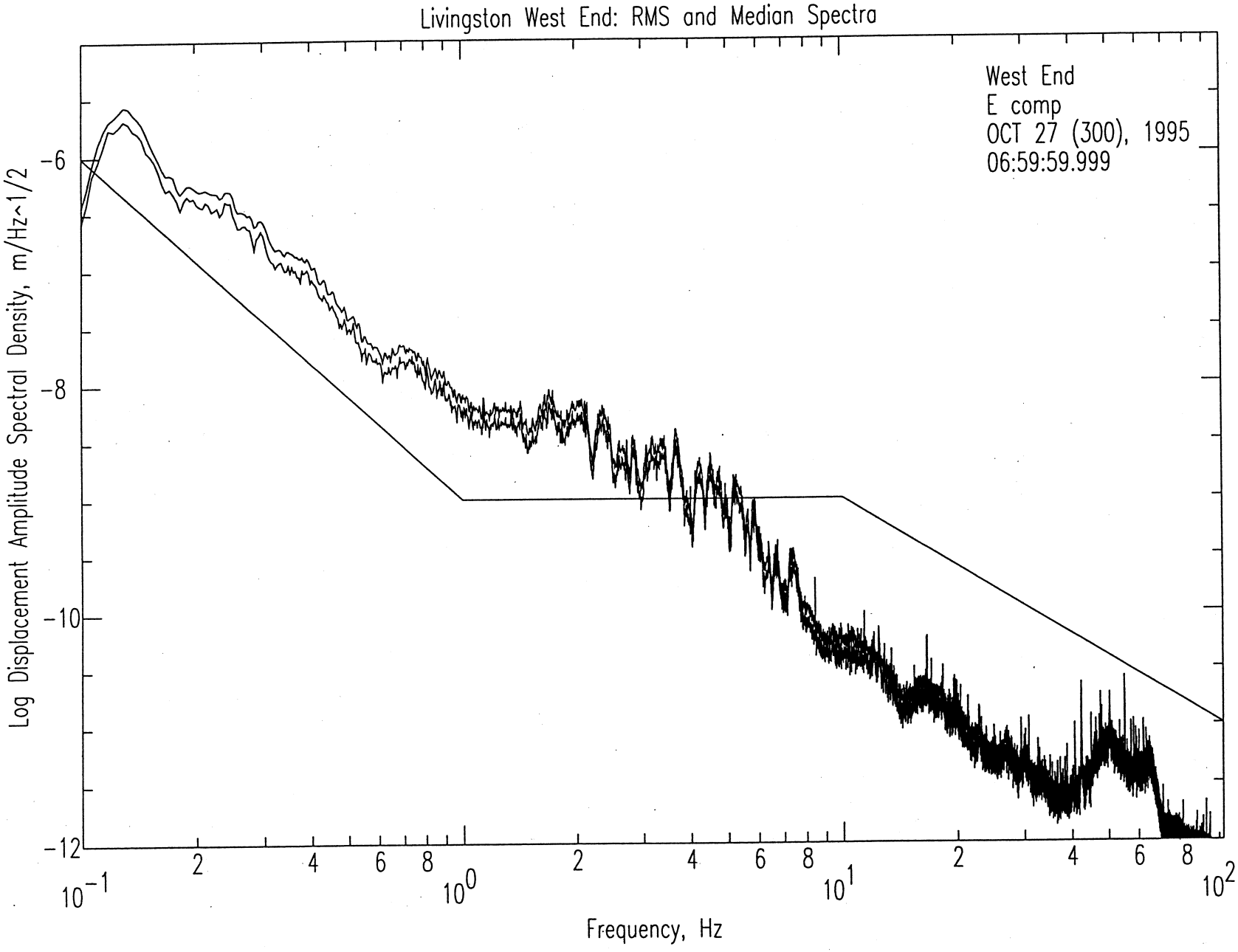

Figure 8.2-7. Amplitude spectra (median and r.m.s.) for a one-hour period at the West End prior to the "Capline" shutdown at 0830 GMT. East component is shown.

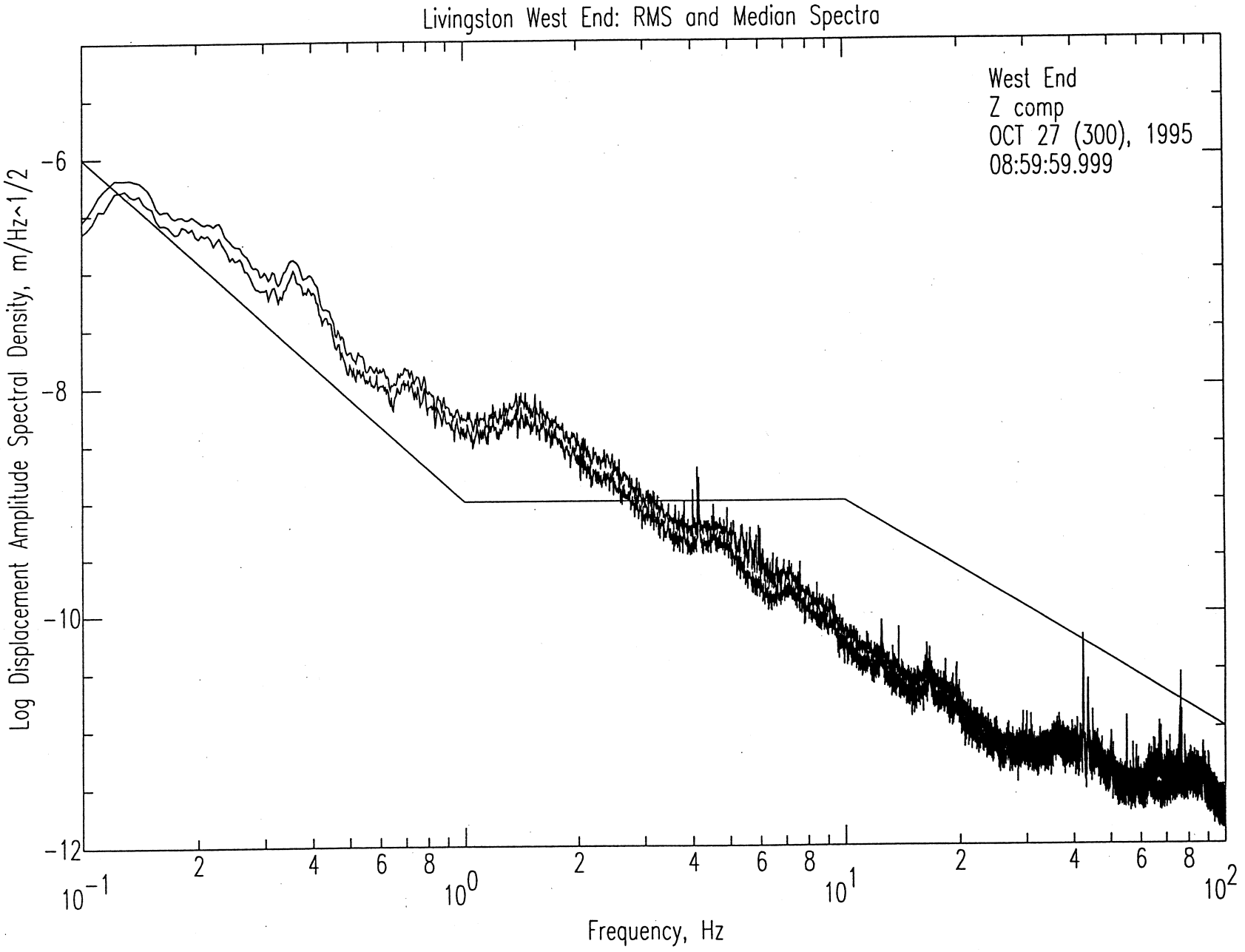

Figure 8.2-8. Amplitude spectra (median and r.m.s.) for a one-hour period at the West End shortly after the "Capline" shutdown at 0830 GMT. Vertical component is shown.

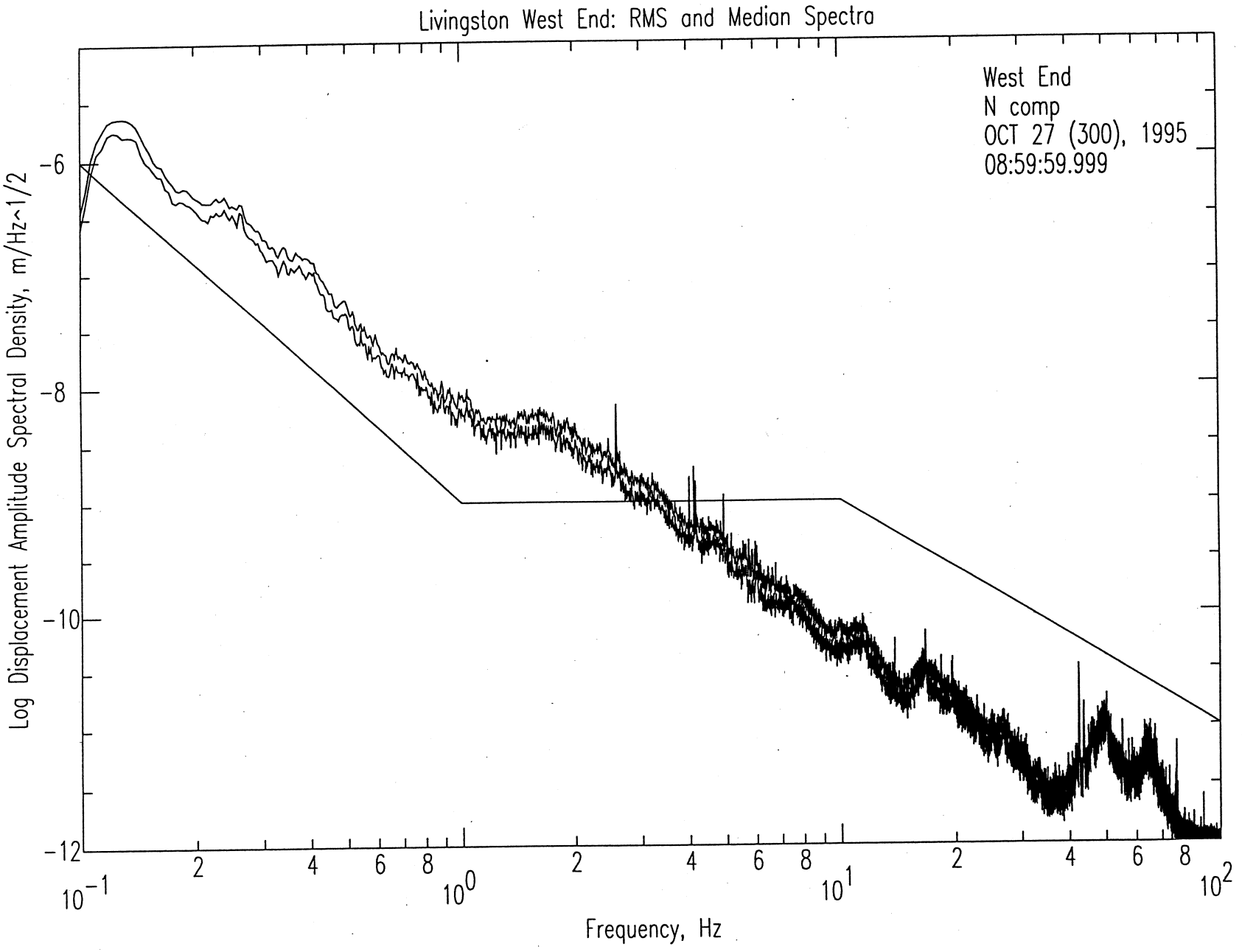

Figure 8.2-9. Amplitude spectra (median and r.m.s.) for a one-hour period at the West End shortly after the "Capline" shutdown at 0830 GMT. North component is shown.

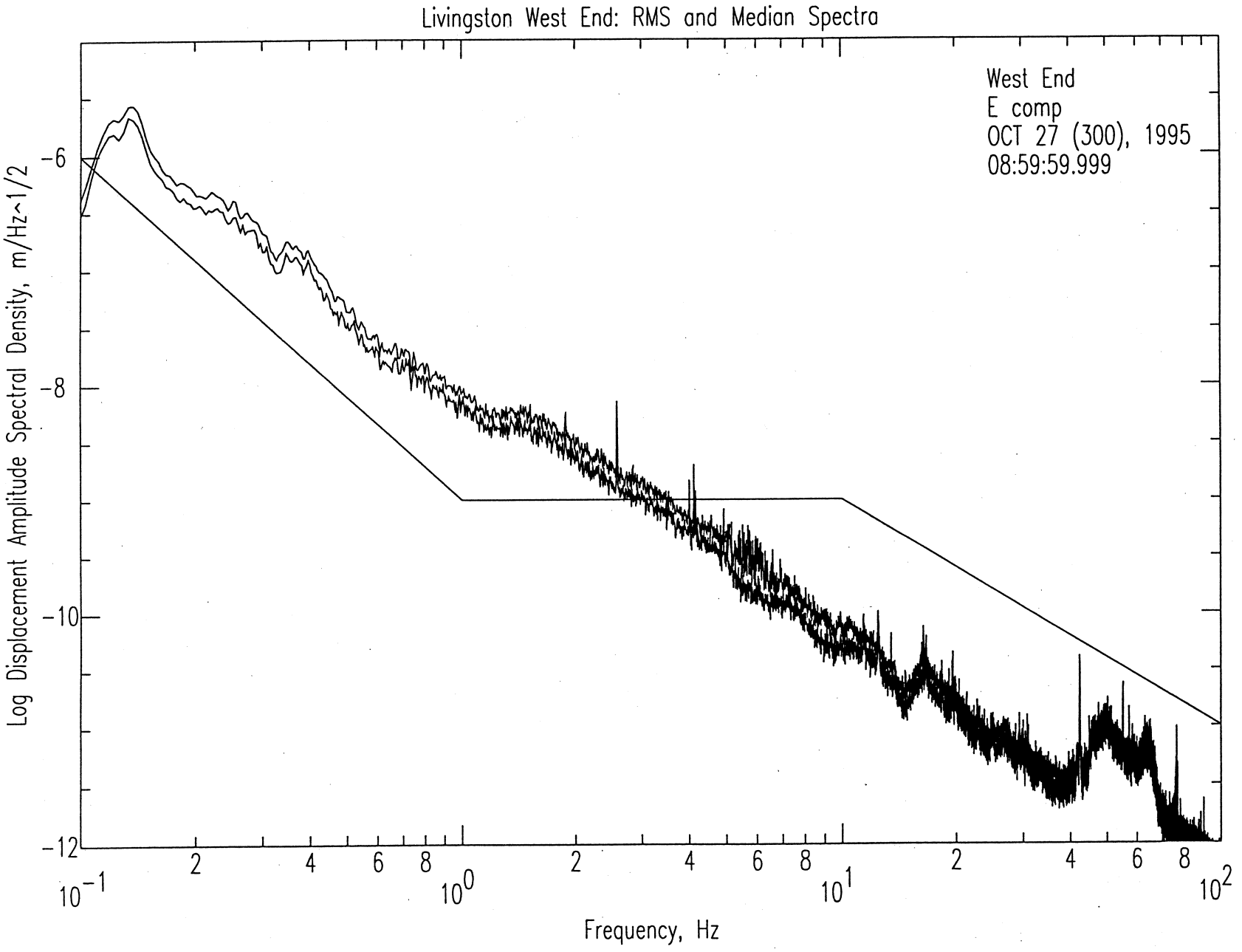

Figure 8.2-10. Amplitude spectra (median and r.m.s.) for a one-hour period at the West End shortly after the "Capline" shutdown at 0830 GMT. East component is shown.

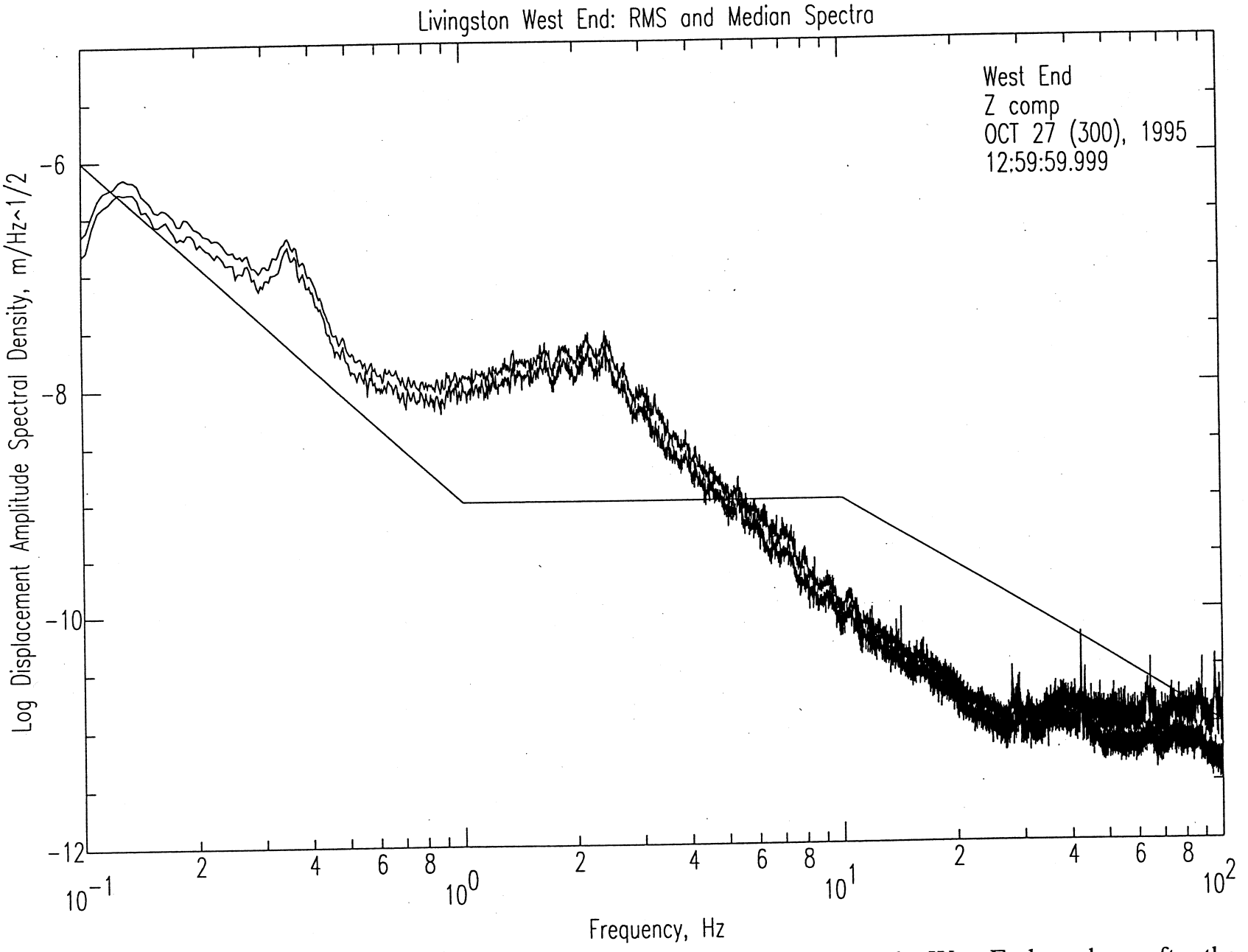

Figure 8.2-11. Amplitude spectra (median and r.m.s.) for a one-hour period at the West End one hour after the "Capline" restarted pumping at 1151 GMT. Vertical component is shown. Note that noise amplitudes are significantly higher than before the shutdown, shown in Figure 8.2-5

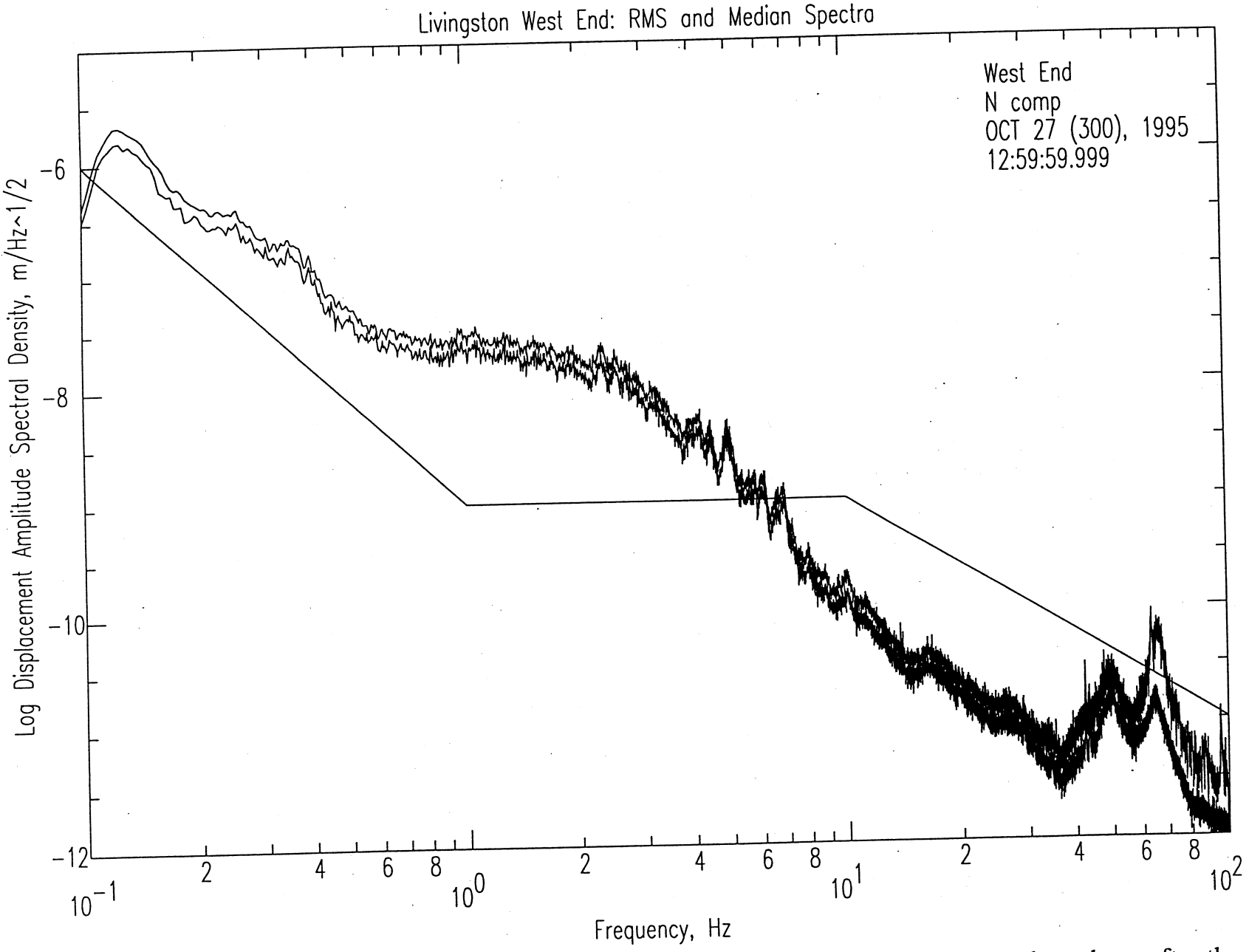

Figure 8.2-12. Amplitude spectra (median and r.m.s.) for a one-hour period at the West End one hour after the "Capline" restarted pumping at 1151 GMT. North component is shown. Note that noise amplitudes are significantly higher than before the shutdown, shown in Figure 8.2-6.

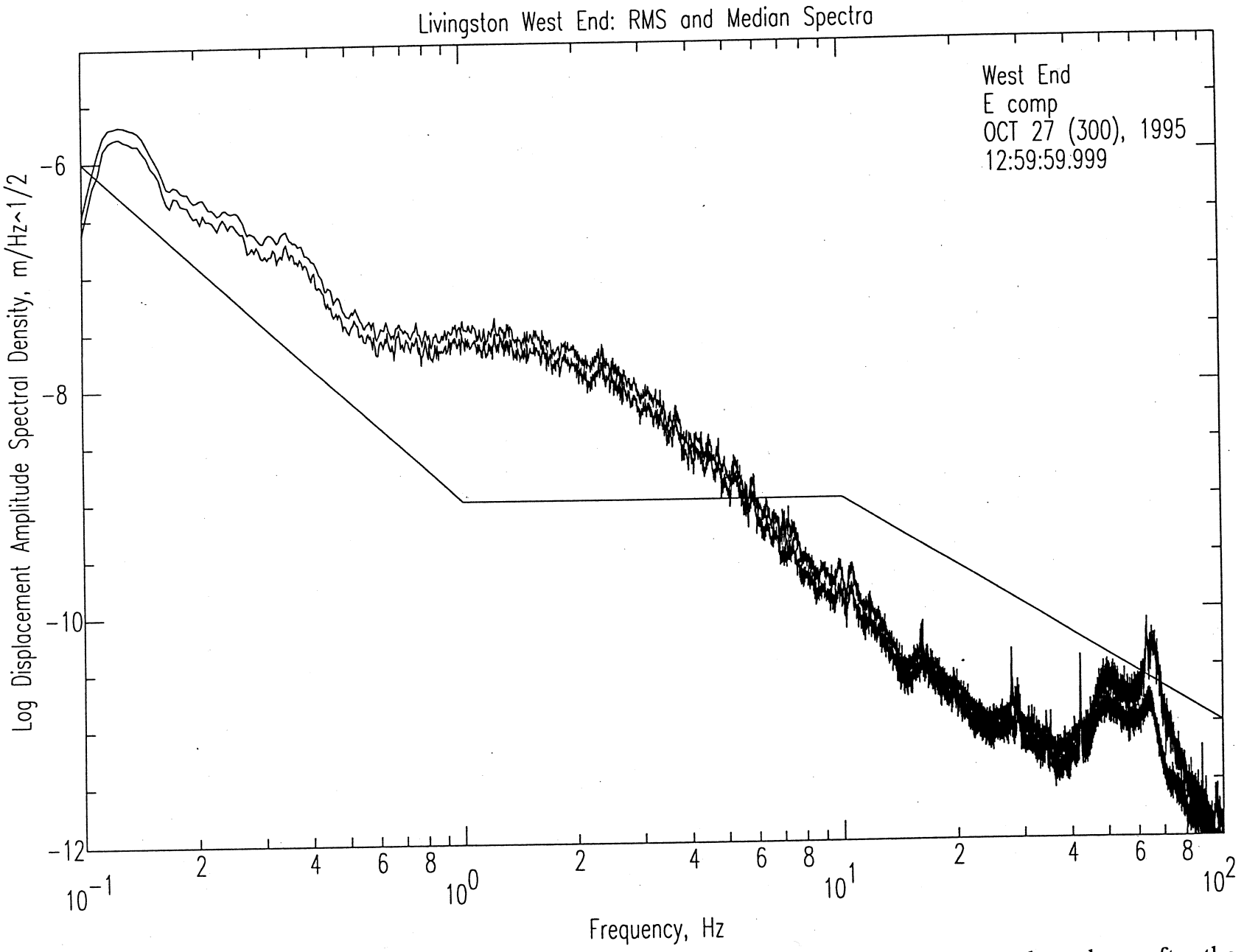

Figure 8.2-13. Amplitude spectra (median and r.m.s.) for a one-hour period at the West End one hour after the "Capline" restarted pumping at 1151 GMT. East component is shown. Note that noise amplitudes are significantly higher than before the shutdown, shown in Figure 8.2-7.

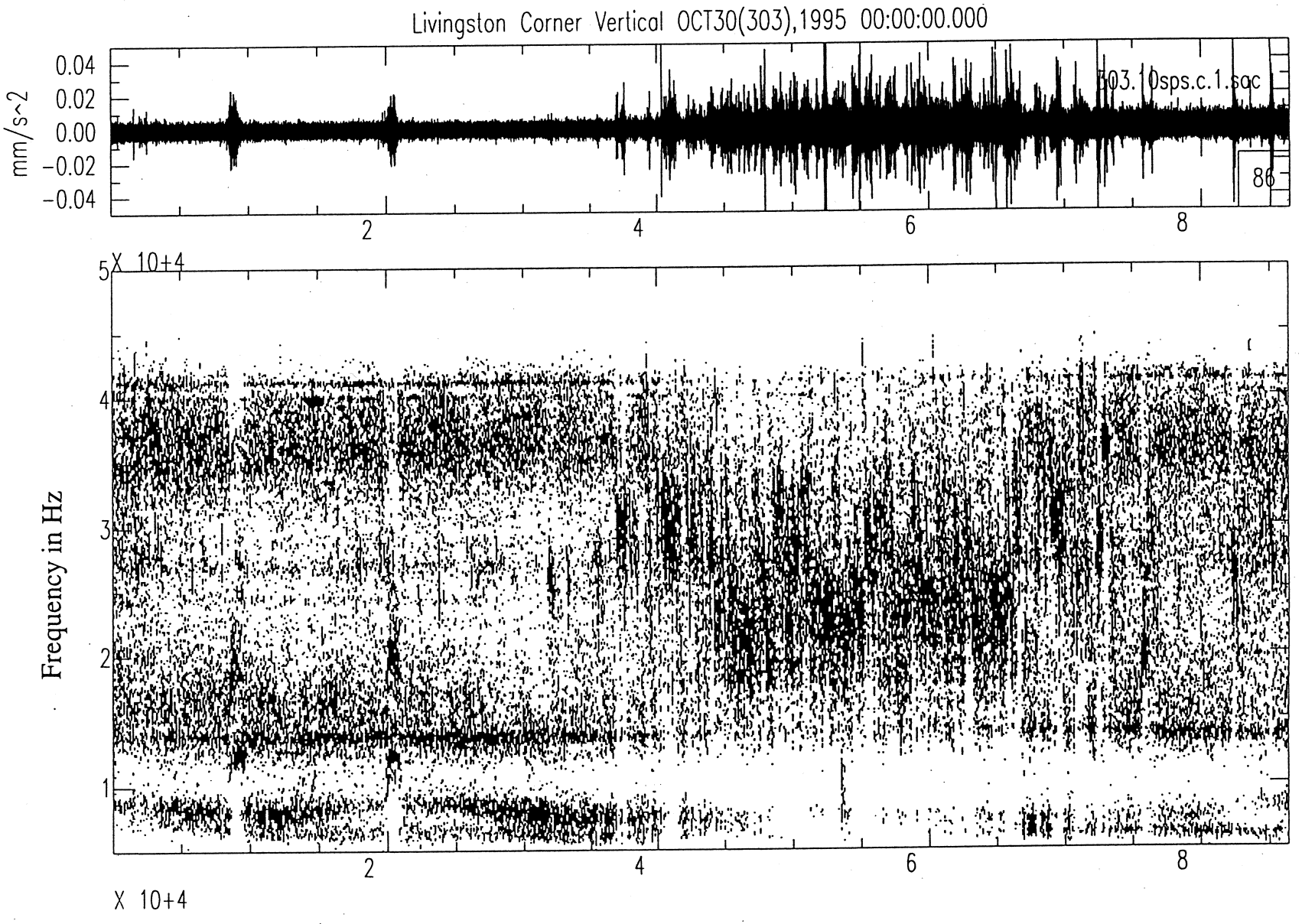

Figure 8.2-14. Black-and-white 0.5-5 Hz spectrogram for a 24-hour period at the Corner. Time period begins at 6 p.m. CST. Note the daily trains at about 10,000 and 20,000 s, and the increase in short-duration noise bursts in the right half of the spectrogram corresponding to daylight hours.

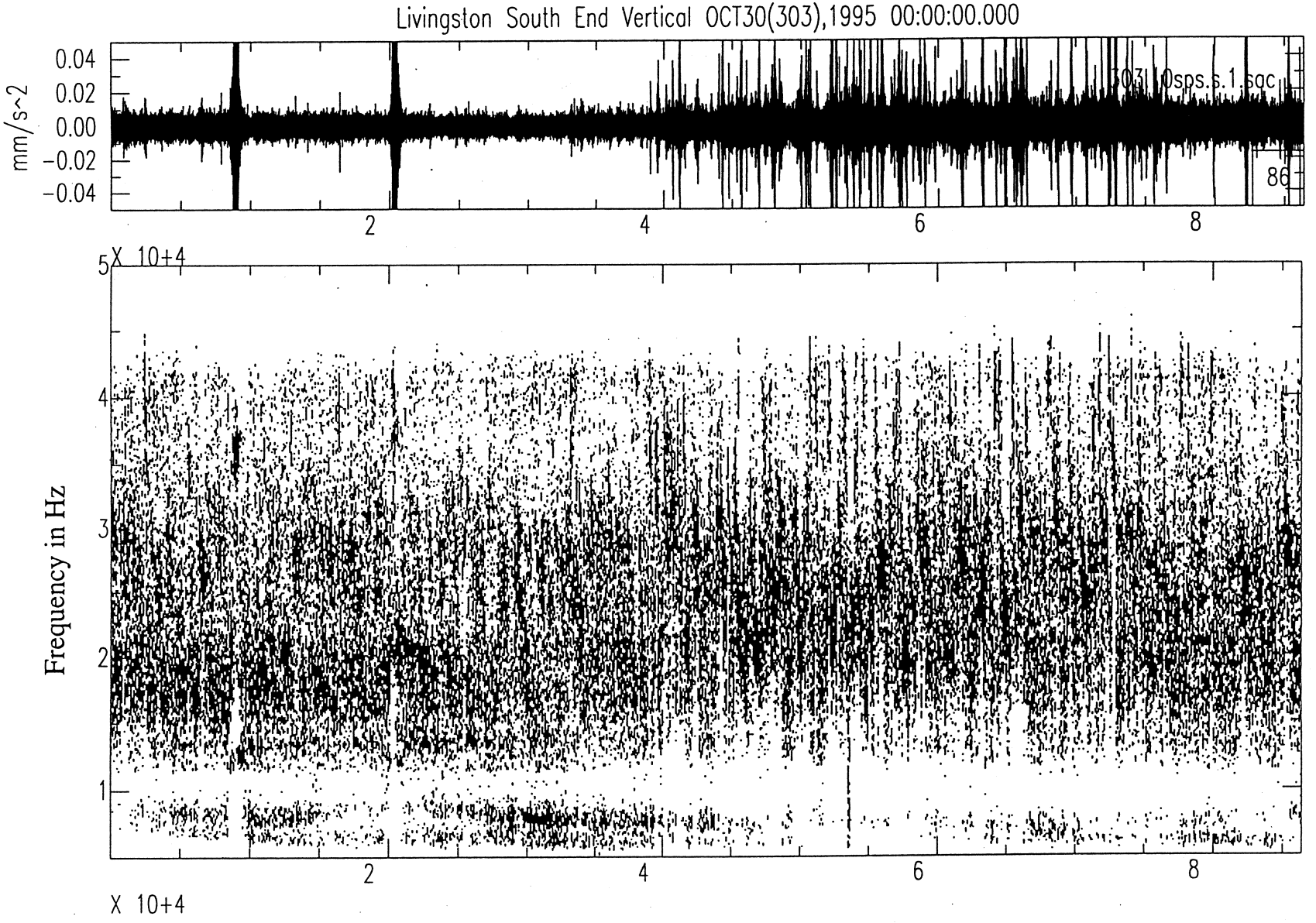

Figure 8.2-15. Black-and-white 0.5-5 Hz spectrogram for a 24-hour period at the South End. Time period begins at 6 p.m. CST. Note the higher-amplitude daily trains at about 10,000 and 20,000 s, and the increase in short-duration noise bursts in the right half of the spectrogram corresponding to daylight hours.

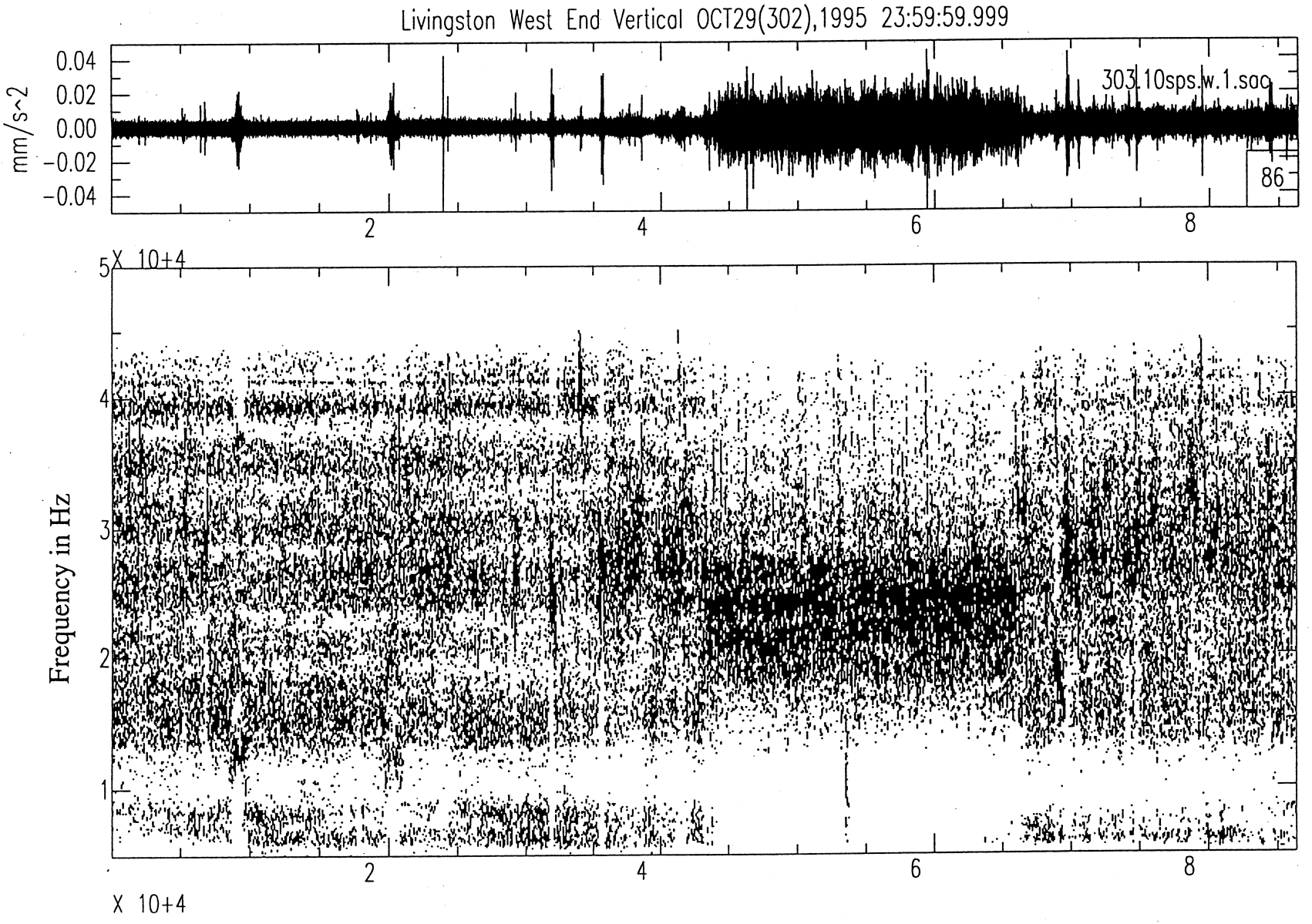

Figure 8.2-16. Black-and-white 0.5-5 Hz spectrogram for a 24-hour period at the West End. Time period begins at 6 p.m. CST. Note the train signals at about 10,000 and 20,000 s. The daylight-hours shown in the right half of the spectrogram show an increase in noise similar to that seen in Figure 8.2-1 when the pipeline was restarted.

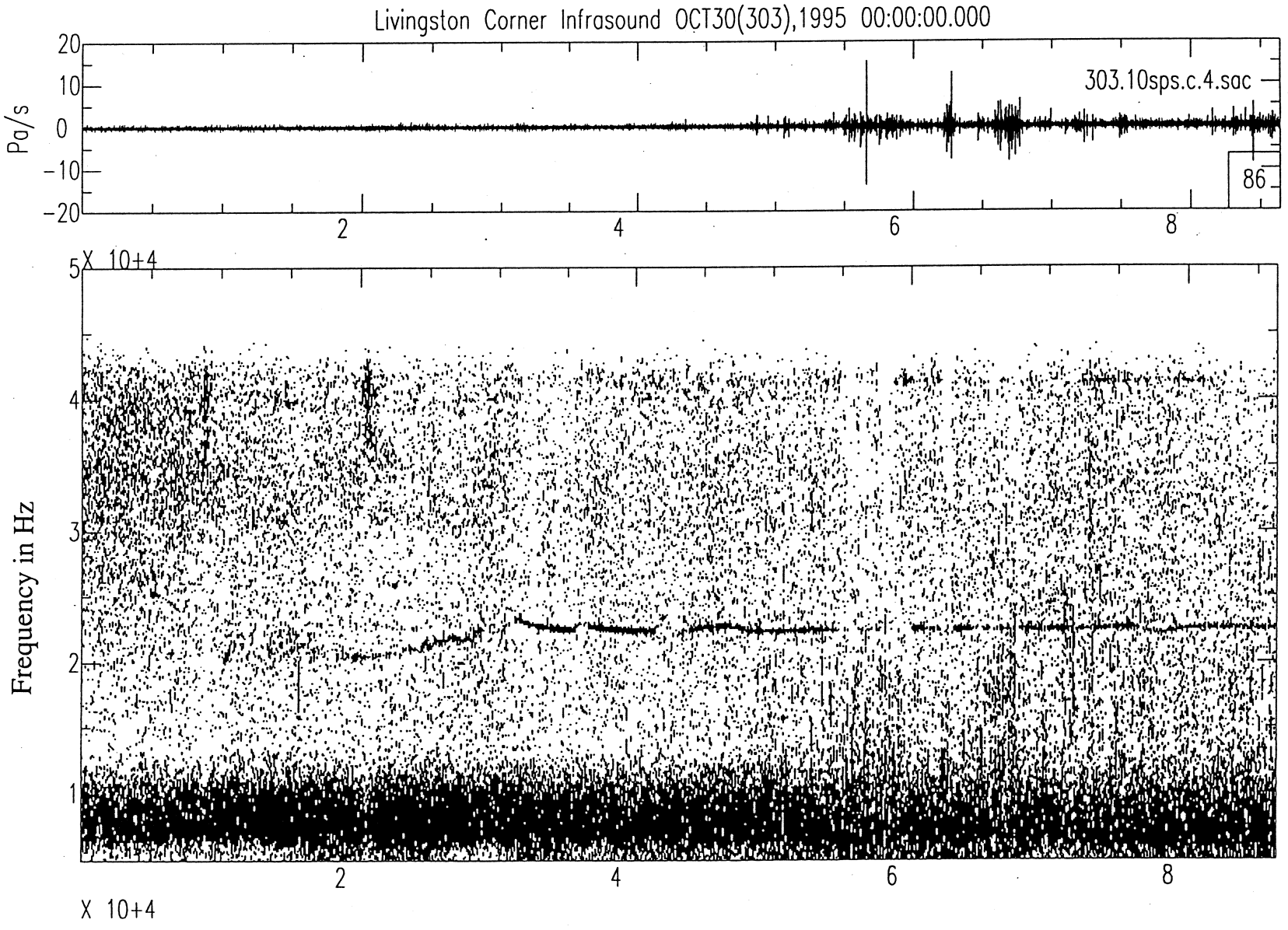

Figure 8.2-17. Black-and-white 0.5-5 Hz infrasound spectrogram for a 24-hour period at the Corner. The infrasound noise is increased during daylight hours (the right half of the spectrogram), but there is little direct comparison to the low-frequency seismic signal at this site for the same time period, shown in Figure 8.2-14.

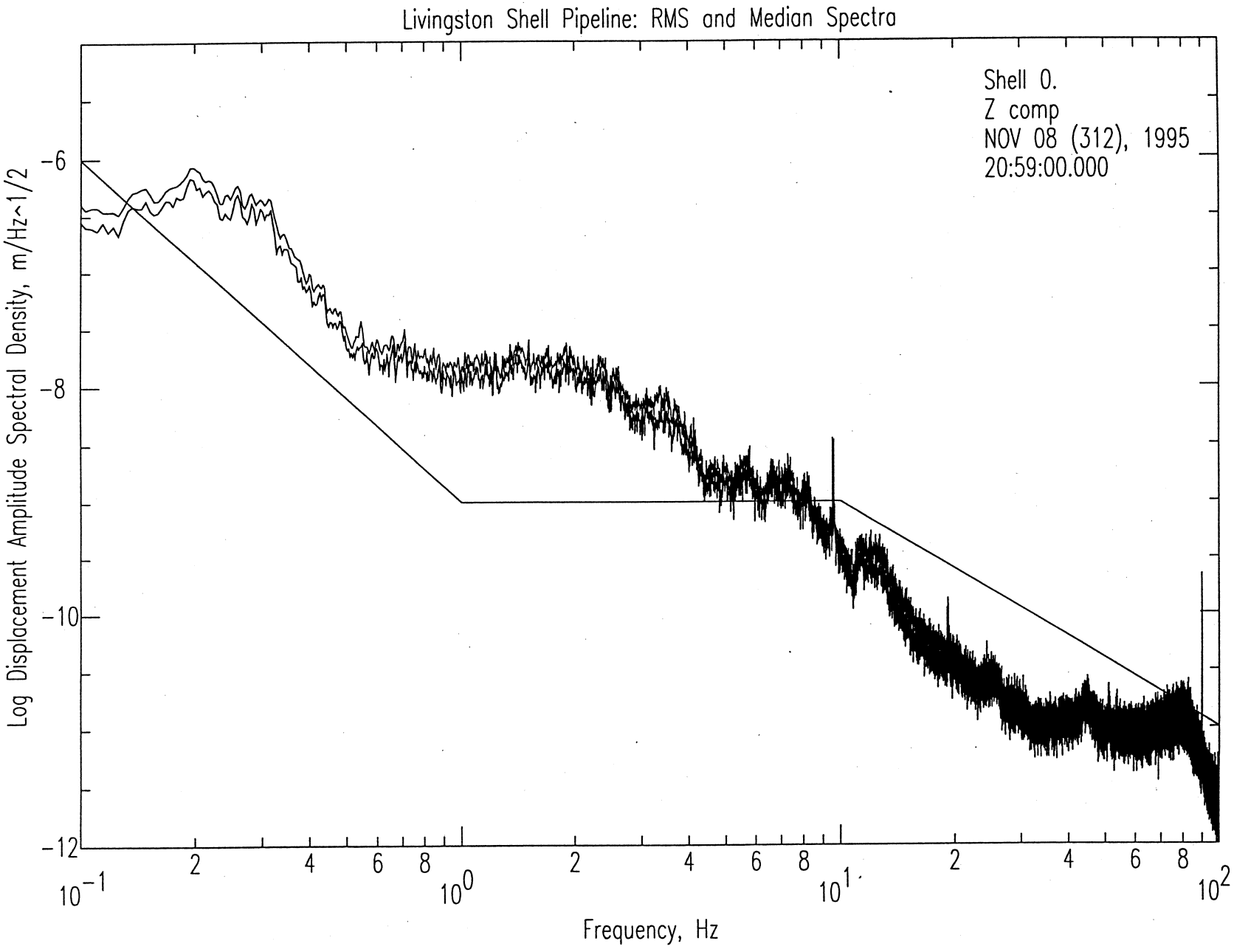

Figure 8.3-1. Amplitude spectra (median and r.m.s.) measured for a half-hour period in the center of the eastern right-of-way of the Shell "Capline" and Choctaw pipelines. The vertical component is shown.

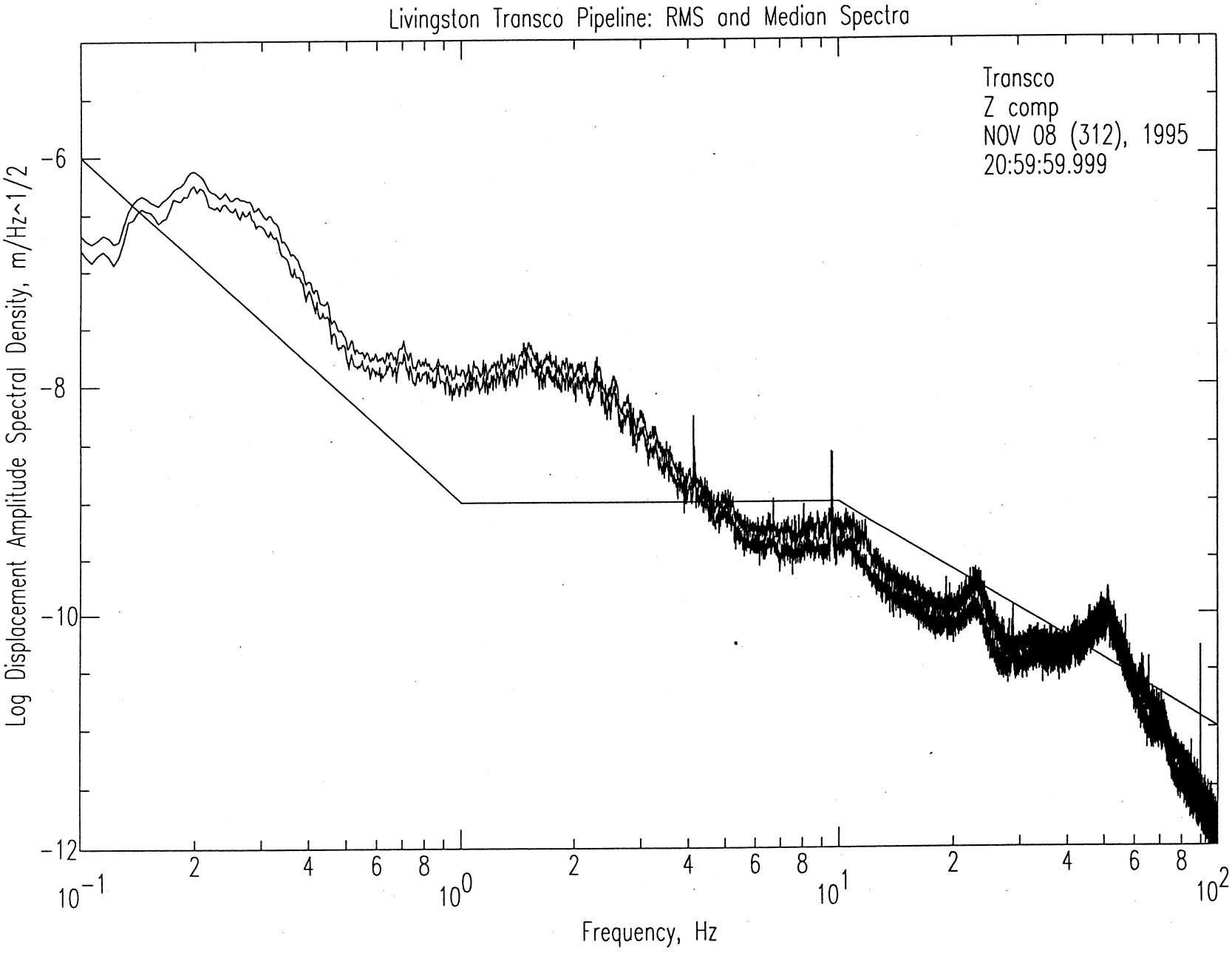

Figure 8.3-2. Amplitude (median and r.m.s.) spectra measured for a half-hour period in the center of the western right-of-way of the three Transcontinental pipelines. The vertical component is shown for the same time period as in Figure 8.3-1.

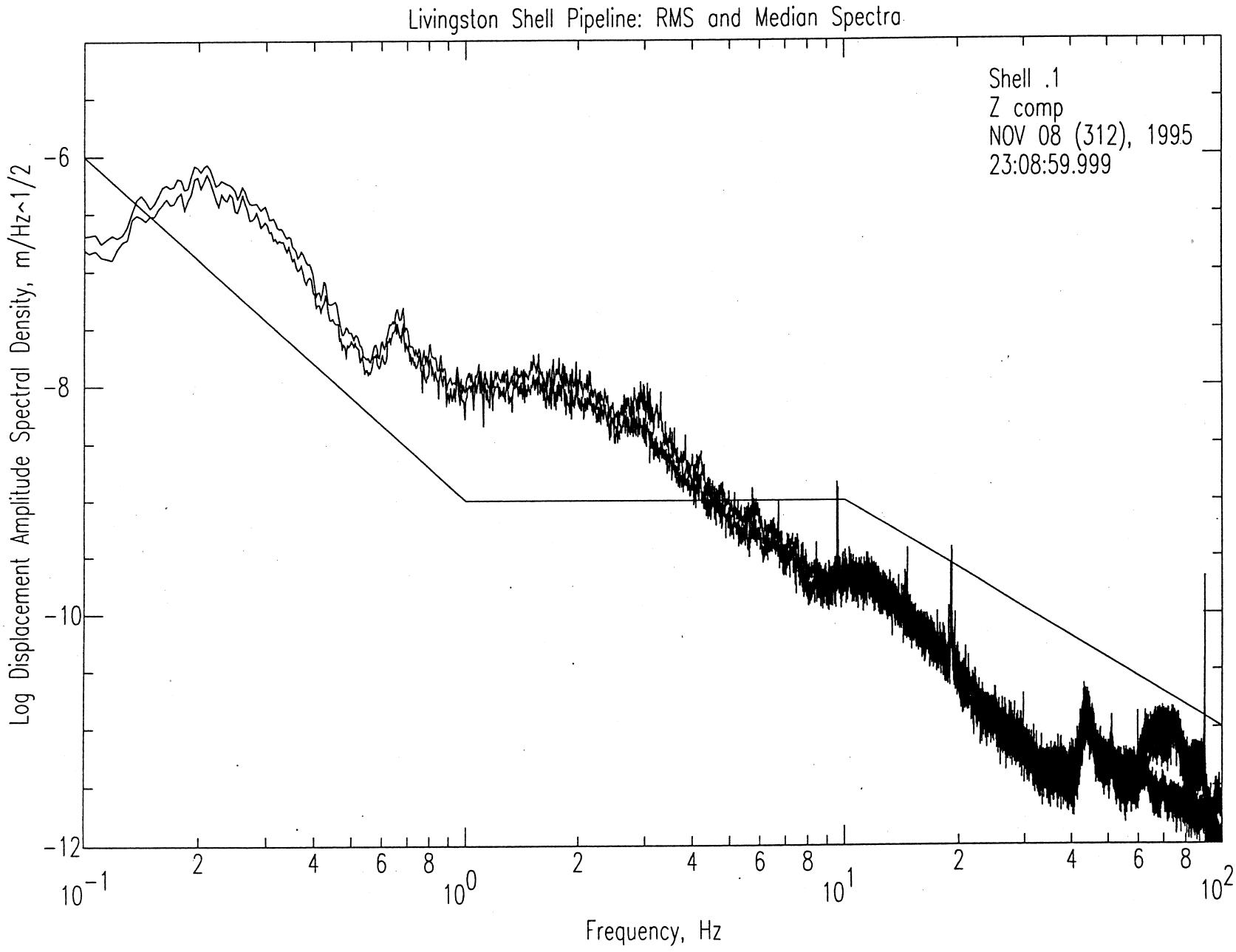

Figure 8.3-3.Amplitude spectra (median and r.m.s.) measured for a half-hour period 0.1 miles east of the eastern right-of-way of the Shell "Capline" and Choctaw pipelines. The vertical component is shown.

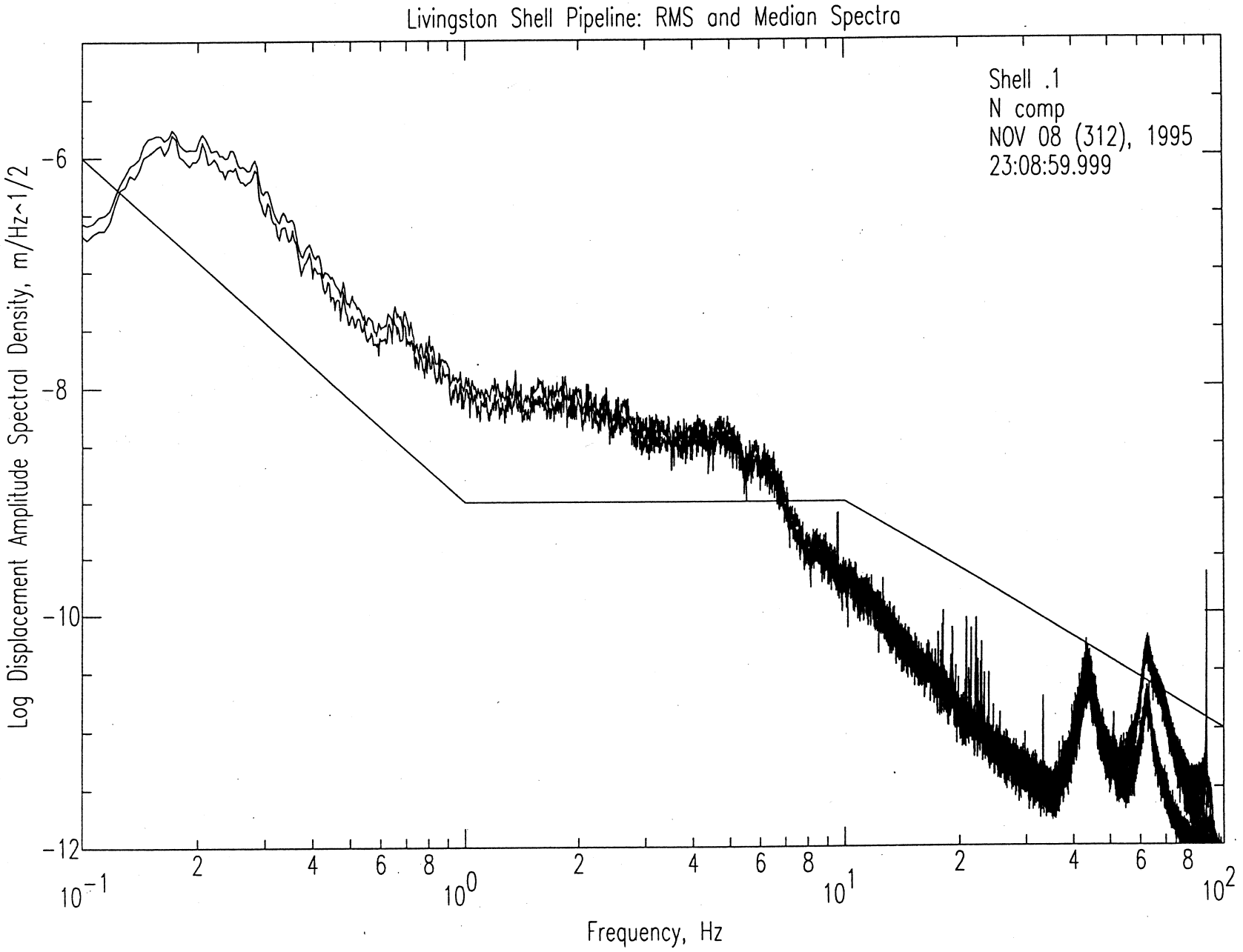

Figure 8.3-4.Amplitude spectra (median and r.m.s.) measured for a half-hour period 0.1 miles east of the eastern right-of-way of the Shell "Capline" and Choctaw pipelines. The north component is shown.

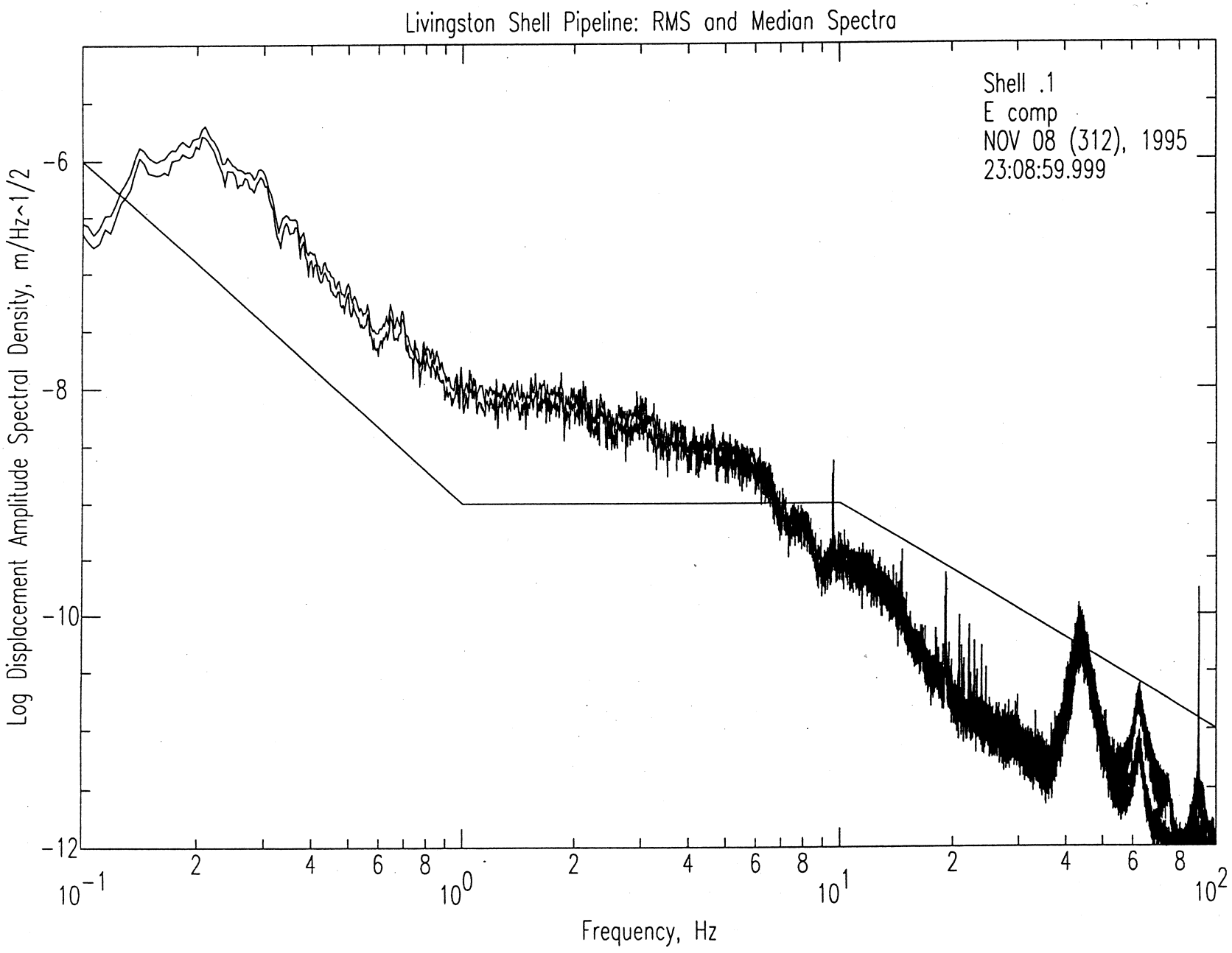

Figure 8.3-5.Amplitude spectra (median and r.m.s.) measured for a half-hour period 0.1 miles east of the eastern right-of-way of the Shell "Capline" and Choctaw pipelines. The east component is shown.

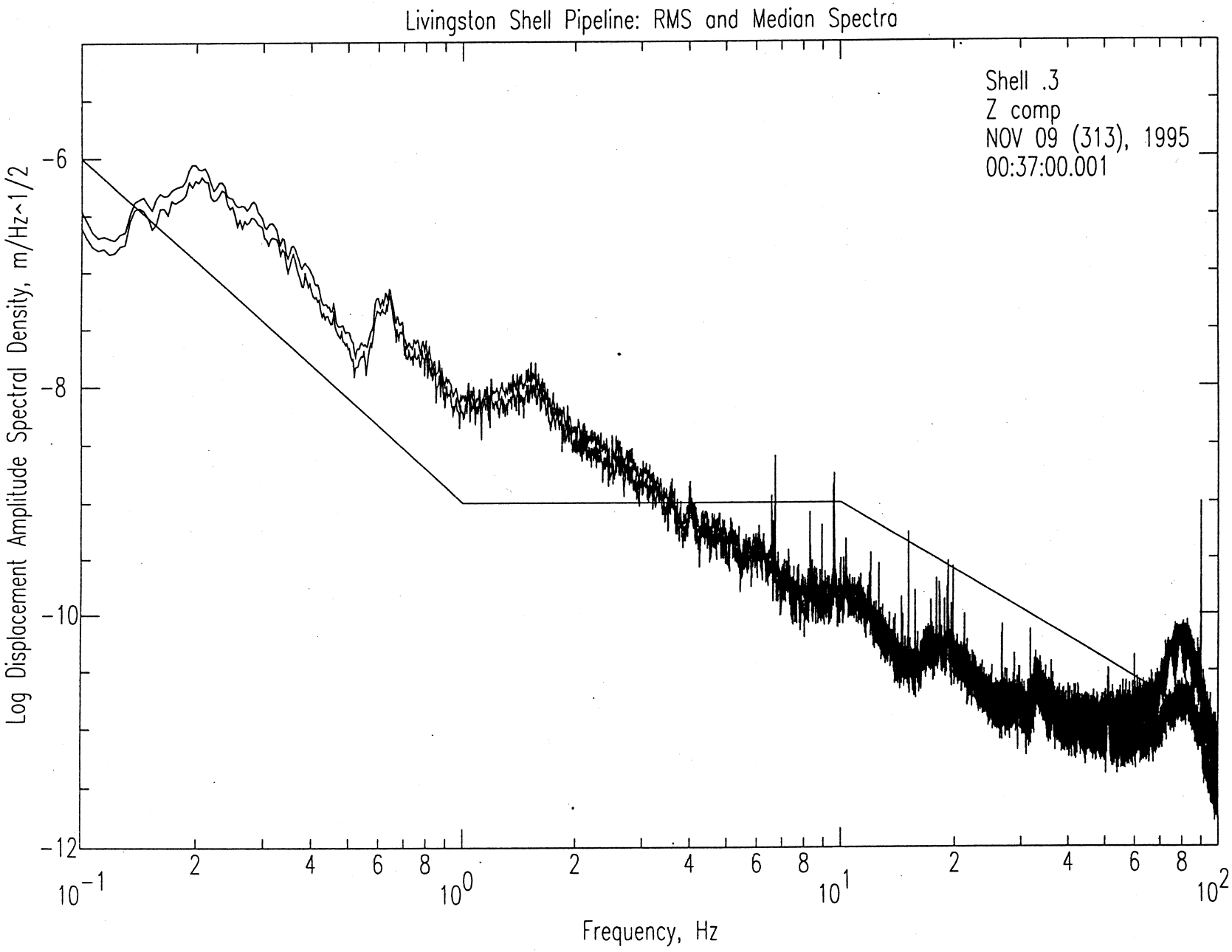

Figure 8.3-6.Amplitude spectra (median and r.m.s.) measured for a half-hour period 0.3 miles east of the eastern right-of-way of the Shell "Capline" and Choctaw pipelines. The vertical component is shown.

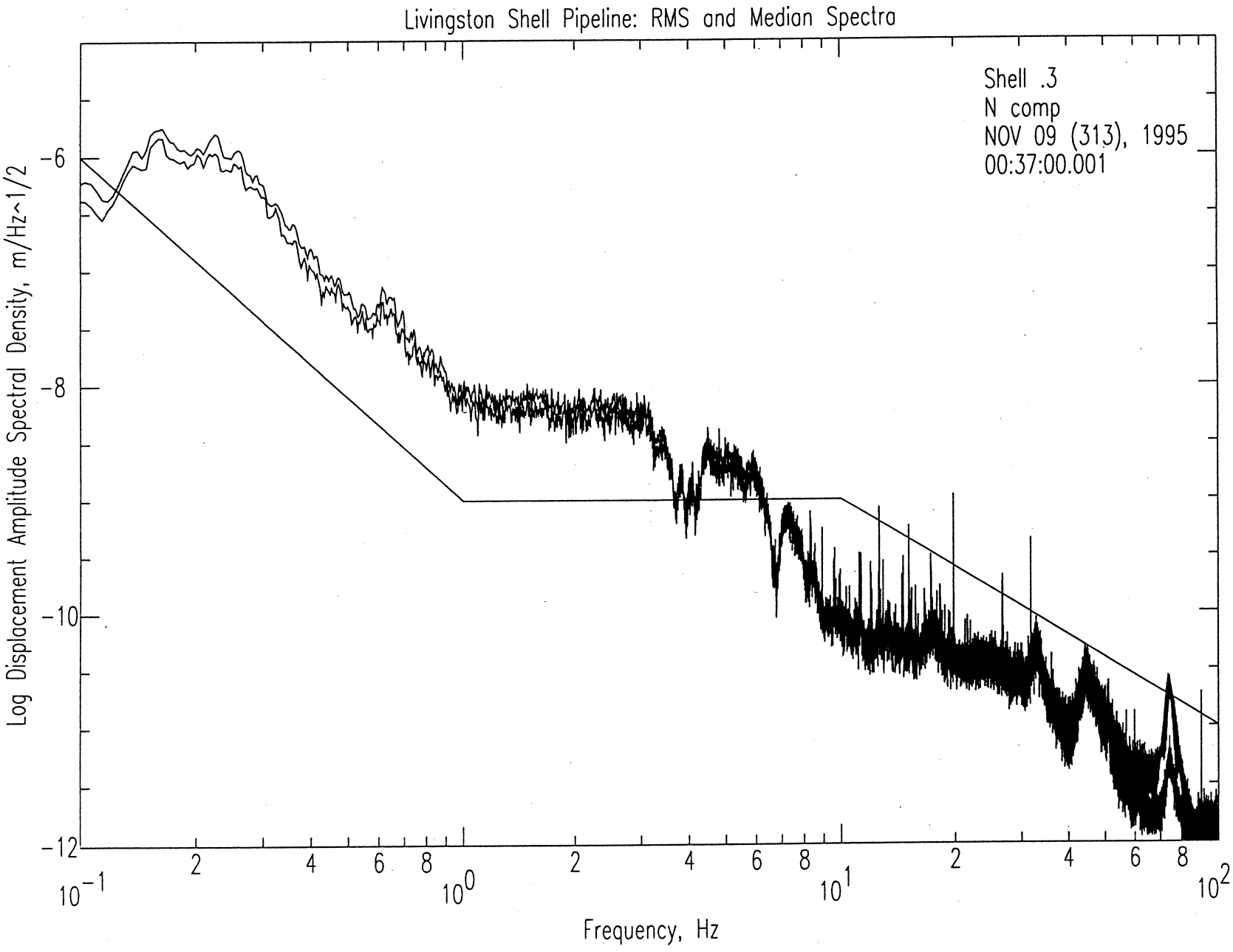

Figure 8.3-7.Amplitude spectra (median and r.m.s.) measured for a half-hour period 0.3 miles east of the eastern right-of-way of the Shell "Capline" and Choctaw pipelines. The north component is shown.

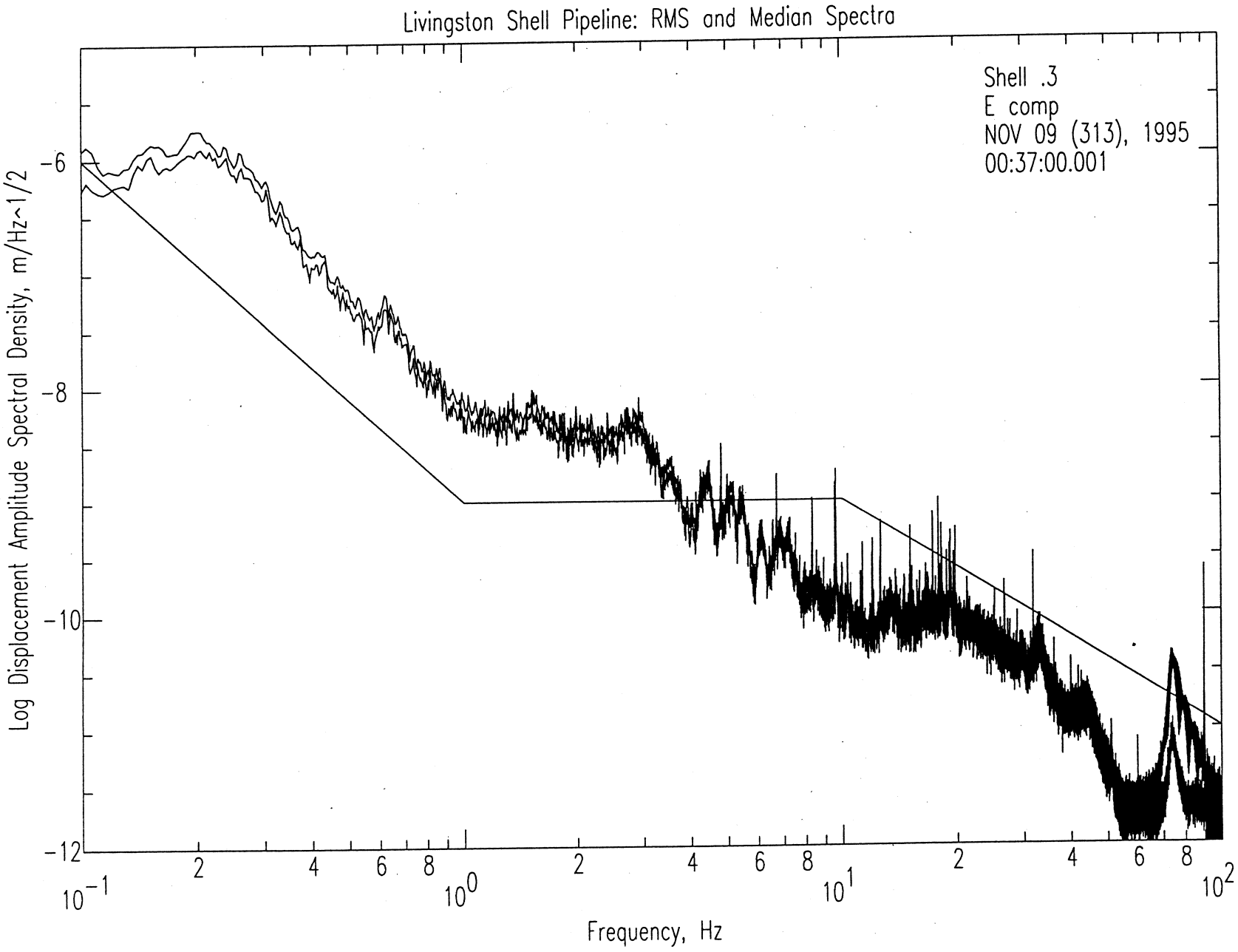

Figure 8.3-8. Amplitude spectra (median and r.m.s.) measured for a half-hour period 0.3 miles east of the eastern right-of-way of the Shell "Capline" and Choctaw pipelines. The east component is shown.

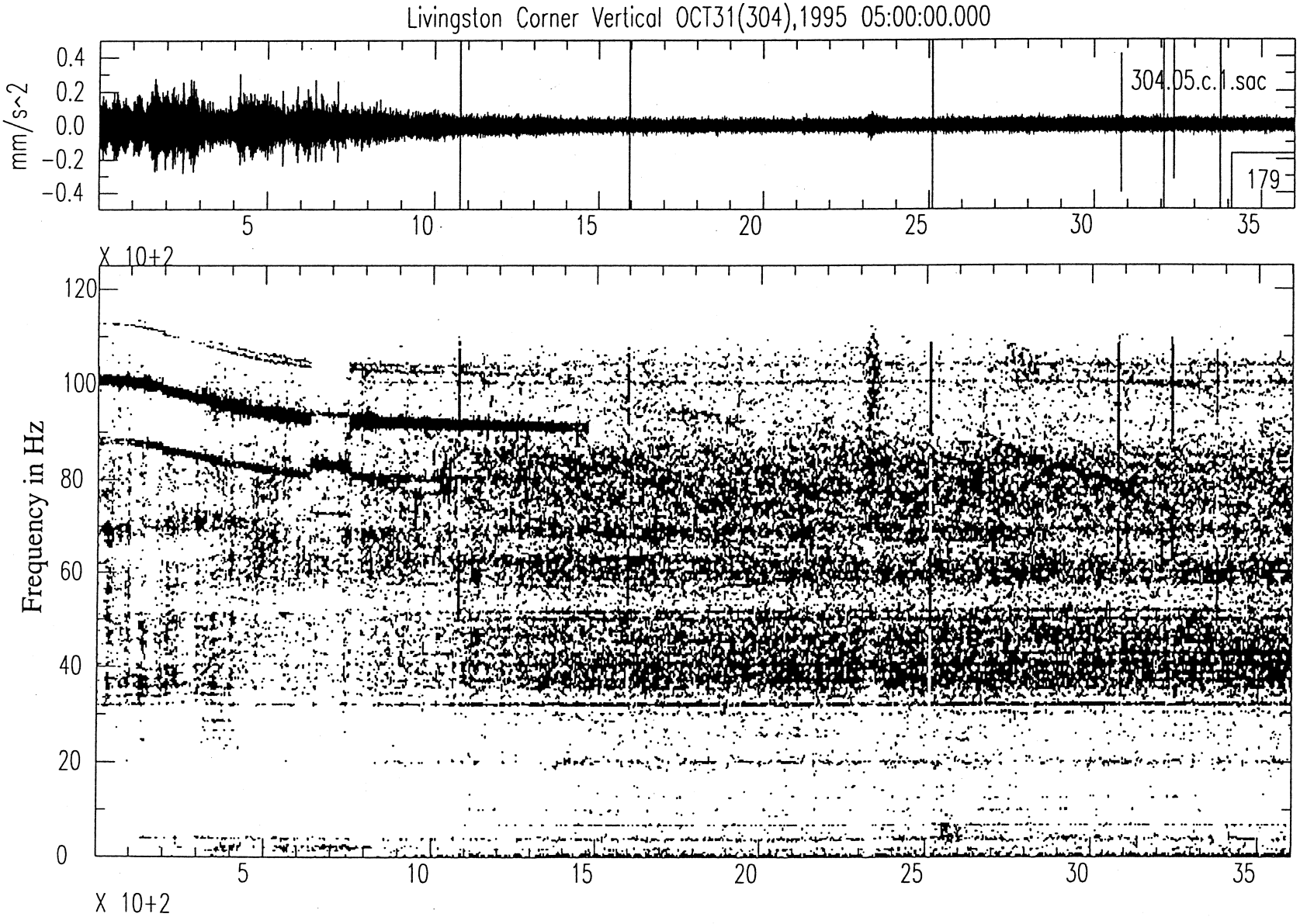

Figure 9.1-1. Black-and-white spectrogram of noise at the Corner from a train passing south of the site.

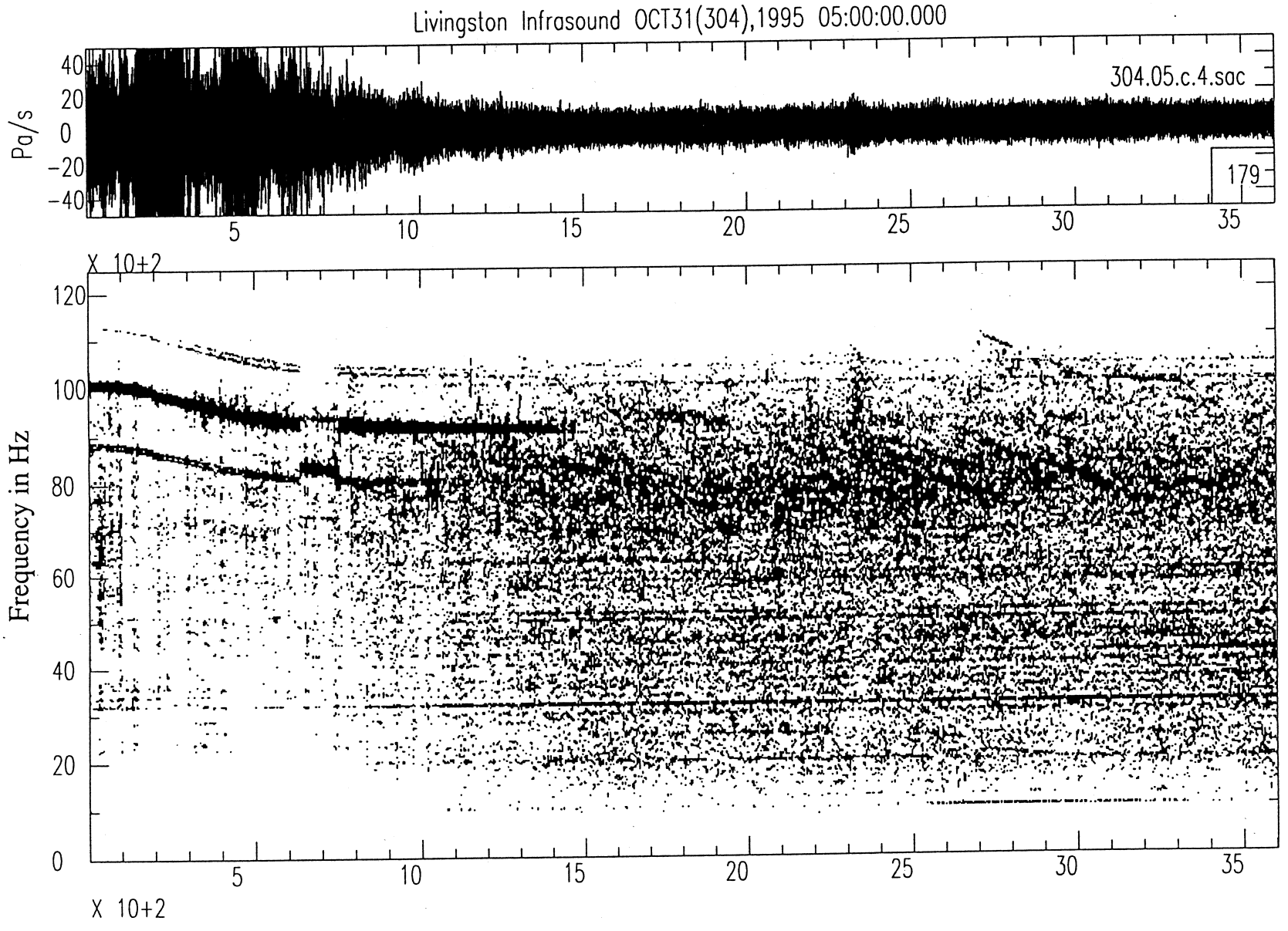

Figure 9.1-2. Black-and-white infrasound spectrogram of noise at the Corner from a train passing south of the site.

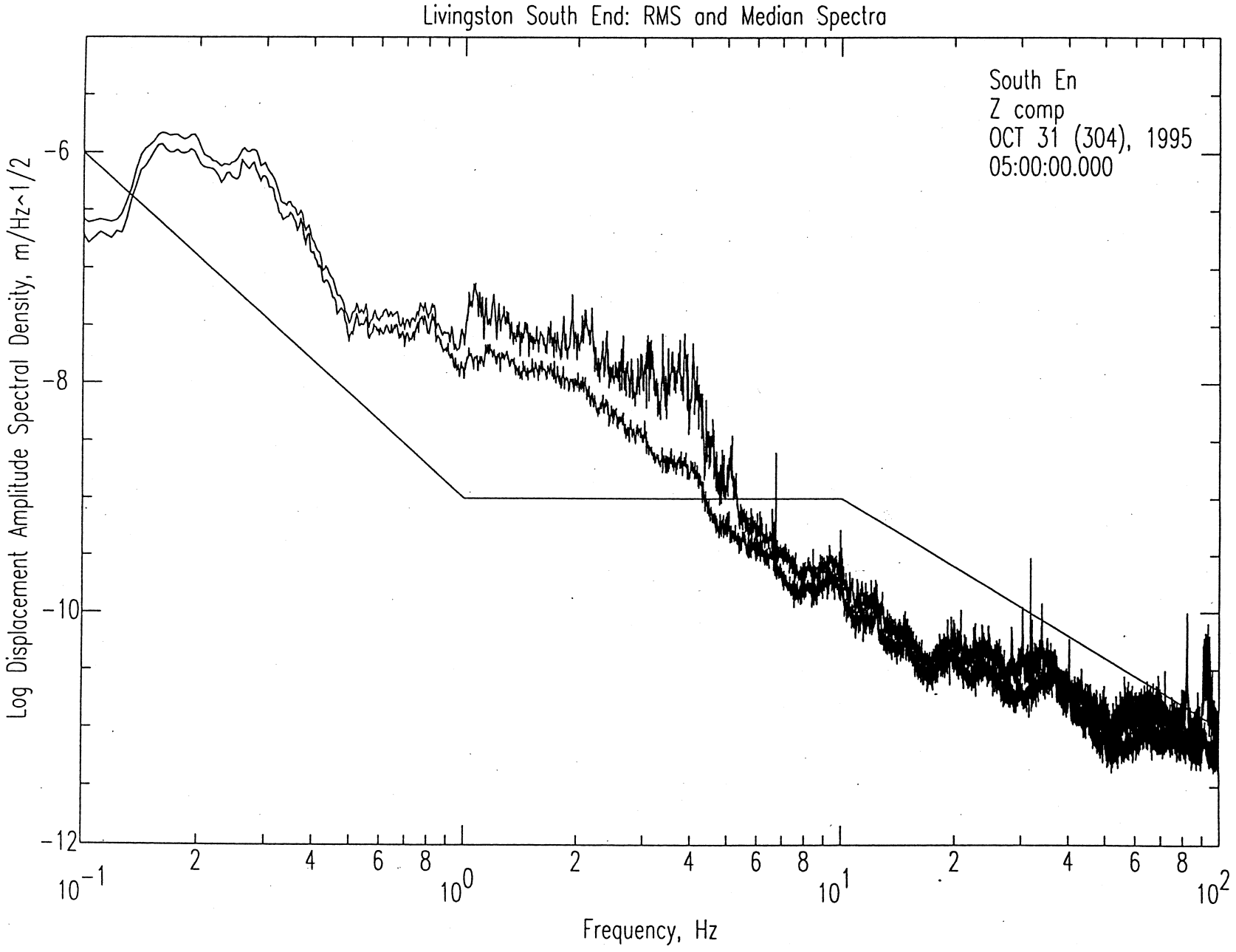

Figure 9.1-3. Amplitude spectra (median and r.m.s.) for a one-hour period at the South End when a train passed south of the site.

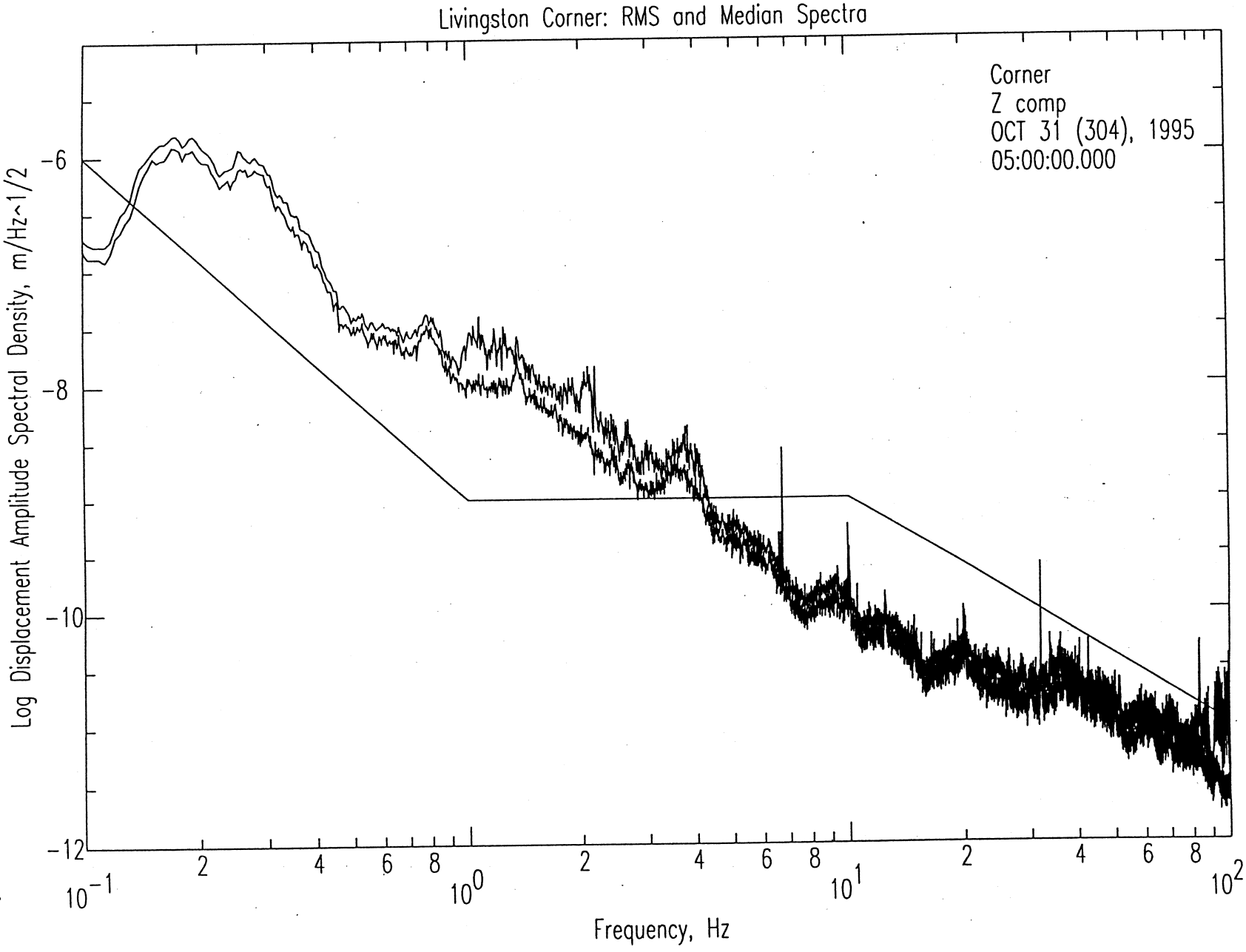

Figure 9.1-4. Amplitude spectra (median and r.m.s.) for a one-hour period at the Corner when a train passed south of the site.

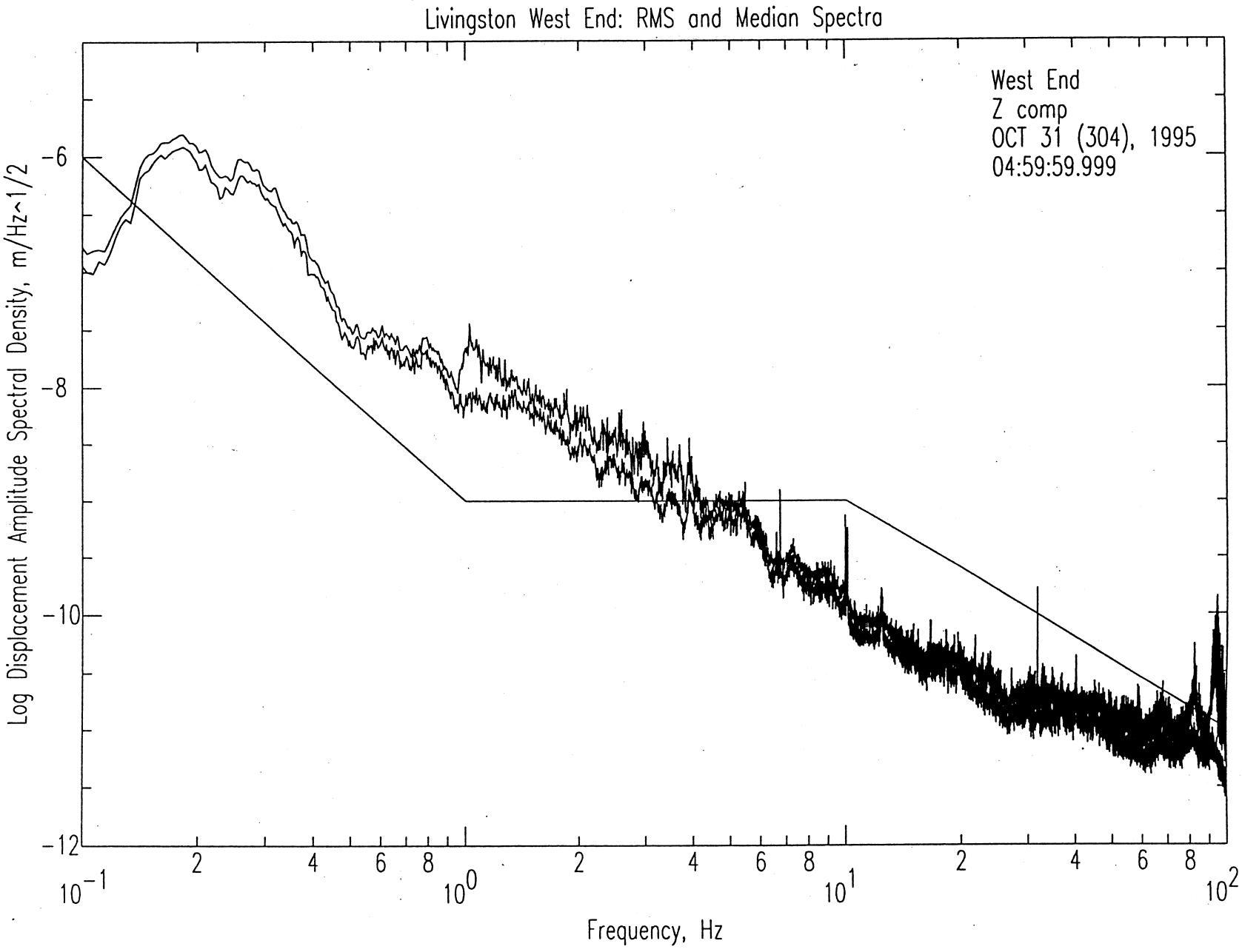

Figure 9.1-5. Amplitude spectra (median and r.m.s.) for a one-hour period at the West End when a train passed south of the site.

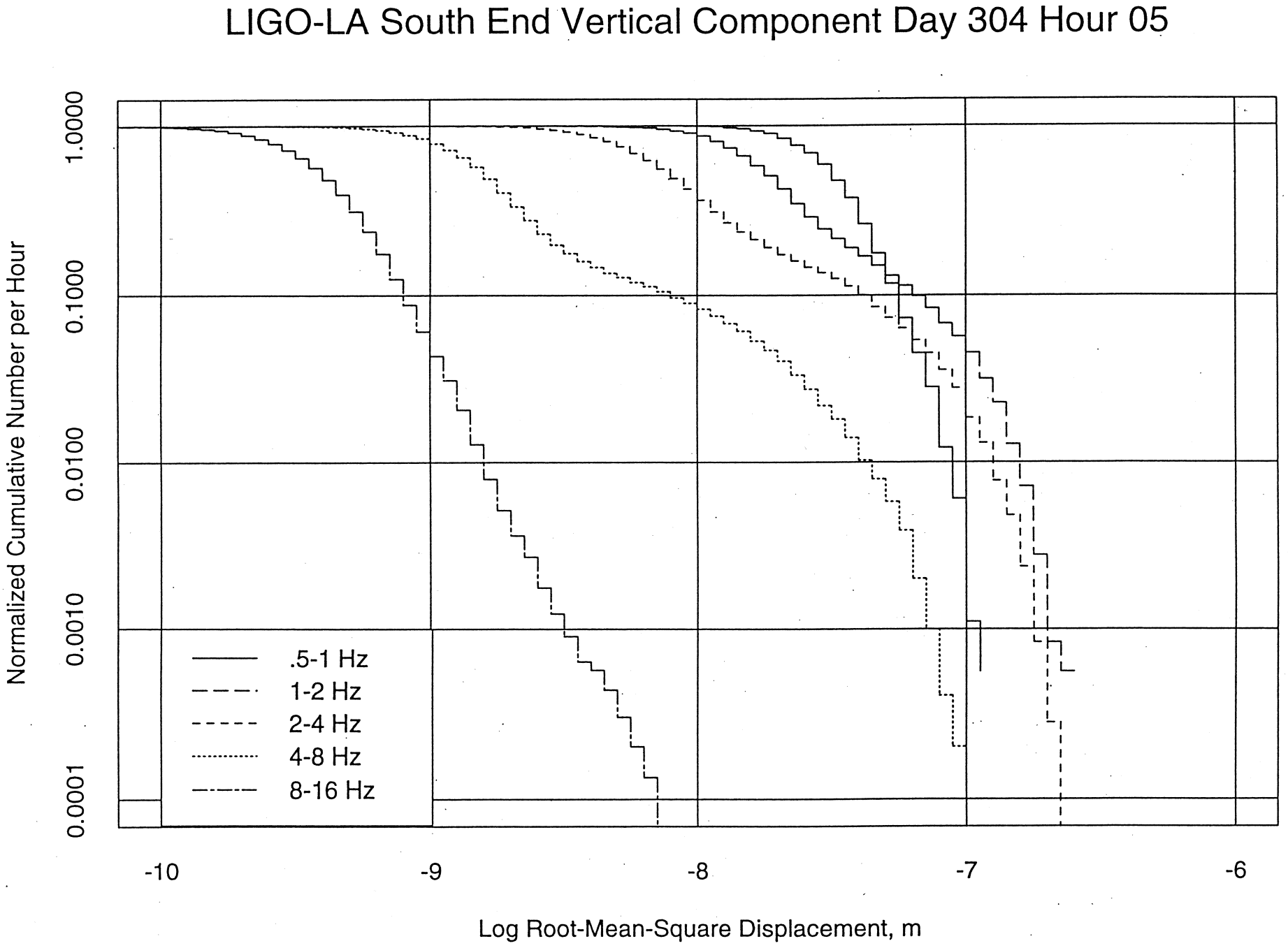

Figure 9.1-6. Amplitude distribution in five frequency bands at the South End when a train passed south of the site. The time period and signal are the same as those forming the amplitude spectra in Figure 9.1-3.

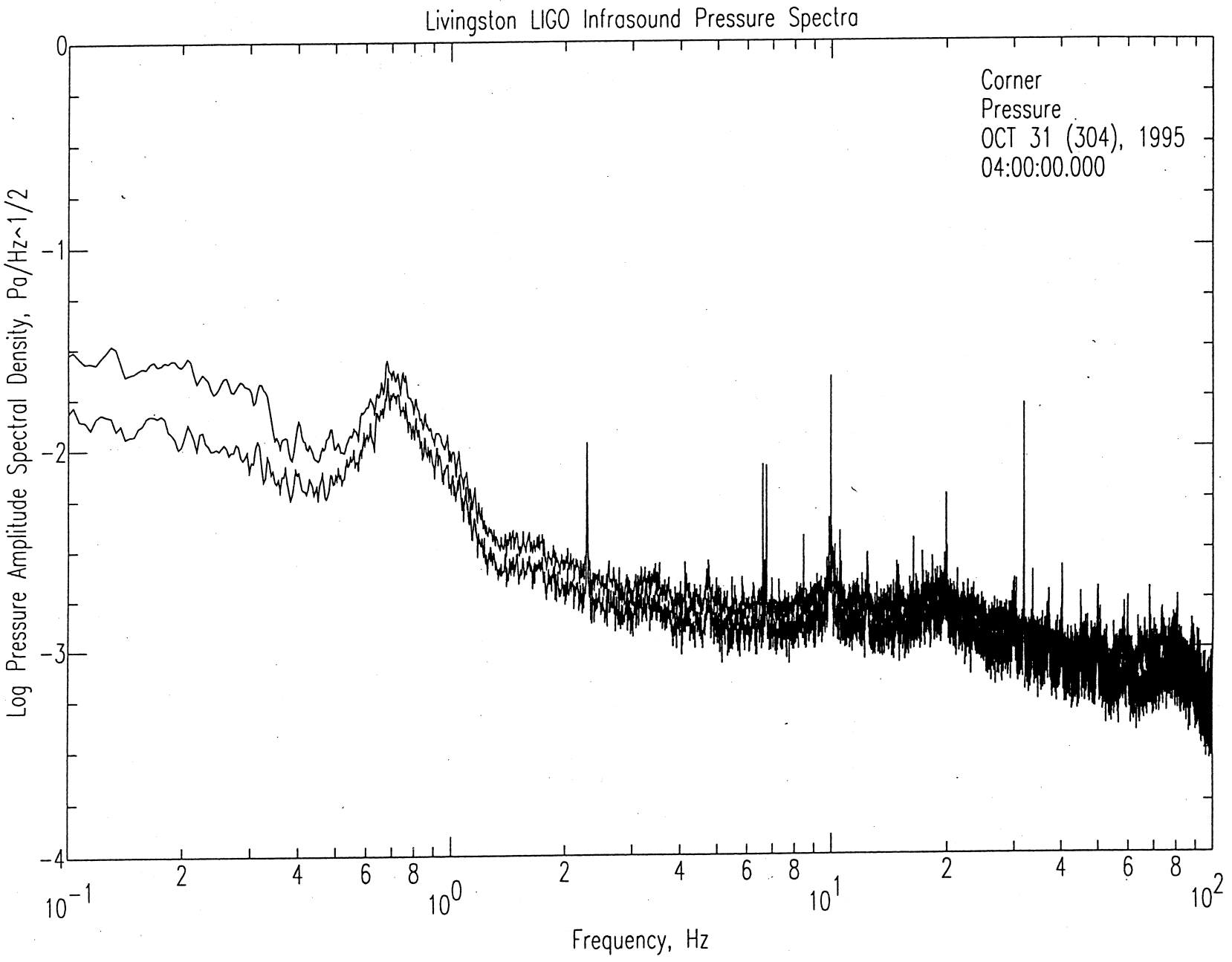

Figure 9.2-1. Infrasound amplitude spectra (median and r.m.s.) for a one-hour period, showing broad noise peaked at 0.7 Hz and multiple spikes or monotones at higher frequencies (e.g. at 10 Hz).

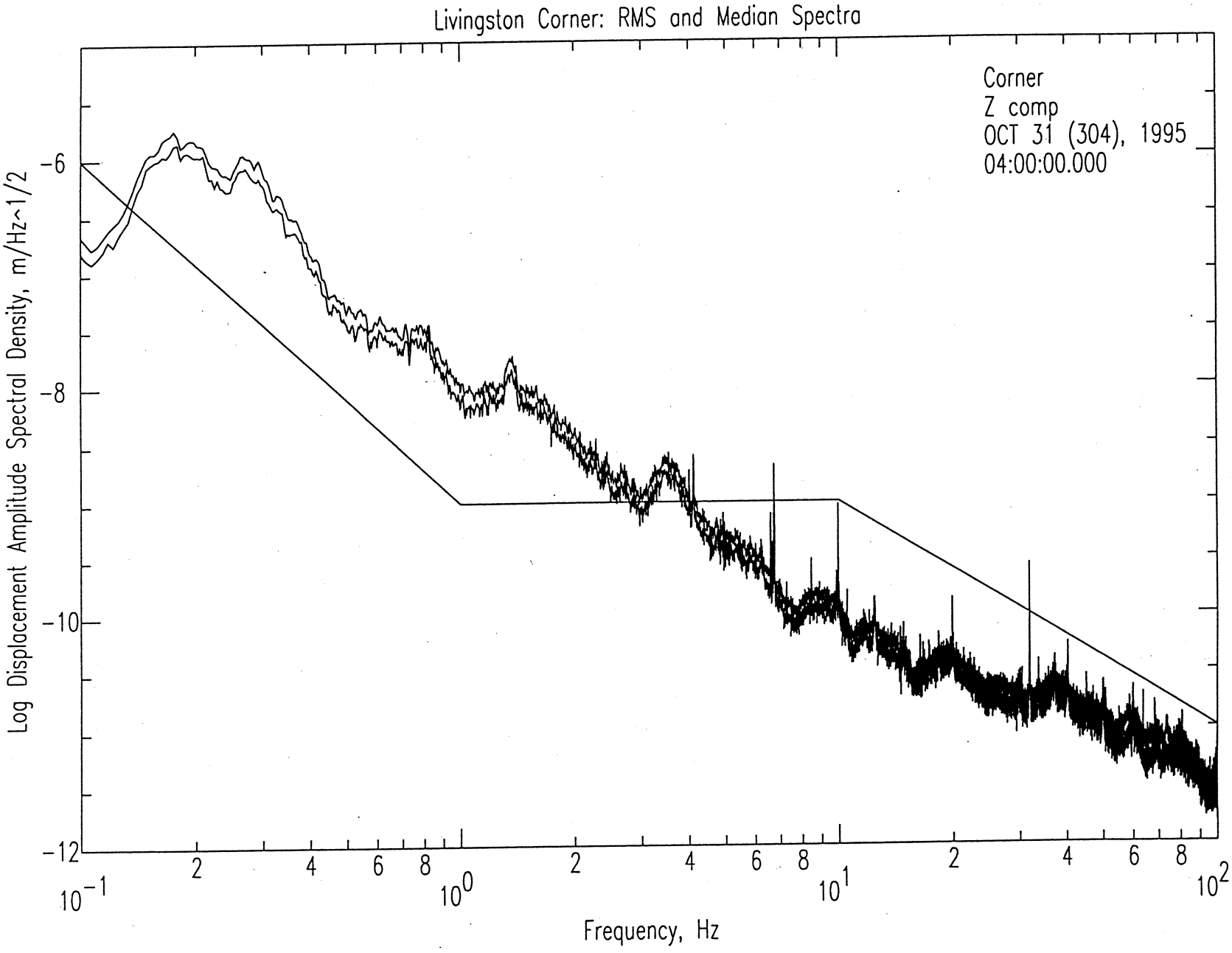

Figure 9.2-2. Vertical component amplitude spectra (median and r.m.s.) for a one-hour period, showing many of the same spikes or monotones as the infrasound spectra shown in Figure 9.2-1. The spikes in the seismic spectrum are interpreted to be due to acoustic signals being transmitted into the ground. The acoustic spectrum spike at 2 Hz is notably absent in the seismic spectrum.

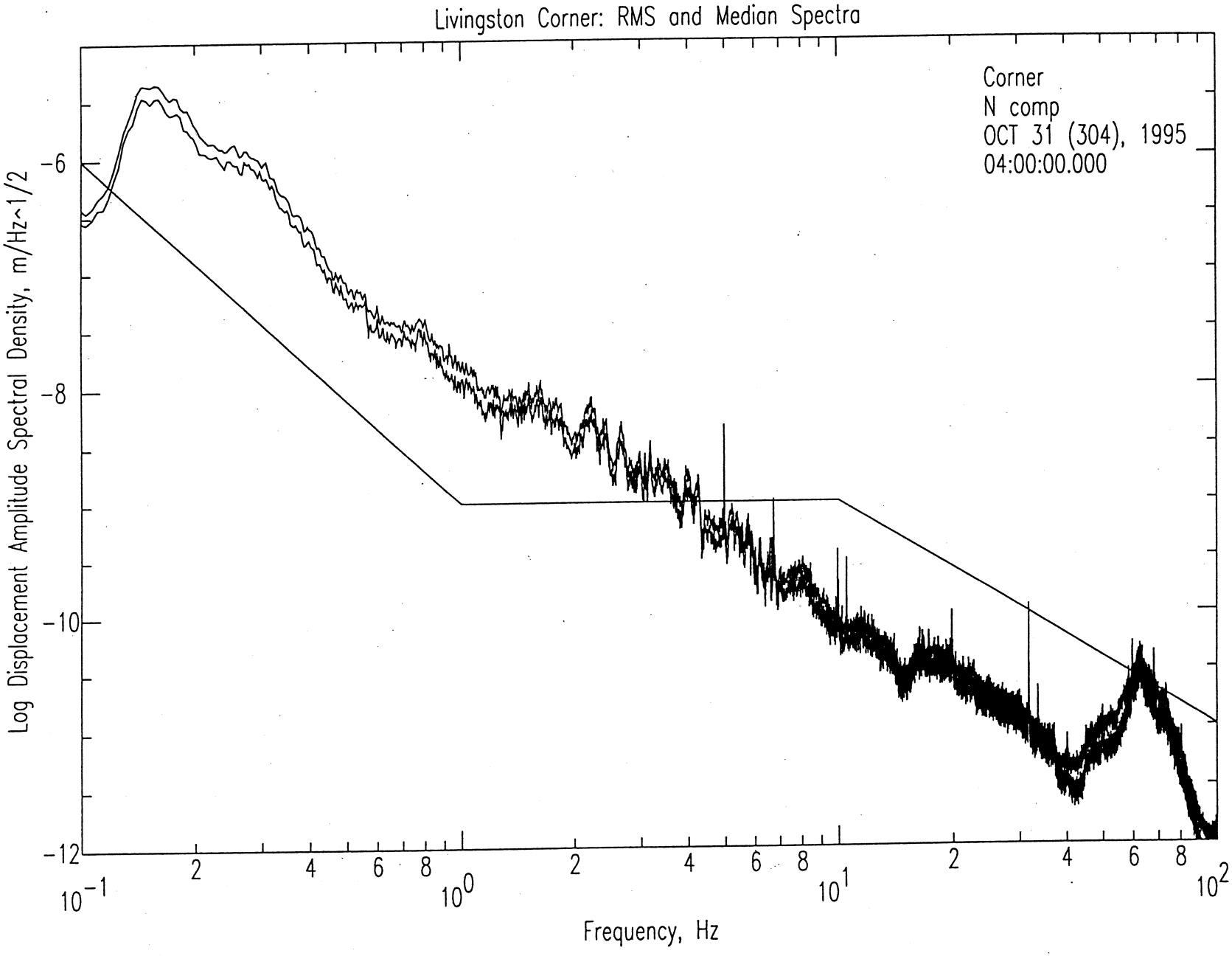

Figure 9.2-3. North component amplitude spectra (median and r.m.s.) or the one-hour period shown in Figures 9.2-1 and 9.2-2. Note the reduced amplitude of the noise spikes at 6.5 and 10 Hz compared to Figures 9.2-1 and 9.2-2.

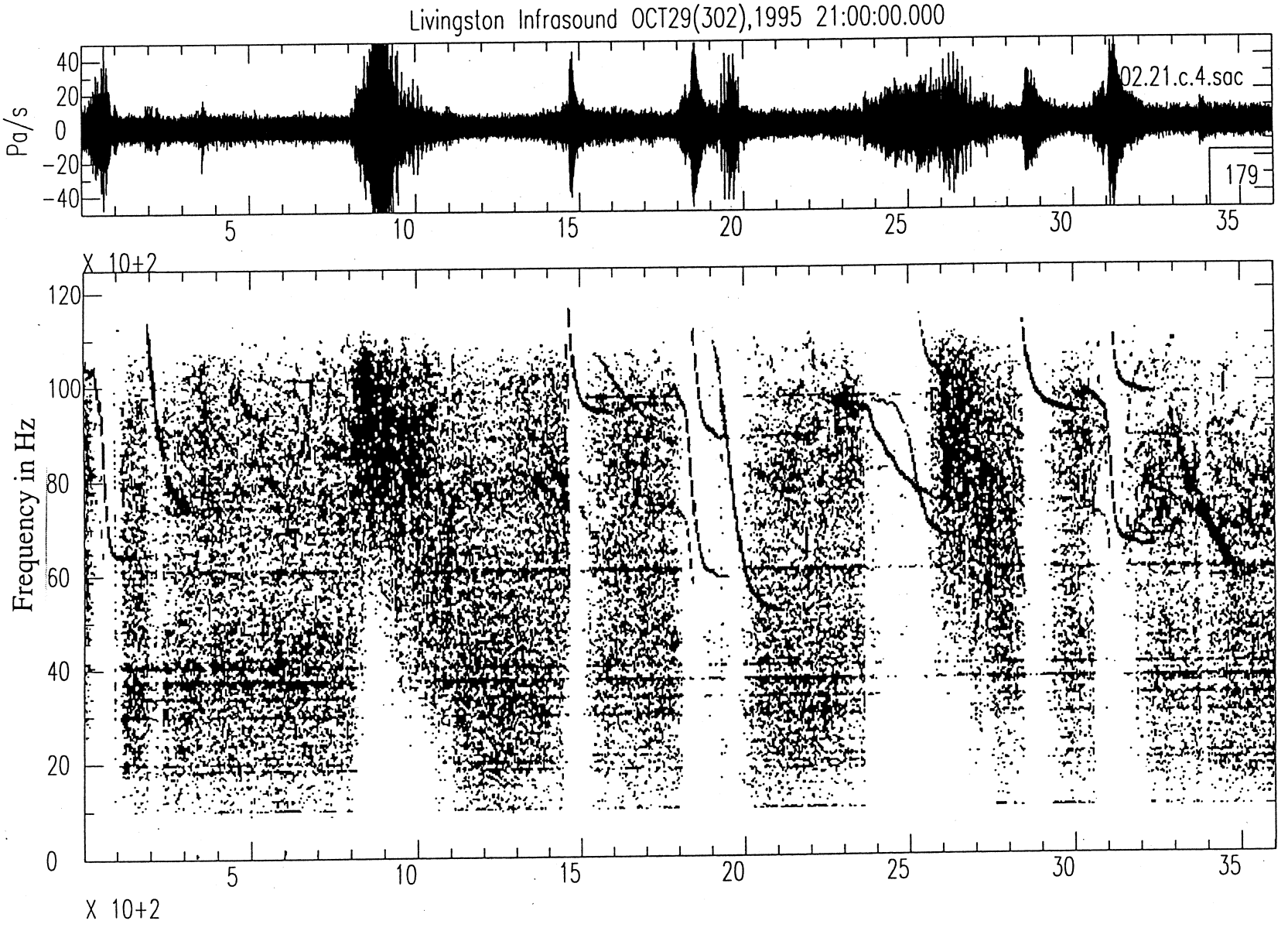

Figure 9.2-4. Black-and-white spectrogram of infrasound signals primarily showing examples of aircraft "glide tones". The noise burst from 800 to 1100 s is referred to as an amorphous acoustic burst in the text.

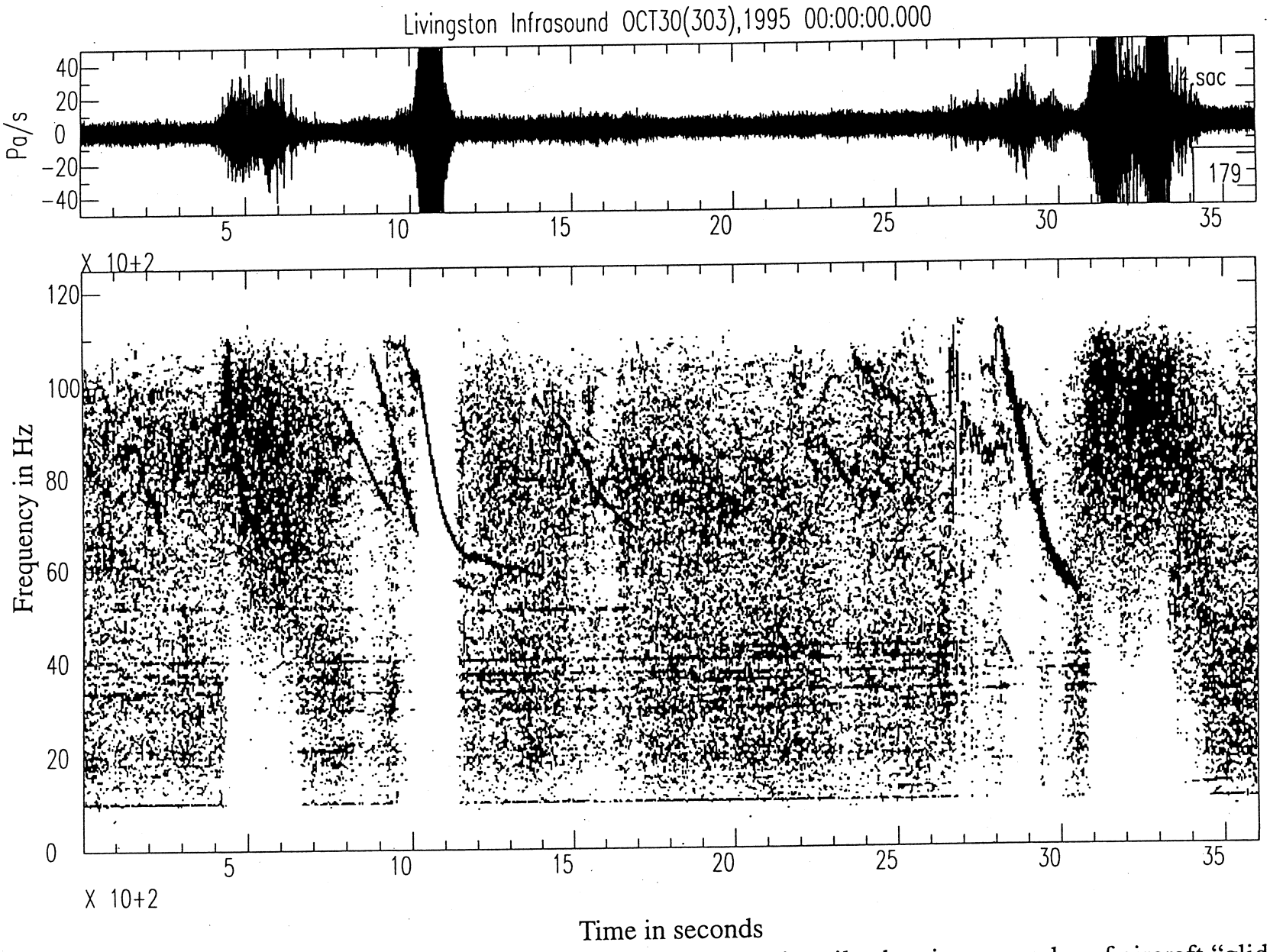

Figure 9.2-5. Black-and-white spectrogram of infrasound signals primarily showing examples of aircraft "glide tones". Two examples of amorphous acoustic bursts are seen at 400-600 and 3000-3500 s, the former showing a subtle doppler phenomenon superposed.

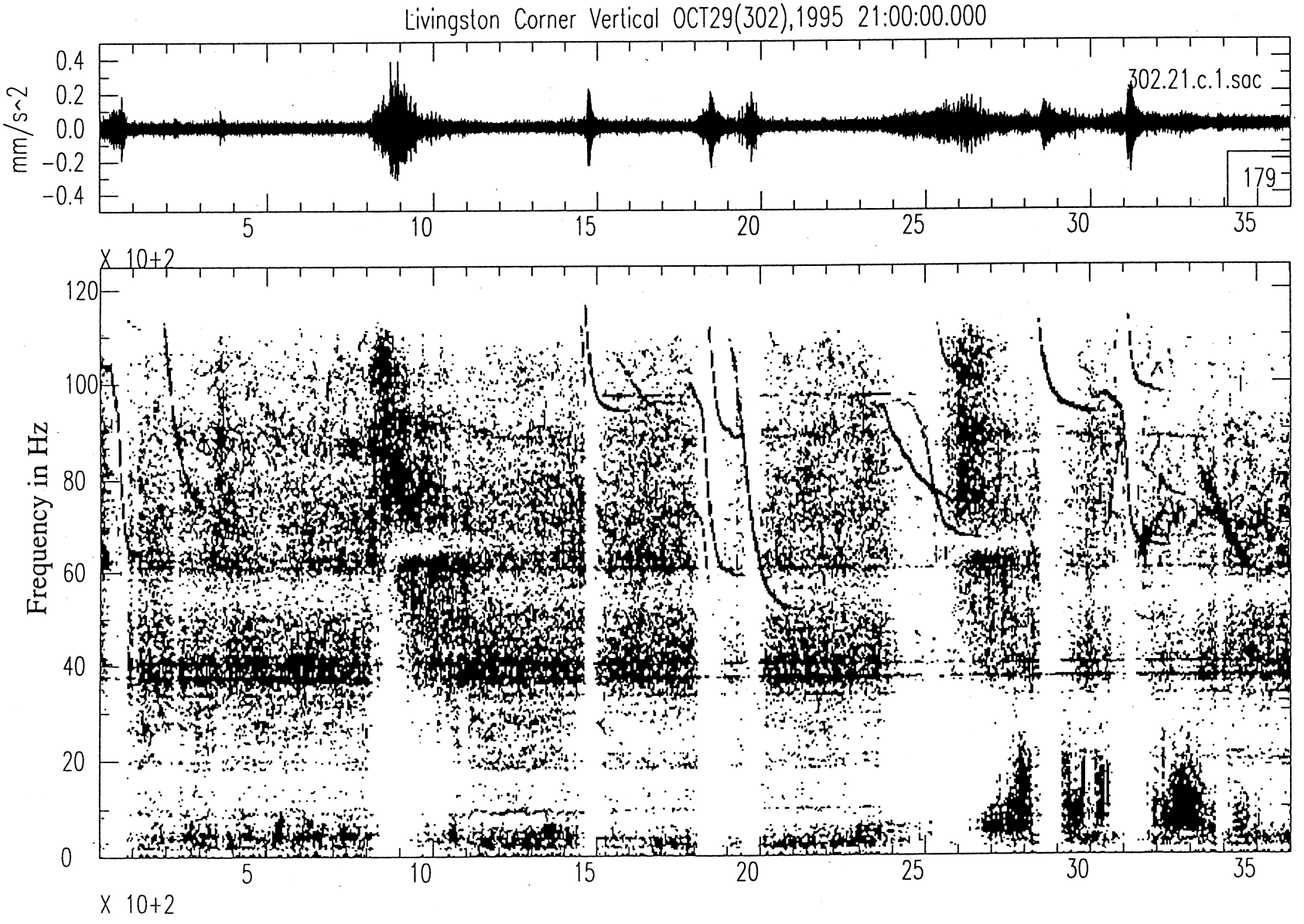

Figure 9.2-6. Black-and-white spectrogram of vertical seismic signals showing examples of aircraft "glide tones" that were observed simultaneously on the infrasound spectrogram in Figure 9.2-4. The noise burst from 800 to 1100 s is referred to as an amorphous acoustic burst in the text.

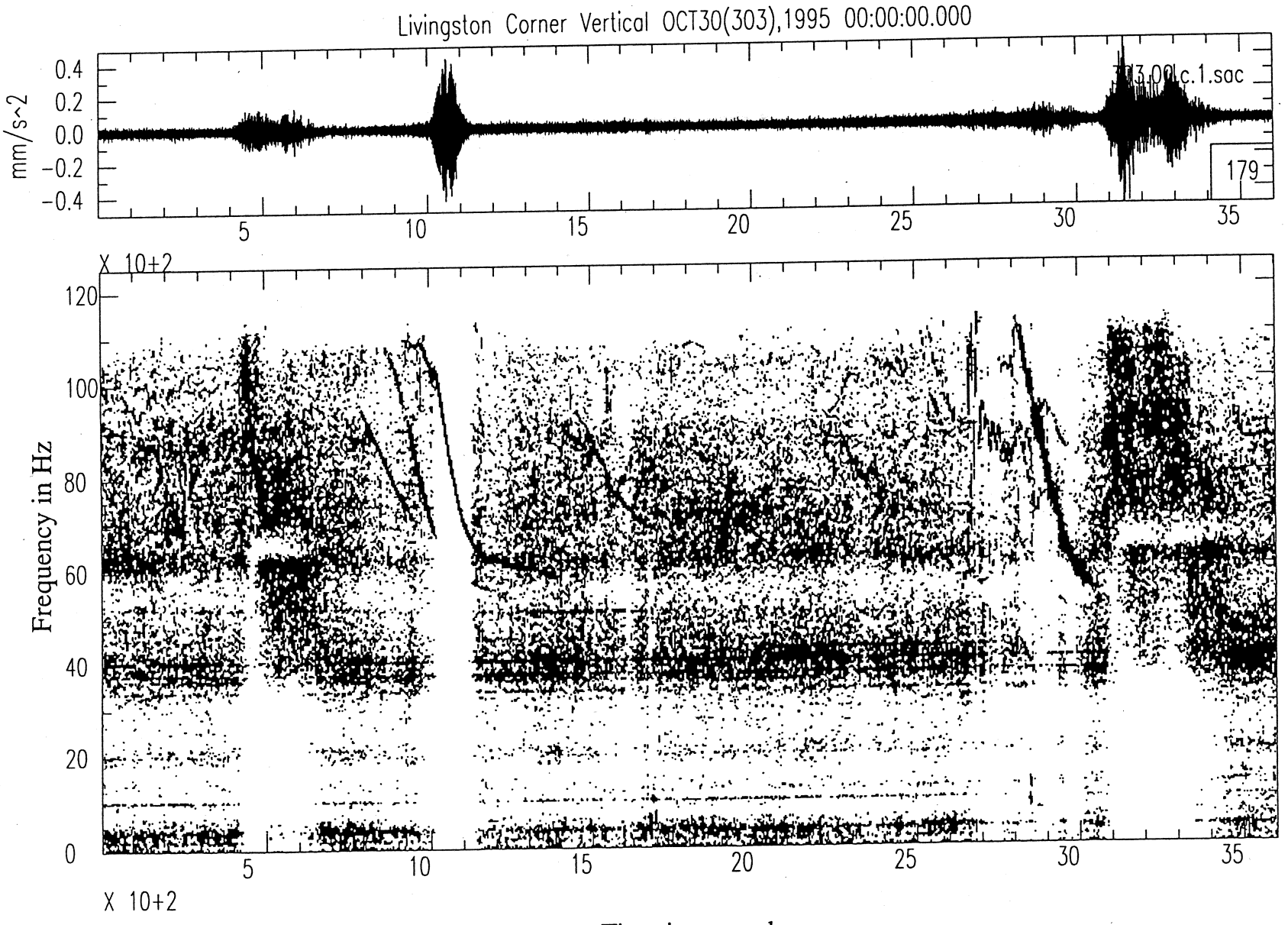

Figure 9.2-7. Black-and-white spectrogram of vertical seismic signals primarily showing examples of aircraft "glide tones" that were observed simultaneously on the infrasound spectrogram in Figure 9.2-5. Two examples of amorphous acoustic bursts are seen at 400-600 and 3000-3500 s, the former showing a subtle doppler phenomenon superposed.

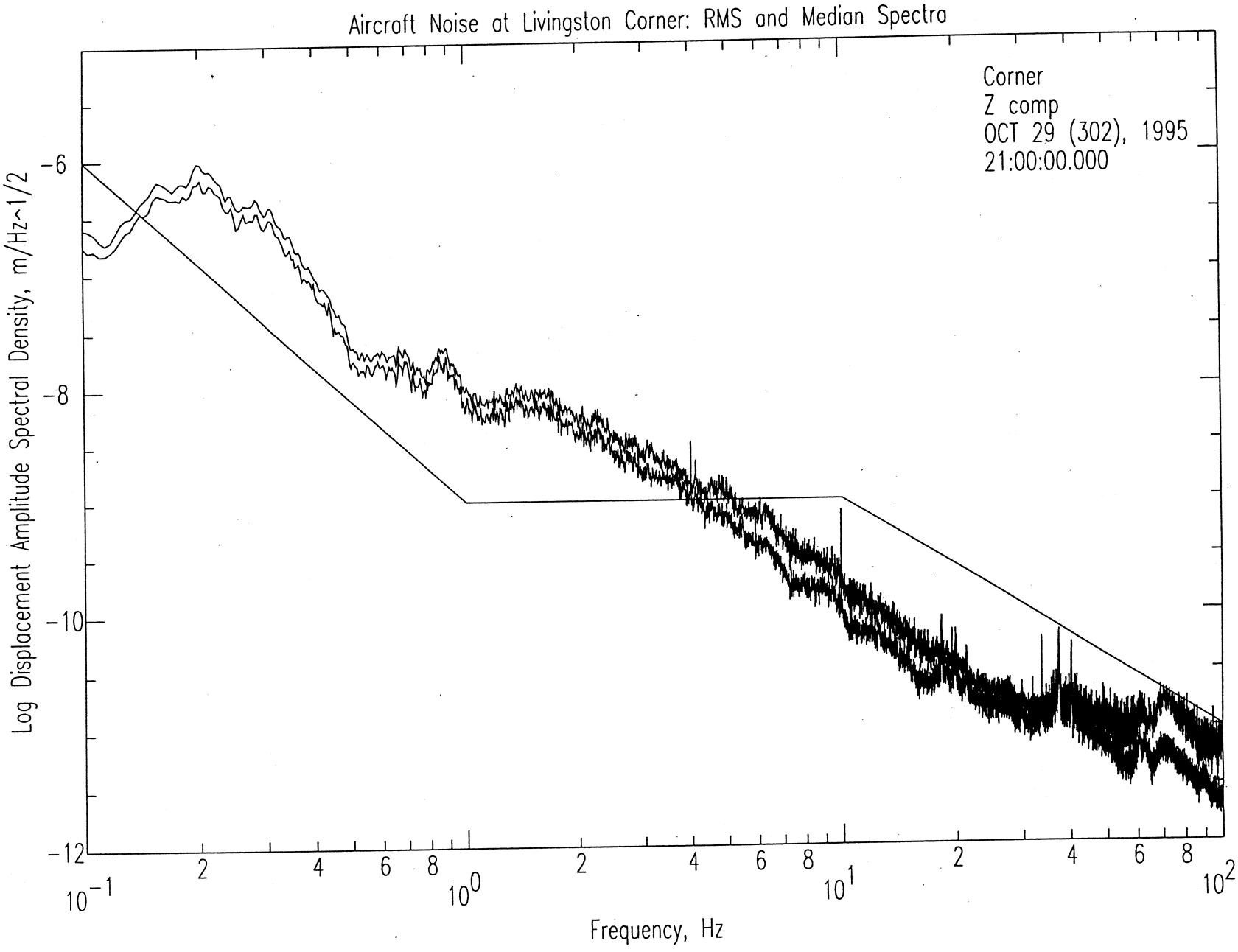

Figure 9.2-8. Amplitude spectra (median and r.m.s.) of vertical seismic signals for a one-hour period with frequent aircraft noise. Vertical seismic channel spectrogram was shown in Figure 9.2-6.

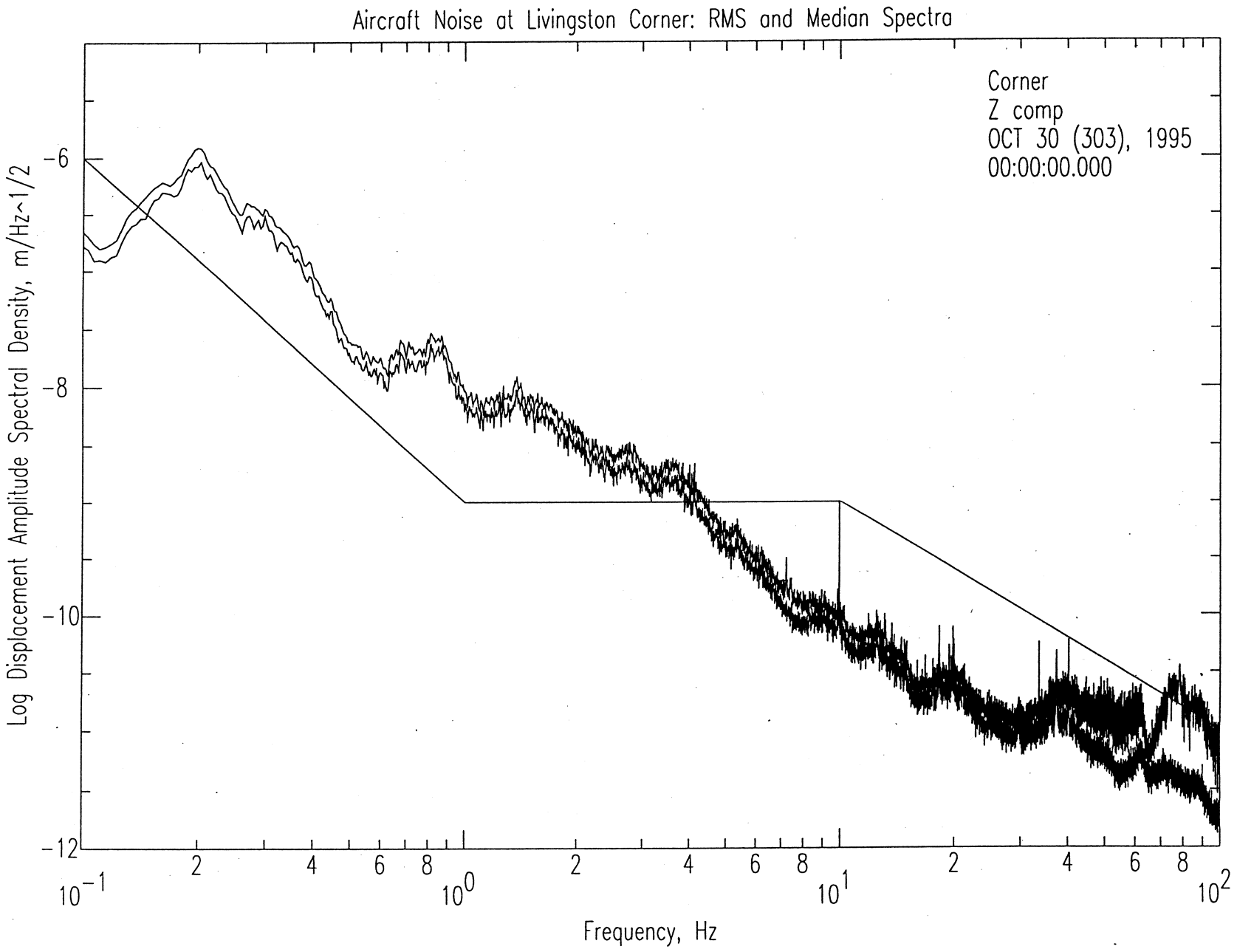

Figure 9.2-9. Amplitude spectra (median and r.m.s.) of vertical seismic signals for a one-hour period with frequent aircraft noise. Vertical seismic channel spectrogram was shown in Figure 9.2-7.

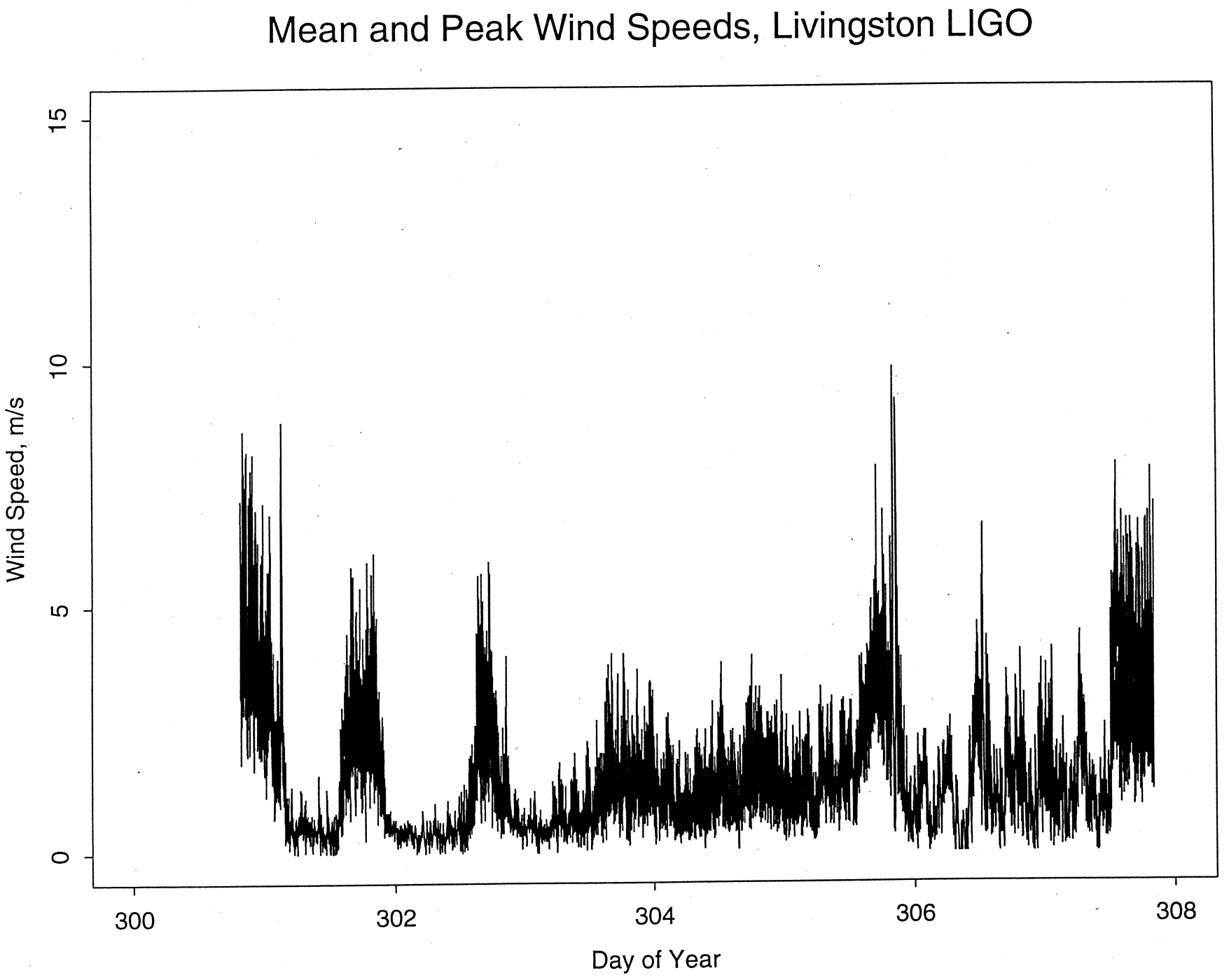

Figure 9.3-1. Mean and peak wind speeds during the entire recording period at Livingston.

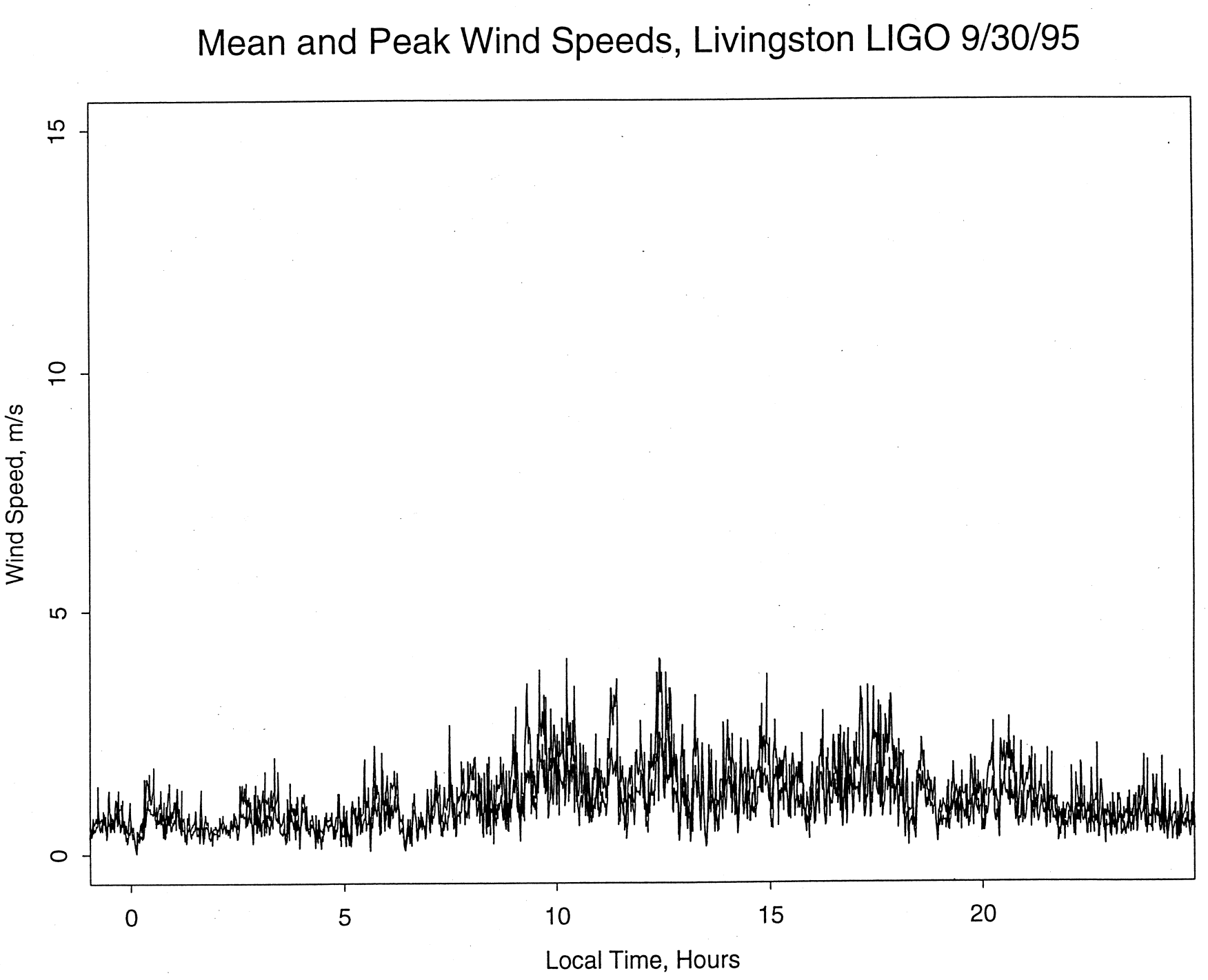

Figure 9.3-2. Mean and peak wind speeds during the 24-hour period analyzed in Appendices B, C, and D.

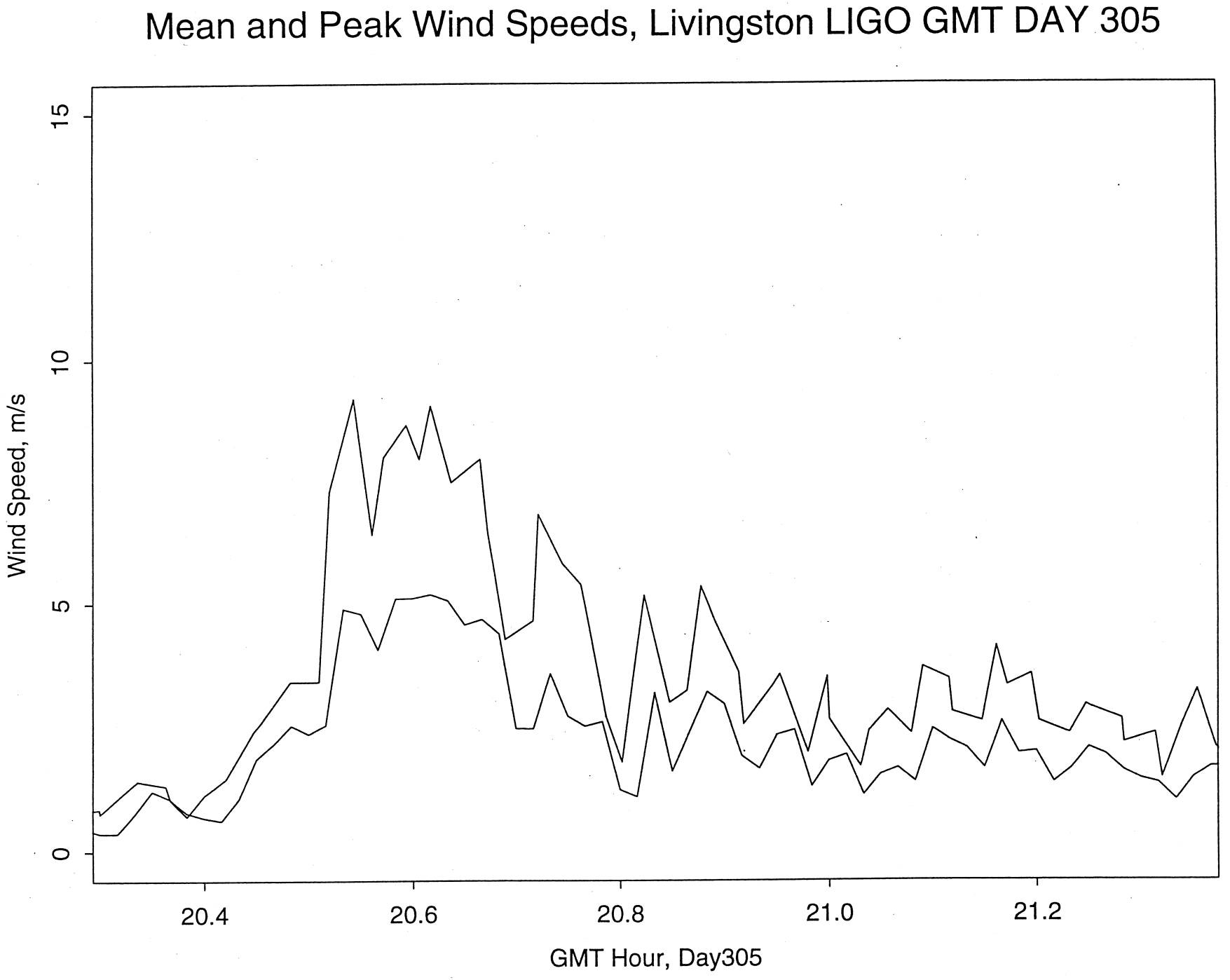

Figure 9.3-3. Mean and peak wind speeds during a one-hour period of moderate wind. This represents the maximum wind speed that was recorded during the Livingston measurement period (shown in Figure 9.3-1).

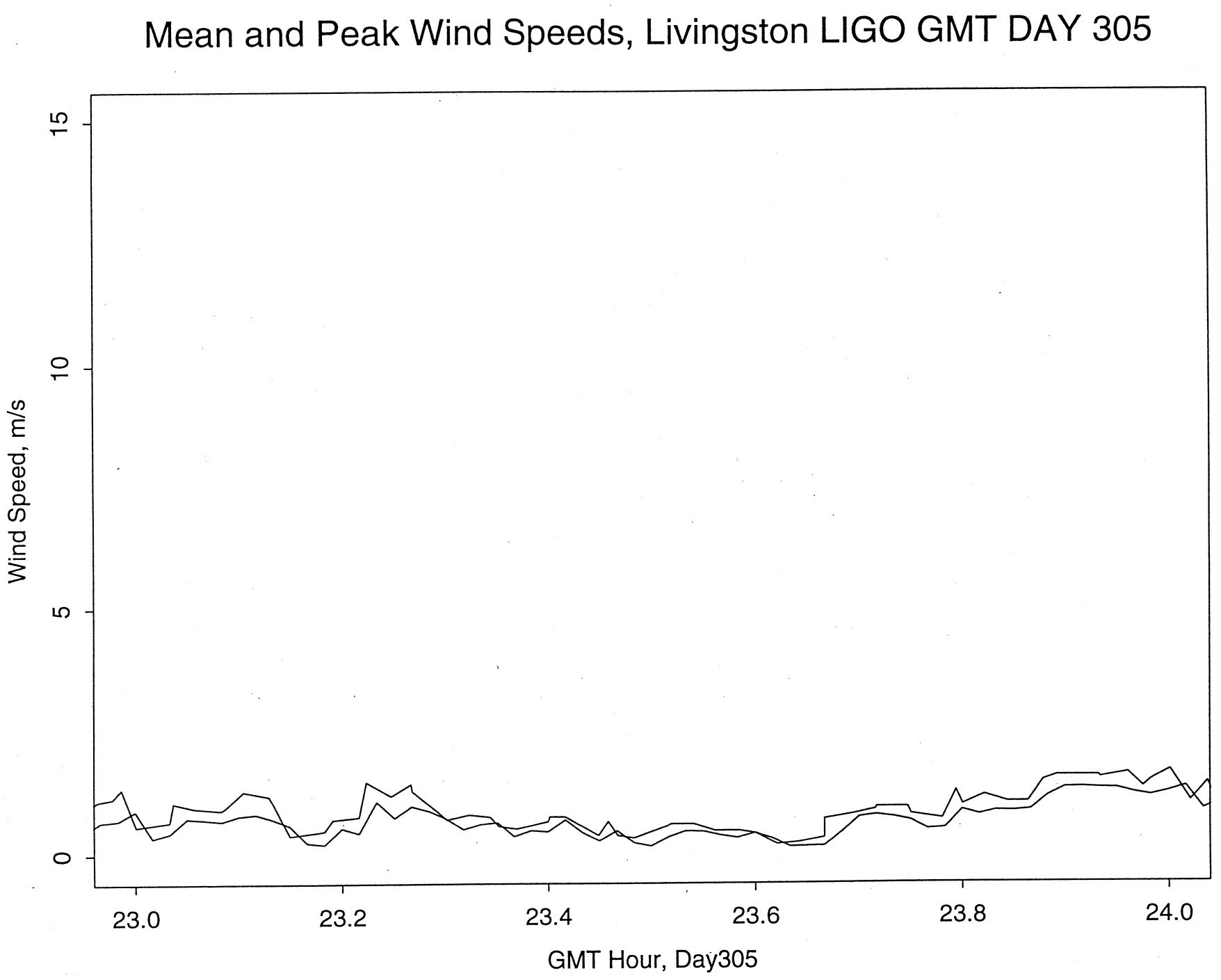

Figure 9.3-4. Mean and peak wind speeds during a one hour period of low wind. This period was chosen as soon as possible following the maximum wind observed in the period shown in Figure 9.3-3.

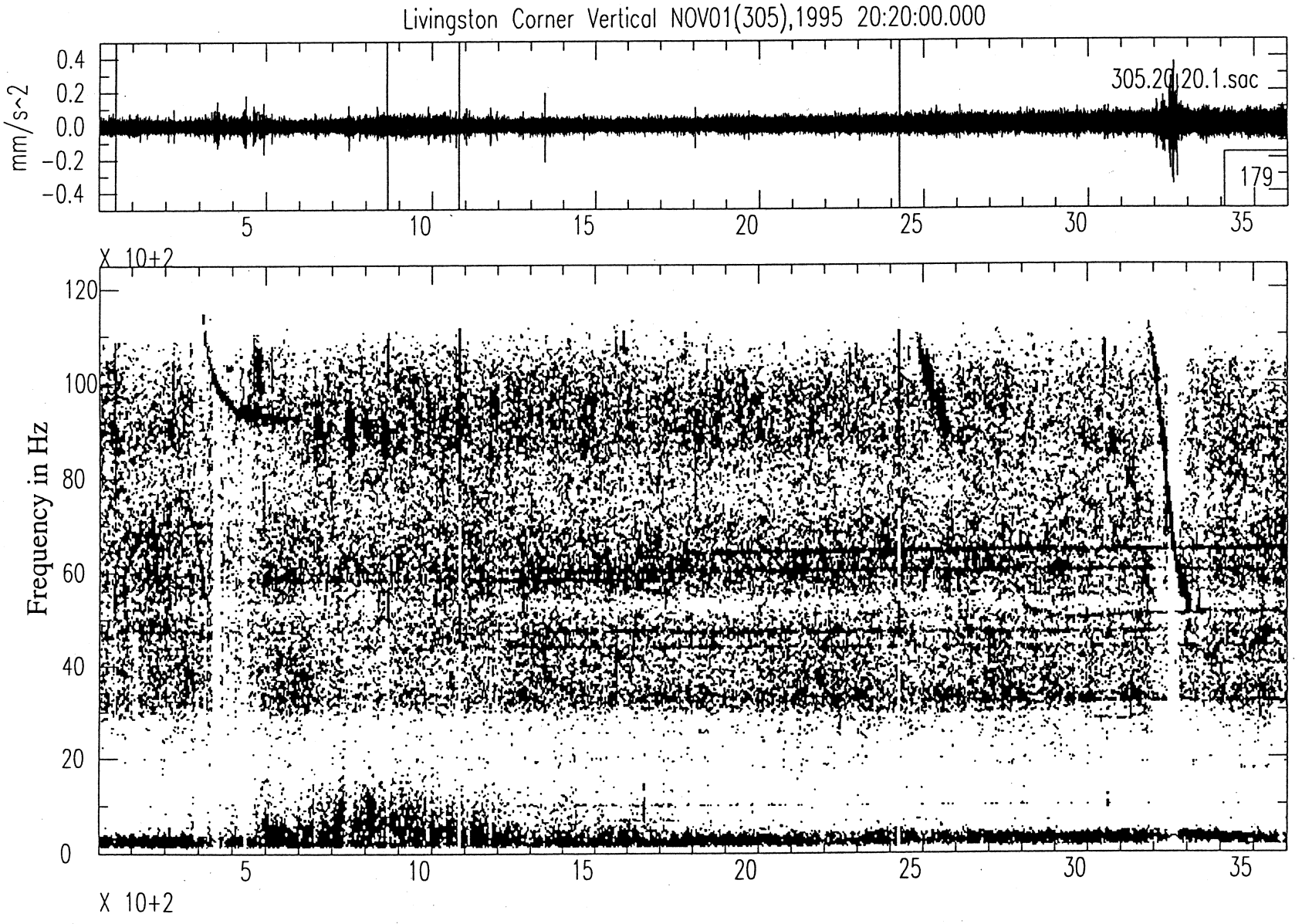

Figure 9.3-5. Black-and-white spectrogram of the vertical component seismic noise signal during the period of moderate wind shown in Figure 9.3-3

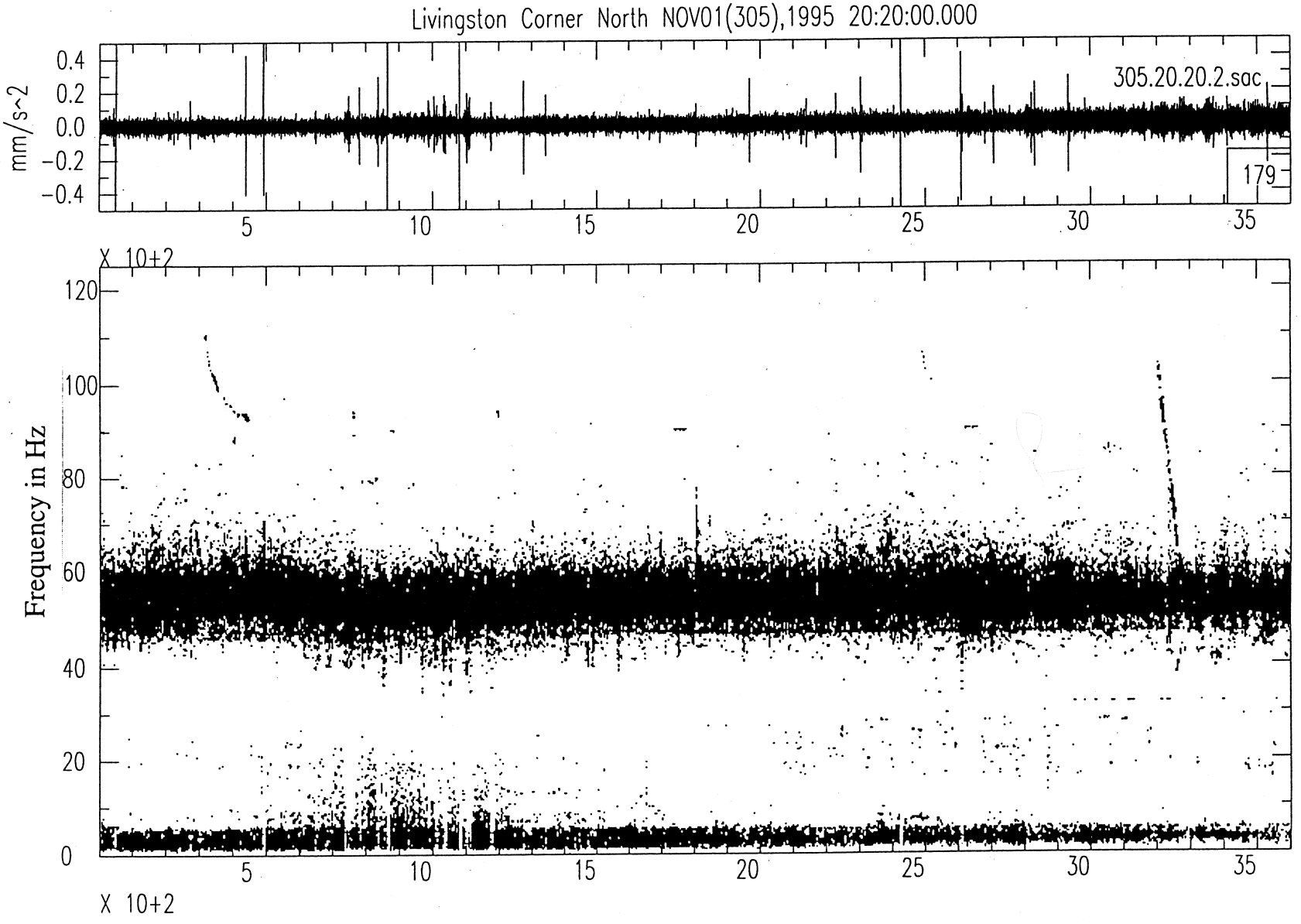

Figure 9.3-6. Black-and-white spectrogram of the north component seismic noise signal during the period of moderate wind shown in Figure 9.3-3

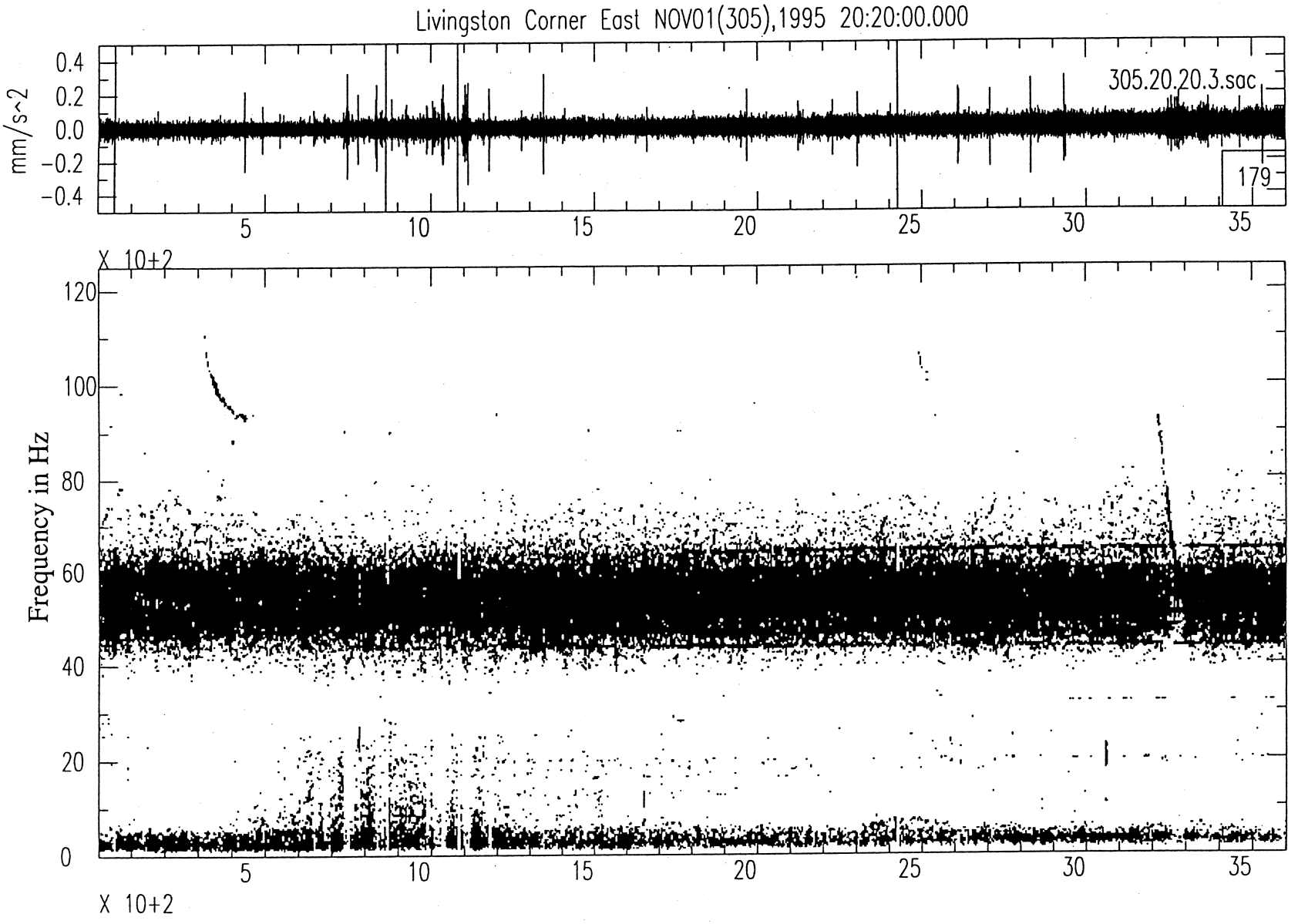

Figure 9.3-7. Black-and-white spectrogram of the east component seismic noise signal during the period of moderate wind shown in Figure 9.3-3

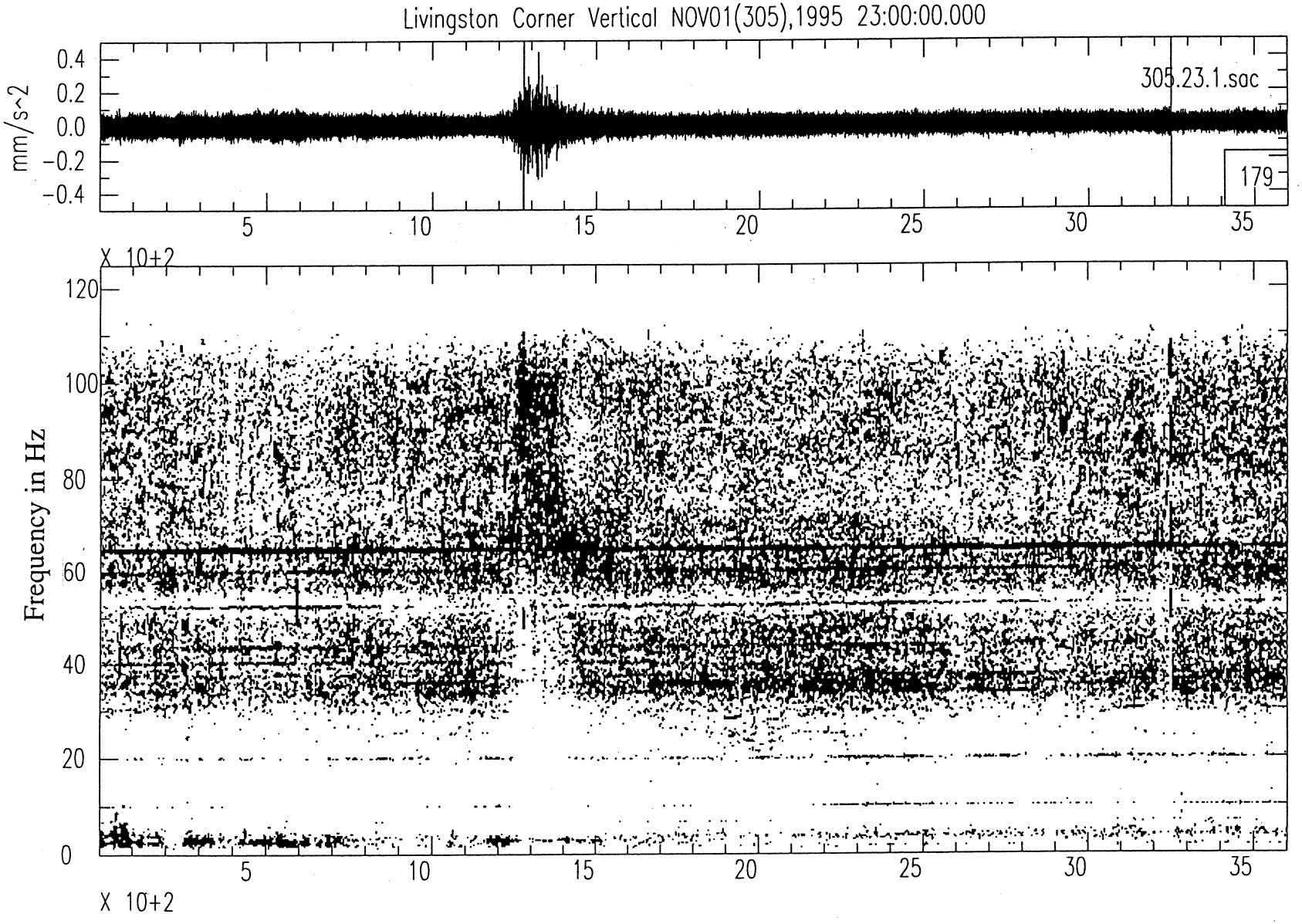

Figure 9.3-8. Black-and-white spectrogram of the vertical component seismic noise signal during the period of low wind shown in Figure 9.3-4

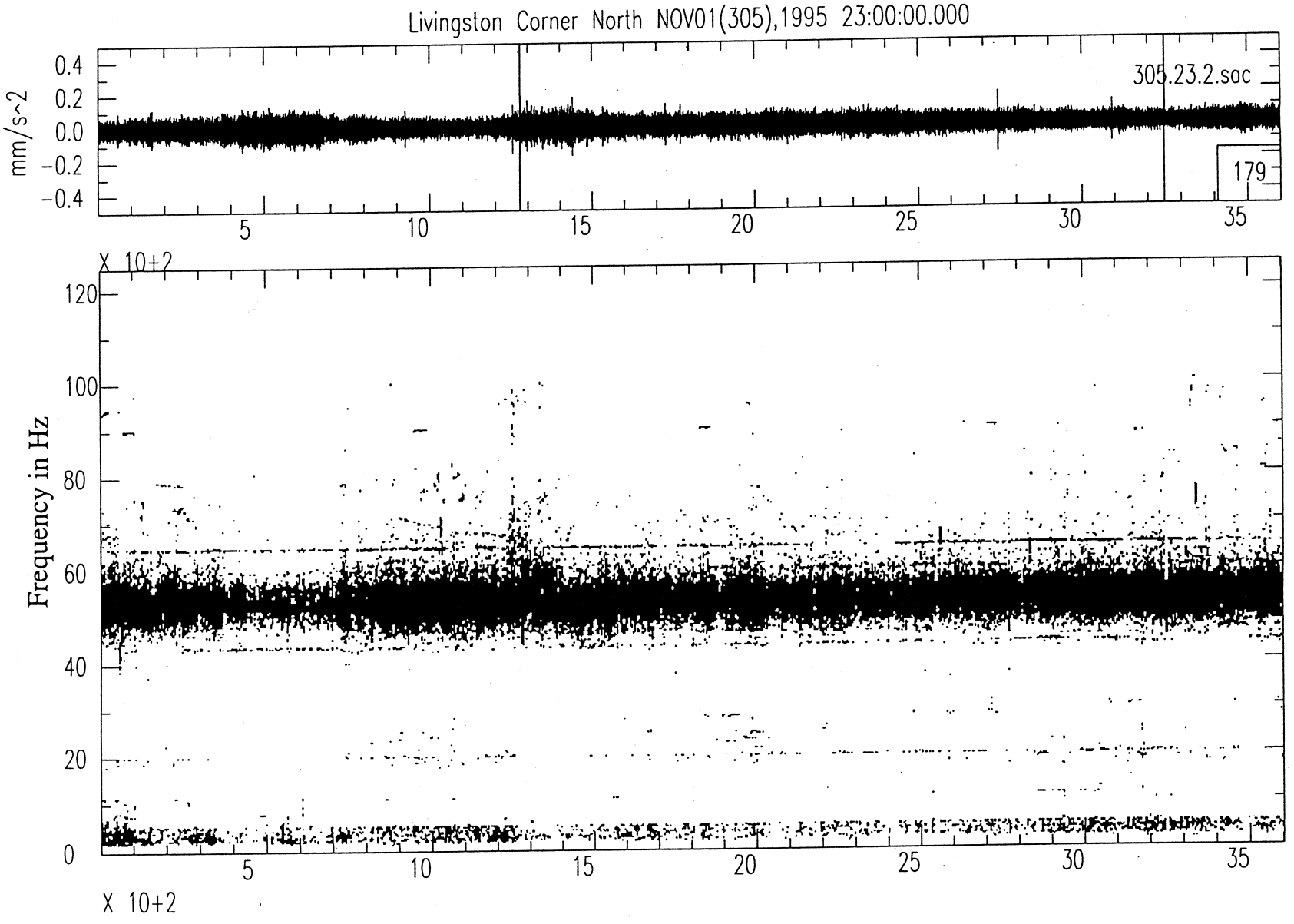

Figure 9.3-9. Black-and-white spectrogram of the north component seismic noise signal during the period of low wind shown in Figure 9.3-4

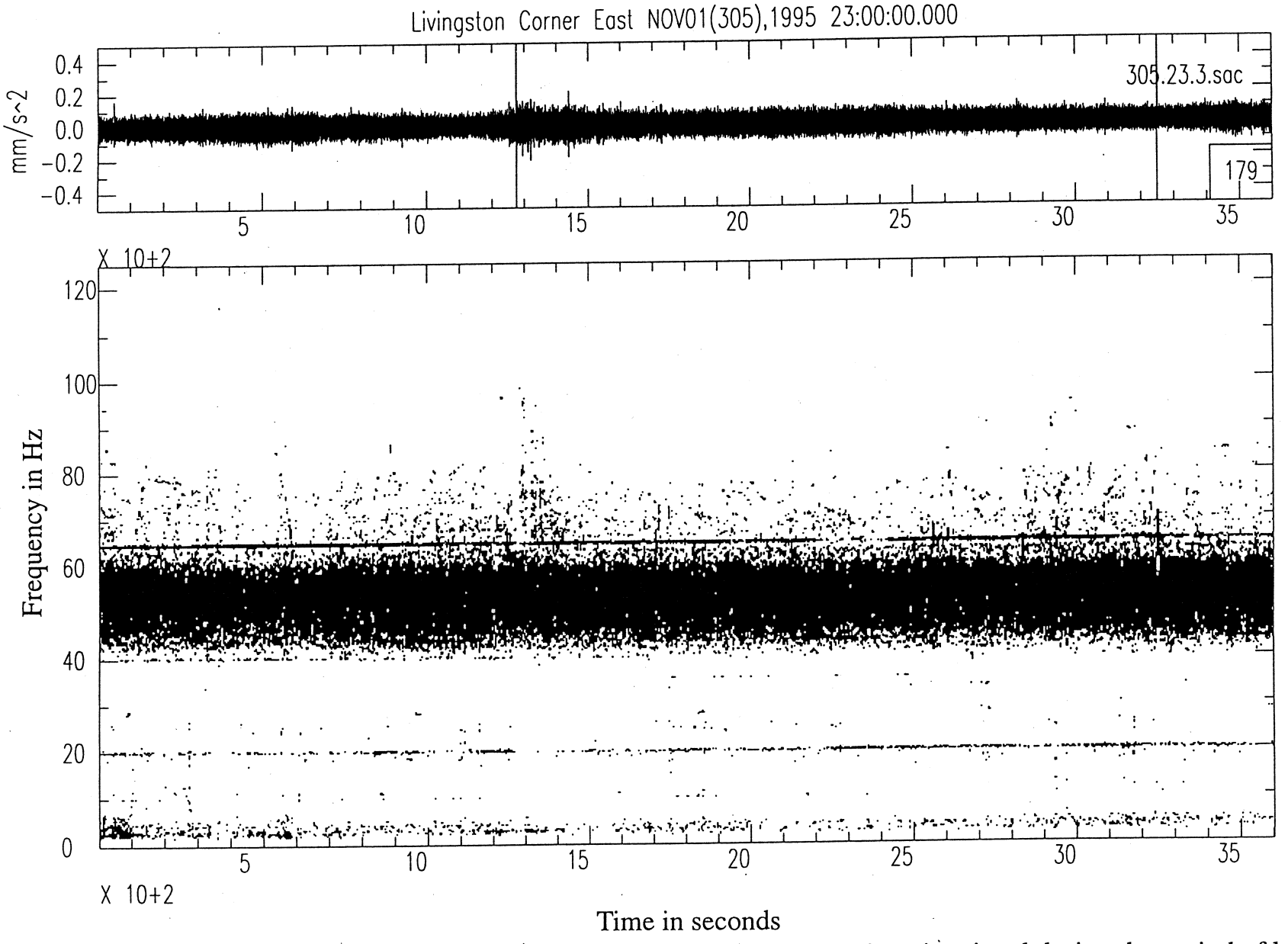

Figure 9.3-10. Black-and-white spectrogram of the east component seismic noise signal during the period of low wind shown in Figure 9.3-4

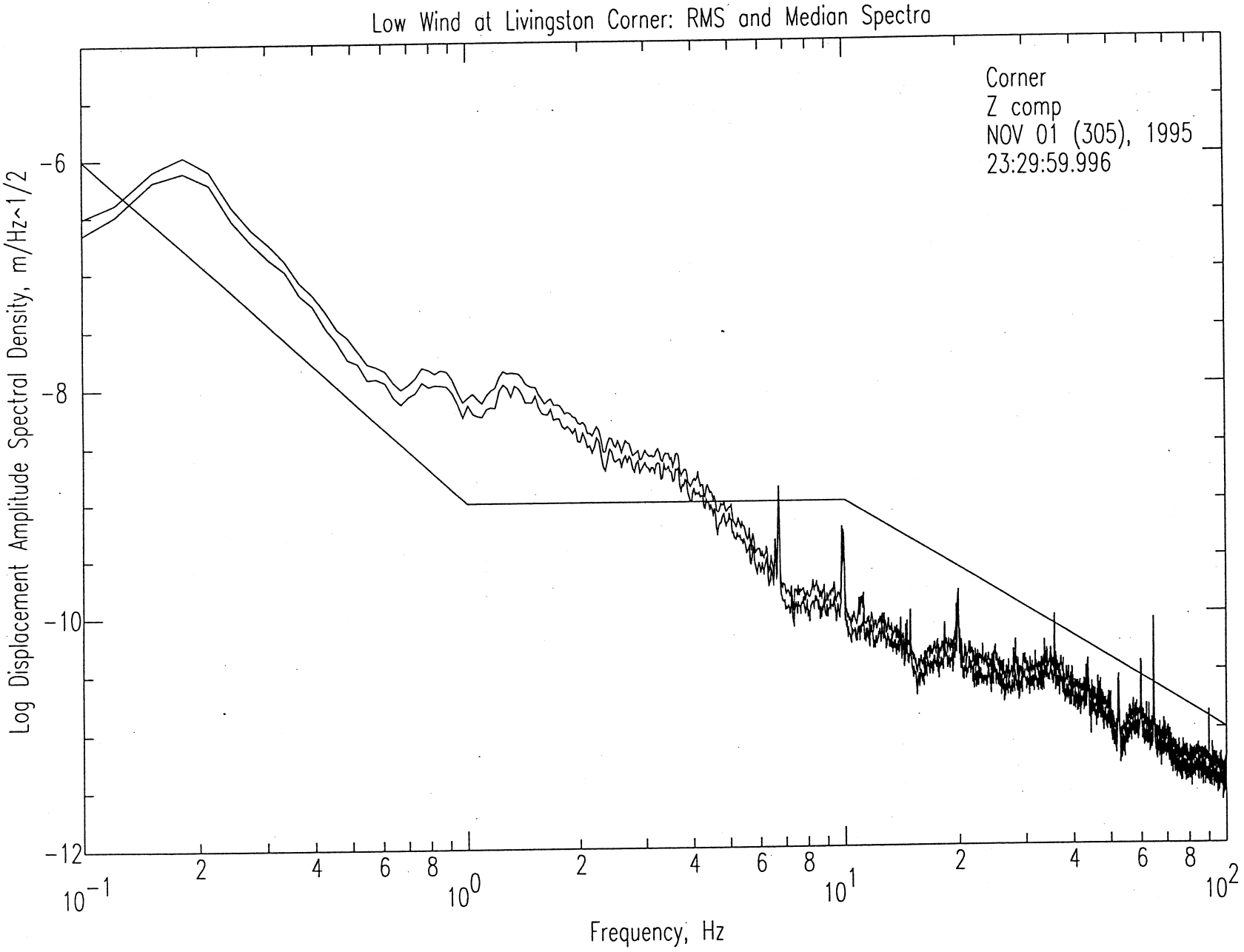

Figure 9.3-11. Vertical component amplitude spectra (median and r.m.s.) for the low-wind period. A 10 minute sample from 23:30 to 23:40 was used, corresponding to the times 23.5 to 23.66 in the wind plot in Figure 9.3-4.

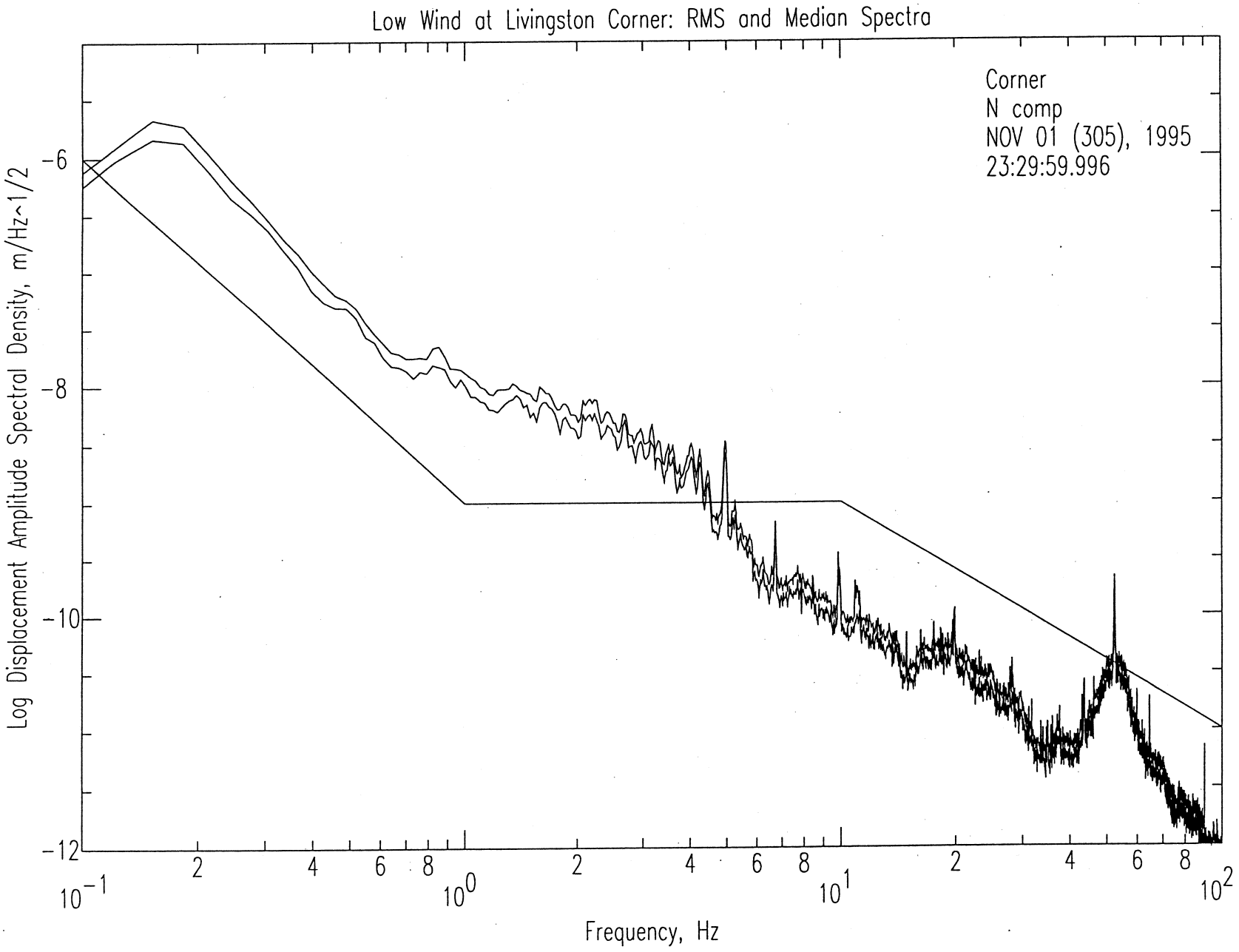

Figure 9.3-12. North component amplitude spectra (median and r.m.s.) for the low-wind period. A 10 minute sample from 23:30 to 23:40 was used, corresponding to the times 23.5 to 23.66 in the wind plot in Figure 9.3-4.

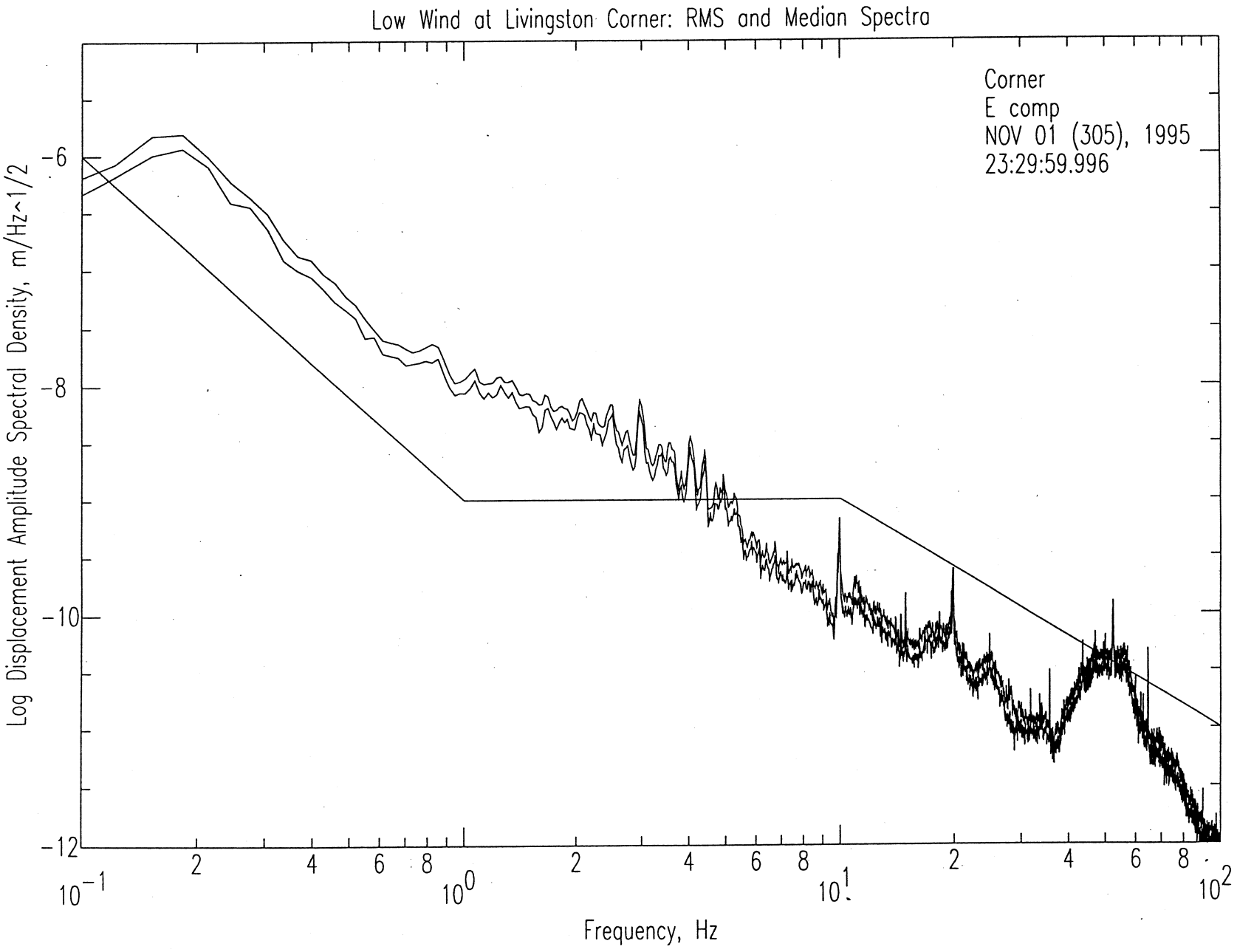

Figure 9.3-13. East component amplitude spectra (median and r.m.s.) for the low-wind period. A 10 minute sample from 23:30 to 23:40 was used, corresponding to the times 23.5 to 23.66 in the wind plot in Figure 9.3-4.

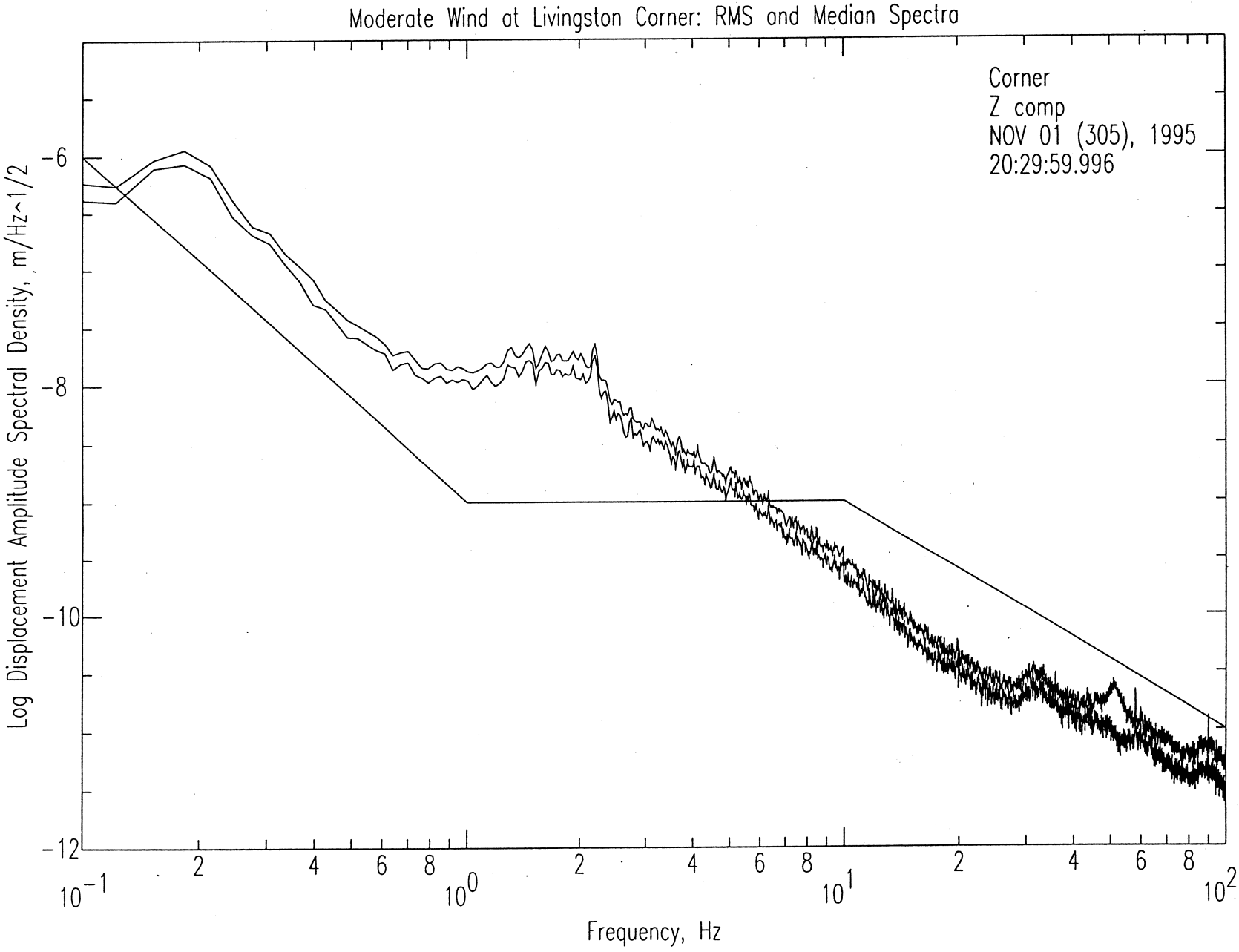

Figure 9.3-14. Vertical component amplitude spectra (median and r.m.s.) for the moderate-wind period. A 10 minute sample from 20:30 to 20:40 was used, corresponding to the times 20.5 to 20.66 in the wind plot in Figure 9.3-3. Noise in the frequency range 1-20 Hz has increased over the low-wind spectra shown in Figure 9.3-11

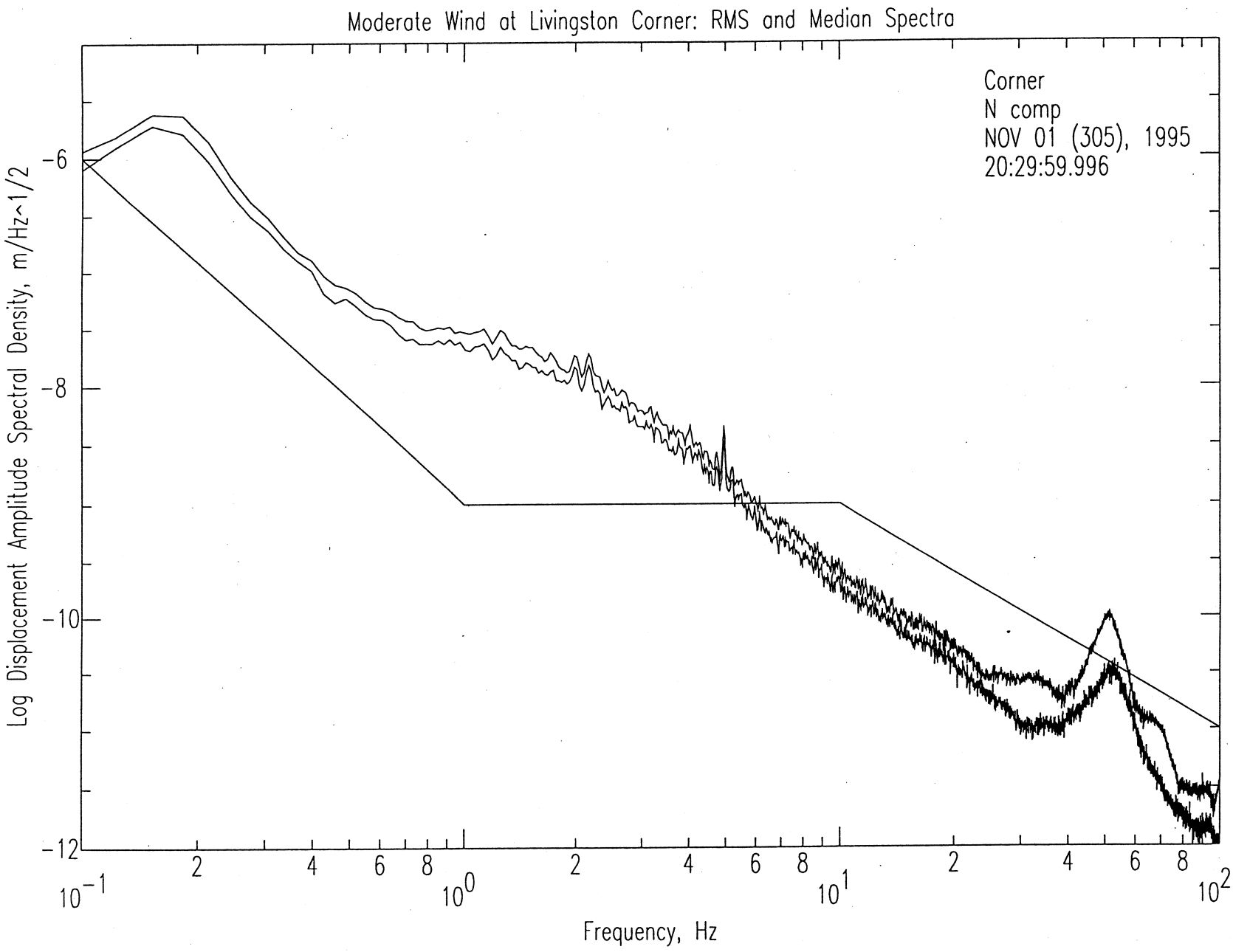

Figure 9.3-15. North component amplitude spectra (median and r.m.s.) for the moderate-wind period. A 10 minute sample from 20:30 to 20:40 was used, corresponding to the times 20.5 to 20.66 in the wind plot in Figure 9.3-3. Noise in the frequency range 1-20 Hz has increased over the low-wind spectra shown in Figure 9.3-12

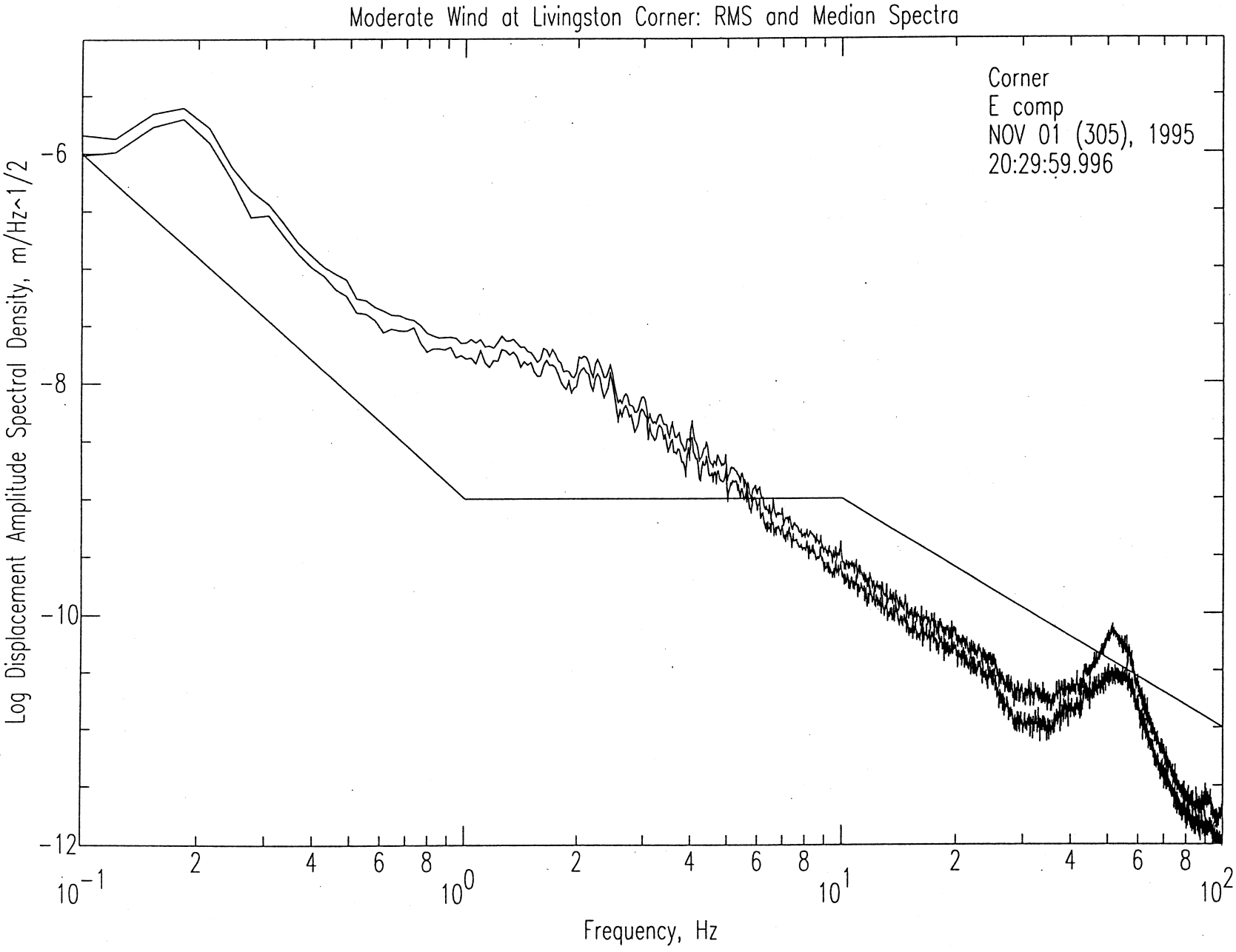

Figure 9.3-16. East component amplitude spectra (median and r.m.s.) for the moderate-wind period. A 10 minute sample from 20:30 to 20:40 was used, corresponding to the times 20.5 to 20.66 in the wind plot in Figure 9.3-3. Noise in the frequency range 1-20 Hz has increased over the low-wind spectra shown in Figure 9.3-13